THE EFFECT OF HIGH MYOPIA ON CORNEAL CHANGES IN CHICKEN

BYUNG SOO KANG

PhD

The Hong Kong Polytechnic University

2020

The Hong Kong Polytechnic University

School of Optometry

The Effect of High Myopia on Corneal Changes in Chicken

Byung Soo Kang

A thesis submitted in partial fulfillment of the requirements for the degree of Doctor of Philosophy

March 2020

Certificate of Originality

I hereby declare that this thesis is my own work and that, to the best of my knowledge and belief, it reproduces no material previously published or written, nor material that has been accepted for the award of any other degree or diploma, except where due acknowledgement has been made in the text.

Signature:

Name: Byung Soo Kang

To

my parents

my family

&

my wife

Abstract

Purpose: To investigate changes in corneal biometric and biomechanical parameters by applying custom-made instruments and proteomic analysis during the development of high myopia in form-deprivation treated chicks.

Methods: White Leghorn chicks (*Gallus gallus domesticus*) were used. Form-deprivation myopia was induced by occluding the right eyes for a week from day 5 post-hatching, while left eyes served as fellow contralateral controls. Refractive status, ocular axial dimensions, and corneal curvature were measured by a modified Hartinger refractometer, high-frequency A-scan ultrasonography, and custom-made videokeratography, respectively.

Experiment 1 (Chapter 2): The applicability of a custom-made air-jet optical coherence tomography system for corneal biomechanics measurement on chicks was tested. An intraocular-pressure control system was also validated.

Experiment 2 (Chapter 3): The applicability of a custom-made optical-coherence-tomography-indentation probe system for corneal biomechanics measurement on chicks was tested. The relationship between corneal biomechanical properties (tangent modulus and stiffness coefficient) and ocular biometric parameters was investigated.

Experiment 3 (Chapter 4): Generation and application of the chicken corneal proteome for a screening of differentially expressed corneal proteins during the

change of corneal biometric and biomechanical properties in high myopia.

Results:

Experiment 1 (Chapter 2): The custom-made air-jet optical coherence system was applicable for the measurement of chicks' eyes and a reduced corneal stiffness coefficient was found in form-deprivation treated eyes (mixed two-way ANOVA; main effect of myopia treatment: F (1, 24)= 17.13, $p<0.001$).

Experiment 2 (Chapter 3): The custom-made optical-coherence-tomography-indentation probe system was shown to be reliable and valid for corneal biomechanics measurements. Highly myopic chicks had a reduced corneal tangent modulus and stiffness coefficient (mixed two-way ANOVAs, all $p<0.01$). A significant correlation was observed between corneal biomechanical properties and ocular biometric parameters (with spherical equivalent refractive error, all $r>+0.52$, $p<0.05$; with vitreous chamber depth, all $r>–0.61$, $p<0.05$).

Experiment 3 (Chapter 4): A large corneal proteome of the chick (n= 2096) was established (1 % Global FDR). Using this first reported spectral library for highly myopic chicks, three upregulated (Reactive intermediate imine deaminase A homolog, Cadherin-1, and RuvB-like helicase) and five downregulated (Fibrinogen alpha chain, Fibrinogen beta chain, Fibrinogen gamma chain, Alpha-2-macroglobulin-like 4, and Chromobox 3 protein) proteins were identified following application of mass-spectrometry based proteomic analysis ($p<0.05$).

Conclusions: These results demonstrated significant changes in the corneal biometric and biomechanical properties as a result of the development of high myopia in chicks. The establishment of a corneal proteome in chicken provides research opportunities to study mechanisms potentially involved in corneal reshaping.

Publications Arising from This Thesis

Kang, B. S., Wang, L. K., Zheng, Y. P., Guggenheim, J. A., Stell, W. K., & Kee, C. S. (2018). High myopia induced by form deprivation is associated with altered corneal biomechanical properties in chicks. PloS one, 13(11), e0207189.

Kang, B. S., Lam, T. C., Cheung, J. K. W., Li, K. K., & Kee, C. S. (2019). Data on corneal proteome and differentially expressed corneal proteins in highly myopic chicks using a data independent quantification approach. Data in brief, 26, 104478.

Kang, B. S., Lam, T. C., Cheung, K. W., Li, K. K., & Kee, C. S. Corneal proteome and differentially expressed corneal proteins in highly myopic chicks using a label-free SWATH-MS quantification approach. (*under review*)

Conference Abstracts Arising from This Thesis

Kang, B. S., Wang, L. K., Zheng, Y. P., & Kee, C. S. (2015). Form-deprived highly myopic chick eyes have lower than normal corneal stiffness. Investigative Ophthalmology & Vision Science. E-Abstract 2158. Poster Presentation.

Kang, B. S., Wang, L. K., Zheng, Y. P., & Kee, C. S. (2016). Reduced corneal stiffness under IOP-controlled conditions in form-deprived highly myopic chicks. Investigative Ophthalmology & Vision Science. E-Abstract 5710. Poster Presentation.

Kang, B. S., Wang, L. K., Zheng, Y. P., Guggenheim, J. A., Stell, W. K., & Kee, C. S. (2018). High myopia induced by form deprivation is associated with altered corneal biomechanical properties in chicks. The 11th Asia Cornea and Contact Lens Conference. Oral Presentation.

Acknowledgements

TO MY SUPERVISOR My deepest appreciation must first go to my chief supervisor, **Dr. Chea-su Kee**, who expertly guided me to become an independent researcher with critical reasoning. His enthusiasm and continuous motivation conveyed a spirit of adventure which kept me constantly engaged with experimental eye research. Without his guidance and advice, the entire works in this dissertation would not have been possible.

TO MY MENTORS I would like to express sincere gratitude to my co-supervisor, Prof. Jeremy Guggenheim, and my advisor, Prof. William Stell for sharing genius insights in myopia research with constructive comments during the preparation of this dissertation and related publications. Special thanks must also go to Prof. Jeong-Sik Son, Prof. Dong-Sik Yoo, Prof. Ho-Won Kwak, Prof. Byeong-Yeon Moon, and Prof. Ji-Hoon Kang who taught me the delight of studying Optometry and encouraged me to pursue graduate study in Hong Kong.

TO MY COLLABORATORS My appreciation extends to key collaborators, Prof. Yong-ping Zheng and Mr. Li-Ke Wang who have been continuously introducing novel technologies for a better understanding of myopia development. In addition, I would like to thank Dr. Chi-wai Do, Dr. Thomas Lam, Mr. K.K. Li, and Mr. Jimmy Cheung for their guidance during the set-up of IOP control and the exploration of micro-level structure in the cornea.

TO MY COLLEAGUES My sincere thanks also go to senior colleagues, Dr. Geoffrey Chu, Dr. Jeffrey Leung, Dr. Yvonne Huang, and Dr. Samantha Shan for teaching the essential research knowledge and technique. I have to thank all lab mates who have helped me adapt to a new living and research environment: Dr. Rachel Chun, Dr. Patrick Ting, Dr. Dede Chan, Dr. Yin Zhi Wong, Dr. Bruce Chin, Dr. Shanica Hon, Dr. Kar Ho Siong, Dr. Serena Li, Ms. Yan Lam, Ms. Hoi Lam Li, Mr. Kai Yip Choi, Mr. Ken Wan, and Mr. Jason Lau. In addition, I thank my fellow lab mates in Special Interest Group on refractive error, Dr. Elie Delestrange-Anginieur, Ms. Sonal Vyas, Ms. Andrea Zhang, Ms. Christie Lam, Ms. Yuanyuan Liang, and Mr. Monkey Kong for sharing innovative ideas in different fields which broadened my perspective on research. I cannot forget my honored colleagues, chicken, who sacrificed and patiently endured the entire experiment process.

TO MY FAMILY Above all, I am indebted to my parents, Yung-Ok Kang and Kyung-Sook Yoo, and my sister Min-Ju Kang for their unconditional support and endless patience. I also deeply thank my new family in Hong Kong who has been generous with their love: Philips Ng, Rosita Kwan, Janice Ng, and Jeffrey Ng.

TO MY WIFE Last but not the least, I am deeply grateful to my beloved wife, Joanne Ka Yiu Ng for her continuous love, sacrifice, understanding, and encouragement as the best friend and companion in my life. Thank YOU.

Table of Contents

List of Figures

Chapter 2

Chapter 3

Chapter 4

List of Tables

Chapter 1

Chapter 3

Chapter 4

List of Abbreviations

A2ML4	Alpha-2-macroglobulin-like 4
ACD	Anterior Chamber Depth
AJ-OCT	Air-Jet Optical Coherence Tomography
ANOVA	Analysis of Variance
ASB14	Ankyrin Repeat and SOCS Box 14
CA	Corneal Astigmatism
CB	Corneal Biomechanical Properties
CBX3	Chromobox 3
CCD	Charged Coupled Device
CCT	Central Corneal Thickness
CDH1	Cadherin 1
CH	Corneal Hysteresis
CHAPS	3-[(3-Cholamidopropyl) Dimethylammonio] Propanesulfonic Acid
CI	Confidence Intervals
COMP	Comprehensive Library
Corvis ST	Corneal Visualization Scheimpflug Technology
CP	Corneal Power
CRF	Corneal Resistance Factor
CS	Corneal Stiffness Coefficient
CT	Choroidal Thickness
CTRL	Unfractionated Control Library
CXL	Corneal Cross-Linking
dF	Differential Force
DIA	Data Independent Acquisition
DTT	Dithiothreitol
$d\delta$	Displacement Interval
E	Modulus of Elasticity
FBA/B/G	Fibrinogen Chain Alpha/Beta/Gamma
FD	Form Deprivation
FD	Frequency-Domain
FDR	False Discovery Rate
FRAC	Fractionated Library
GO	Gene Ontology
h	Height
h	Hour
HCl	Hydrogen Chloride
HRSP12	Heat-responsive Protein 12
IAA	Iodoacetamide

ICC	Intra-class Correlation Coefficients
IDA	Information Dependent Acquisition
IOP	Intraocular Pressure
J0	Refractive Cosine Jackson Crossed-Cylinder Component
J45	Refractive Sine Jackson Crossed-Cylinder Component
LE	Left Eye
LED	Light-Emitting Diode
LT	Lens Thickness
MLR	Most Likely Ratio
MMP-2	Matrix Metalloproteinase-2
MRM-HR	Multiple Reaction Monitoring High-Resolution
MS	Mass Spectrometry
MS/MS	Tandem Mass Spectrometry
MV	MarkerView
OCE	Optical Coherence Elastography
OCT	Optical Coherence Tomography
ORA	Ocular Response Analyzer
p	Pressure
P5	5 Days Post-Hatching
P12	12 Days Post-Hatching
PP	ProteinPilot
PTM	Post Translational Modification
PV	PeakView
r	Pearson's Correlation
r^2	Coefficient of Determination
r_0	Radius of the Full-Contact Area
RA	Refractive Astigmatism
Rc	Radius of Corneal Curvature
RE	Right Eye
RT	Retinal Thickness
RUVBL1	RuvB-like 1
SD	Standard Deviation
SE	Spherical Equivalent
SEM	Standard Error of the Mean
SLD	Superluminescent Diode
ST	Scleral Thickness
SWATH-MS	Sequential Windowed Acquisition of all Theoretical Mass Spectra
t	Corneal Thickness
TD	Time-Domain
TFA	Trifluoroacetic Acid
TGF-β2	Transforming growth factor-beta 2

TIMP-2	Tissue inhibitor of metalloproteinases-2
TM	Corneal Tangent Modulus
v	Poisson's Ratio
VCD	Vitreous Chamber Depth
VIF	Variance Inflation Factor
VKS	Videokeratography System
XIC	Extracted-ion Chromatogram
α	Geometrical Constant
ρ	Density

Keywords

Astigmatism

Corneal Astigmatism

Corneal Biomechanics

Corneal Curvature

Corneal Proteomics

Corneal Thickness

High Myopia

OCT-indentation Probe

Ocular Biometrics

Aims of this Thesis

Myopia is the most common refractive disorder, mainly caused by an abnormally elongated eyeball. High myopia can lead to vision loss. In recent decades, myopia prevalence has increased dramatically worldwide, especially in East Asia. Numerous studies have revealed various factors (optical, genetic, and environmental) affecting myopia development by determining the role of ocular posterior segments (retina, choroid, and sclera) in eye-growth regulation. However, far less attention has been paid to the anterior segments (cornea, anterior chamber, and crystalline lens) and their roles remain unclear. Since increasing evidence suggests that myopia development is associated with the changes of an essential ocular refractive component, the cornea, more extensive research into the causes of these changes and their effects on ocular development is clearly required.

This thesis, therefore, aims to develop chicken as an animal model for investigating the relationship between development of high myopia and changes of corneal biometric/biomechanical properties. A brief overview of each chapter is given below, followed by a general introduction in Chapter 1. Detailed introductions to research background, and relevant descriptions of each experiment and citations can be found in the following chapters.

Chapter 1 provides an introduction to the background of this study. Scope of each chapter and major objectives are also presented.

Chapter 2 presents the application of the air-jet optical coherence tomography system for measuring corneal stiffness coefficient of form-deprived highly myopic chicks at controlled intraocular pressures. Technological limitations are discussed for instrument improvements in Chapter 3.

Chapter 3 presents the development and application of the optical coherence tomography indentation probe system by addressing instrumental limitations found in Chapter 2. This improved and validated instrumentation can measure corneal stiffness coefficient and tangent modulus of form-deprived highly myopic chicks at controlled intraocular pressures. The associations between ocular biometric parameters and corneal biomechanical properties were examined.

(Note: knowledge learned from Chapters 2 and 3 were used to produce the following paper: Kang, B. S., Wang, L. K., Zheng, Y. P., Guggenheim, J. A., Stell, W. K., & Kee, C. S. (2018). High myopia induced by form deprivation is associated with altered corneal biomechanical properties in chicks. PloS one, 13(11), e0207189.)

Chapter 4 presents the application of analytical proteomic approaches to understand the mechanism behind corneal biometric and biomechanical changes in form-deprived, highly myopic chicks. The first chicken corneal proteome was established and potential biomarker proteins were further screened. This study has been submitted for publication and is currently under review.

Chapter 5 provides general conclusions and discussions on future directions arising from this study.

Chapter 1

General Introduction

Myopia, or nearsightedness, is a refractive condition in which reflected light from distant objects focuses in front of rather than on the retina, causing blurred distance vision. Myopia is typically caused by an excessively elongated eyeball or increased refractive power of the eye, or a combination of these two elements (Edwards & Lam, 2004). Although the adverse optical effect of myopia can be easily corrected by visual aids and refractive surgery, high levels of myopia are associated with various ocular pathologies resulting in permanent vision loss (Celorio & Pruett, 1991; Ko et al., 2002; Saw et al., 1996; Wong et al., 2003; Xu et al., 2006; Younan et al., 2002; Yura, 1998). In recent years, myopia has become of particular concern in East Asia, due to extremely high prevalence (Ding et al., 2017; He et al., 2004; Jung et al., 2012; Kim et al., 2013; Koh et al., 2014; Lin et al., 2004; Morgan et al., 2018; Pan et al., 2012; Zhao et al., 2000); however, the increasing prevalence of myopia is expected to become global in the next decades (Dolgin, 2015; Holden et al., 2016).

The cornea is a transparent collagen-rich optical component located at the

front part of the eye, serving as a protective shield against harmful materials. Optically, the cornea is responsible for around 60 % of the human eye's refractive power. Minor irregularities of shape and surface produce an adverse influence on visual performance (Hayashi et al., 2015; Huang et al., 2002; McLellan et al., 2001; Suzuki et al., 2007; Tan et al., 2008). Thus, maintaining a good corneal integrity structure throughout life is imperative. It has been recognized that balanced microstructure and biomechanical strength across the corneal region is responsible for sustaining its fine structure, based on observation of disrupted structural equilibrium in various corneal pathologies and post-refractive surgery (Bao et al., 2016; Blackburn et al., 2019; Dawson et al., 2008; Pallikaris et al., 2001; Rad et al., 2004; Wolffsohn et al., 2012).

Human cornea is composed of five parallel layers. The epithelium is the outermost layer consisting of three distinctive cells (squamous cell, wing cell, and basal cell) and responsible for the absorption of nutrition/oxygen from tear film and distribution to other corneal layers (Berman, 2013; Ehlers & Hjortdal, 2005; Forrester et al., 2015). Below the epithelium is Bowman's layer, containing collagen randomly arranged (type I, III, IV, V, and VI) (Konomi et al., 1984; Marshall et al., 1991; Newsome et al., 1981) and is associated with stromal wound healing and transparency maintenance (Hayashi et al., 2002; Lagali et al., 2009; Wilson & Hong, 2000)). The corneal stroma, a hydrated matrix, is the middle layer accounts for 90 % of the total corneal thickness and composed primarily of collagens (type I, III, IV, V,

VI, VII, VIII, XII, XIII, and XVII). Stromal collagen fibrils, small and uniform in diameter, are regularly arranged and stacked to one another to form lamellae; this arrangement ensures minimal light scattering to maintain corneal transparency (Meek & Knupp, 2015). The Descemet's membrane, a supporting basement membrane to endothelial cells (Last et al., 2009), is composed of type II, IV, VI, and VII collagens (Marshall et al., 1991; Marshall et al., 1991). Although this layer is tough and highly elastic, its contribution to overall corneal biomechanics may be minimal (Jue & Maurice, 1986; Last et al., 2009); instead, it plays a key role in fluid regulation (e.g., tissue damage leads to endothelial cell loss (Hull et al., 1984)). The endothelium is a single cellular layer composed of around 400,000 uniform and hexagonal shaped cells (Yokoi et al., 2012), it maintains fluid and ion homeostasis that regulates corneal hydration and transparency (Berman, 2013; Fischbarg & Maurice, 2004).

Factors including the organization of stromal collagen fibril, interaction with proteoglycan, and corneal biomechanical strength have been suggested to modulate the corneal shape (Boote et al., 2005; Boote et al., 2006; Meek et al., 2005; Quantock & Young, 2008). In human and monkey, a novel X-ray scattering technique demonstrated that collagen fibrils in the central cornea are preferentially oriented in the inferior-superior and nasal-temporal directions (Daxer & Fratzl, 1997; Meek et al., 1987). In the peripheral cornea, collagen fibrils are oriented circumferentially and coalesced with annulus of fibrils that confine the cornea —

which may maintain the corneal shape (curvature) by reinforcing the limbus (Meek & Boote, 2004; Newton & Meek, 1998; Newton & Meek, 1998). It has long been questioned whether causal relationships exist between myopia development and corneal shape because of its significant role as a primary refractive component of the eye. Investigation has revealed a notable reduction of two well-defined corneal geometrical elements in both human and animals myopes: thickness and radius of curvature (Table 1.1) (Gottlieb et al., 1987; Graham & Judge, 1999; Guggenheim & McBrien, 1996; Hayes et al., 1986; Howlett & McFadden, 2006; Irving et al., 1992; Jiang et al., 2018; Kang et al., 2018; Kee et al., 2005; Lu et al., 2006; McBrien et al., 2001; Napper et al., 1995; Norton & Rada, 1995; Qiao-Grider et al., 2004; Qiao-Grider et al., 2010; Siegwart & Norton, 1998; Troilo et al., 1995; Troilo & Nickla, 2005; Wallman et al., 1978; Zhou et al., 2007). There are two hypothetical explanations of these changes: 1) a self-tissue-remodeling upon visual stimulus, based on the observations of the sclera in myopia-developing eyes: specifically, changes in scleral thickness and biomechanical properties are driven by altered collagen fibril orientation and molecular expression to facilitate ocular expansion during abnormal eye growth; and 2) as a consequence of corneal stretching by acute ocular elongation during myopia development.

Corneas and sclera are attached and possess a structural similarity of a compressed collagen scaffold to function as the outer coat of the eyeball. Evidence of vision-dependent corneal reshaping in animal models and its role in

Table 1.1. Ocular anterior segments changes during the development of myopia in animal models.

Authors	Species	Treatment	SE	CCT	CRC	ACD
Wallman et. al (1978)	Chicks	Diffuser	-12.00	·	·	Deeper*
Hayes et al (1986)	Chicks	Diffuser	-14.88	NS	Steeper†	Deeper*
Gottlieb et al (1987)	Chicks	Diffuser	-31.00	·	Steeper*	Deeper*
Irving et al (1992)	Chicks	Lens (-10D)	-9.70	·	NS	·
Troilo & Nickla (1995)	Chicks	Diffuser	-21.80	·	Steeper†	Deeper†
Napper et al (1995)	Chicks	Diffuser	-23.58	·	Steeper†	Deeper†
Kang et al (2018)	Chicks	Diffuser	-26.40	Thinner*	Steeper*	Deeper*
Norton et al (1995)	Tree Shrews	Diffuser	-11.30	·	NS	Deeper*
Guggenheim & McBrien (1996)	Tree Shrews	Diffuser	-7.40	·	NS	NS
Siegwart & Norton (1998)	Tree Shrews	Diffuser	-2.50	·	NS	NS
McBrien et al (2001)	Tree Shrews	Diffuser	-11.80	·	NS	NS
Graham & Judge (1999)	Marmoset	Lens (-4D)	-2.80	·	NS	NS
Troilo & Nickla (2005)	Marmoset	Diffuser	-8.65	·	Steeper*	·
Qiao-Grider et al (2004)	Rhesus monkeys	Diffuser	-4.06	·	Steeper*	·
Kee et al (2005)	Rhesus monkeys	Diffuser	-5.62	·	NS	·
Qiao-Grider et al (2010)	Rhesus monkeys	Diffuser/Lens	-1.00	·	Steeper*	NS
Lu et al (2004)	Guinea Pigs	Diffuser	-2.21	·	NS	NS
Howlett & McFadden (2006)	Guinea Pigs	Diffuser	-6.60	·	·	Deeper*
Zhou et al (2007)	Guinea Pigs	Diffuser	-2.55	·	NS	NS
Jiang et al (2018)	Mouse	Lens (-10D)	-15.00	·	NS	Deeper*

Abbreviations: SE, spherical equivalent (D); CCT, central corneal thickness; CRC, corneal radius of curvature; ACD, anterior chamber depth ; NS, not significantly differ; * statistically differ; †, statistical test not performed

emmetropization in early eye growth suggest that corneal remodeling can be influenced by visual experiences (Cohen et al., 2008; Gottlieb et al., 1987; Howlett & McFadden, 2006; Kee & Deng, 2008; Kee et al., 2005; Qiao-Grider et al., 2004; Rucker et al., 2015; Troilo et al., 1995). There have been limitations to the investigation of myopia-cornea relationships because myopia development typically occurs during the early years of life and opportunities to collect corneas for biological and biomechanical analysis are scarce. The primary aim of this thesis, therefore, was to develop an animal model to investigate the relationship between myopia development and corneal structural changes and their underlying mechanisms. Three experiments were conducted to evaluate the effectiveness of using chicken as the animal model in myopia-cornea research, to reveal corneal structural and biomechanical changes in experimentally induced high myopia, and to understand the molecular basis of the corneal changes.

Chapter 2: Corneal Stiffness Coefficient of Highly Myopic Chicks Measured by an Air-jet Optical Coherence Tomography System

Scientific interest in corneal biomechanics has greatly increased with the introduction of the commercial instruments for their measurement, Ocular Response Analyzer (Luce, 2005), and Corvis ST (Bekesi et al., 2016). Both of these instruments have significantly expanded our knowledge of the role of biomechanics in various corneal conditions, such as keratoconus (Caporossi et al., 2010; Elham et al., 2017; Henriquez et al., 2011; Pena-Garcia et al., 2016; Schweitzer et al., 2010; Shah & Laiquzzaman, 2009; Spoerl et al., 1998; Vinciguerra et al., 2016; Wollensak et al., 2003) and post-refractive surgery complications (Dawson et al., 2008; Dupps & Wilson, 2006; Frings et al., 2015; Kamiya et al., 2009), but there has been limited research into effects of corneal biomechanical changes in myopia. However, applying commercially available corneal biomechanics instruments for myopia research has several limitations, such as problems with interpretation of mechanical parameters and difficulty in mechanistic experiments using human subjects. Therefore, this study aimed to investigate: 1) identifying corneal biomechanical properties of highly myopic chicks, the most widely used animal model in experimental myopia research (Norton, 1999; Schaeffel & Feldkaemper, 2015; Troilo et al., 2019; Wallman et al., 1978), and 2) evaluating the applicability of stiffness coefficient measurement by a custom-made instrument with air-jet optical coherence tomography (Chao et al., 2013; Huang et al., 2009). Stiffness coefficient measurements were conducted while intraocular pressure was controlled since intraocular pressure is one of the contributing factors to corneal

biomechanics (Kling & Marcos, 2013; Lu et al., 2019). The result indicated that close associations existed between a reduced corneal stiffness coefficient and high myopia induced by form-deprivation.

Chapter 3: High Myopia Induced by Form Deprivation Alters Corneal Biomechanical Properties in Chicks.

In a previous chapter, corneal biomechanical properties measurements on experimental myopia animal models were successfully investigated. The result of reduced corneal stiffness coefficient in highly myopic chicks has not been previously reported and was also aligned with clinical research results (Altan et al., 2012; Hon et al., 2017; Lee et al., 2016; Plakitsi et al., 2011; Qiu et al., 2016; Shen et al., 2008; Wang et al., 2015). However, several technological limitations were also identified (possible measurement error caused by whole eye movement, corneal dehydration effect by air-jet, inflexible instrument setting, and the potential role of corneal biometric parameters on biomechanical properties calculation) (Kling & Marcos, 2013; Ko et al., 2013; Terai et al., 2012). Therefore, in this study, an improved instrument was developed and validated to accurately derive corneal biomechanical properties from highly myopic eyes (Wang et al., 2016). Enhancement Included: 1) reference surface detection (crystalline lens surface) to reduce confounding error caused by whole eye movement during corneal indentation (Ko et al., 2013); 2) indentation method altered from air-jet to probe-contact-based, and 3) calculating corneal tangent modulus to consider the effect of corneal thickness and curvature changes on biomechanical properties. Validation tests of OCT-indentation probe system showed satisfactory results for research purposes. In form-deprivation treated highly myopic chicks, reduced corneal biomechanical properties (both corneal tangent modulus and stiffness coefficient) and altered corneal biometrics (steeper and thinner corneas) were

observed. Additionally, a significant correlation with ocular refractive power and biometric parameters was observed. These results indicate a potential association between high myopia development and anterior ocular segments, specifically the cornea.

Chapter 4: Corneal proteome and differentially expressed corneal proteins in highly myopic chicks using a label-free SWATH-MS quantification approach.

High myopia development by form-deprivation treatment in chicks showed significant corneal structural and biomechanical alterations, specifically thinning, steepening, and softening (Kang et al., 2018). These trends are interesting because similar results have been reported from human myopes, as well as from conjunctival ocular tissue, sclera, from both human and animal myopes (Avetisov et al., 1983; Gottlieb et al., 1990; Phillips et al., 2000; Siegwart & Norton, 1999). Extensive investigations have revealed that a series of molecular actions occurred to remodel collagen structure (Gentle et al., 2003; Norton & Rada, 1995; Rada & Brenza, 1995; Rada & Matthews, 1994; Rada et al., 1999) and extracellular matrix (Norton & Rada, 1995; Rada et al., 2000; Rada & Matthews, 1994; Rada et al., 2000), resulting in altered biomechanical properties and thickness (Gottlieb et al., 1990; Phillips et al., 2000; Siegwart & Norton, 1999), ultimately allowing for accelerated ocular expansion during myopia development(Harper & Summers, 2015; McBrien et al., 2009; Moring et al., 2007; Rada & Hollaway, 2011). There is a lack of supporting evidence that changes in the sclera and cornea can be explained by the same mechanism, but it is plausible to assume their close relationship because of similarities in their collagen-dominated structural compositions and anatomical connections. Unlike the sclera, whose role in myopia development is already well recognized (Harper & Summers, 2015; McBrien et al., 2009; Metlapally & Wildsoet, 2015; Rada et al., 2006), the role of the cornea remains elusive. This chapter describes the molecular basis of corneal changes in highly myopic eyes by applying

a proteomic approach to fill the current research gap. Recently, proteomics has gained growing attention because of a better understanding of disease etiology by looking directly into the cellular expression of functional proteins (Chambers et al., 2000; Hanash, 2003; Xiao et al., 2005). A hybrid quadrupole time-of-flight mass spectrometer (MS) (Andrews et al., 2011; Shan et al., 2018) was applied to explore the chicken corneal proteome and the protein pool was extended by utilizing independent data acquisition analysis with the offline high-pH reversed-phase peptide fractionation technique (Scientific, 2016). This first of its kind comprehensive chicken corneal proteome was further used in the sequential windowed acquisition of all theoretical mass spectra (SWATH-MS) analysis (Gillet et al., 2012; Shan et al., 2018) to screen differentially expressed proteins in highly myopic chicken corneas. The result indicated that molecular activities might be involved in the regulation of corneal biometrics/biomechanics during high myopia progression.

Chapter 2

Corneal Stiffness Coefficient of Highly Myopic Chicks Measured by an Air-jet Optical Coherence Tomography System

Abstract

Purpose: To determine whether corneal stiffness coefficient differed between normal and highly myopic eyes in the chick model of myopia.

Methods: Starting on day 5 post-hatching, the right eyes of 13 chicks were covered with translucent occluders for 7 days to induce form-deprivation myopia (FDM). At the end of the treatment period, spherical equivalent (SE) refractive error was measured under anesthesia by Hartinger refractometer. Chicks were then euthanized, and their intraocular pressures (IOP) were controlled by intravitreal cannulation. *In-situ* corneal stiffness coefficient (CS) was measured by a custom-made air-jet optical coherence tomography system (AJ-OCT) while IOP was controlled at 0, 5, and 10 mmHg. At each IOP level, three sets of 5-cycled ascending-descending air pressure were applied on the corneal surface. Corneal deformation images in response to air pressure were analyzed by a custom MATLAB algorithm,

generating the slope of the load-deformation curve followed by cross-correlation analysis to derive CS.

Results: Compared to the fellow untreated eyes, form-deprived eyes developed significant myopia (mean±SEM: SE= –24.85 ± 1.80 D vs. –1.42 ± 0.54 D; paired *t*-test, $p<0.001$) and exhibited reduced CS (mixed two-way ANOVA, $p<0.001$). No significant difference was found between fellow untreated eyes and both eyes of age-matched control chicks (Kruskal-Wallis H test, $p>0.05$). Expressing the corneal stiffness as a percentage of interocular difference in CS [100 %*(treated eye – fellow eye)/fellow eye], nine birds (77 %) had at least 12 % reduction in CS. When data from treated eyes and right eyes of age-matched control chicks were pooled for Pearson's correlation analyses, SE was moderately correlated with CS at IOP 0 mmHg ($r= +0.66$, $p<0.01$).

Conclusions: Form-deprivation induced high myopia and reduced CS. The correlation between SE and CS suggests that the changes occurring in the corneal biomechanical properties may be related to those occurring in the myopic sclera as previously reported in tree shrews.

Introduction

The cornea is a distensible, extracellular matrix-rich tissue that provides nearly 60% of the human eye's focusing power. Anatomically, the cornea merges with the posterior coat of the eye, the sclera, and the two tissues share many structural properties. The cornea has long been a primary target for surgical intervention and refractive correction, and cumulative evidence using different approaches has indicated the importance of understanding corneal biomechanical properties in the diagnosis and management of intervention involving corneal tissue (Kling & Hafezi, 2017; Pinero & Alcon, 2015). However, despite extensive studies on the role of corneal biomechanics – in the diagnosis (Elham et al., 2017; Pena-Garcia et al., 2016; Schweitzer et al., 2010; Shah & Laiquzzaman, 2009; Vinciguerra et al., 2016) and treatment (Caporossi et al., 2010; Henriquez et al., 2011; Spoerl et al., 1998; Wollensak et al., 2003) of keratoconus, in deriving accurate intraocular pressure (IOP) measurements (Hamilton & Pye, 2008; Liu & Roberts, 2005; Medeiros & Weinreb, 2006), and in evaluating corneal stability after refractive surgeries (Dawson et al., 2008; Dupps & Wilson, 2006; Frings et al., 2015; Kamiya et al., 2009) – comparatively little is known regarding whether the biomechanical properties of the cornea are altered in the development of high myopia. This contrasts with the wealth of information that has been obtained about the structural and biomechanical changes occurring in the sclera of eyes developing high myopia, which include reduced thickness (Avetisov et al., 1983; Curtin, 1985; Curtin et al., 1979; McBrien et al., 2001), tissue loss (McBrien et al.,

2001; McBrien & Gentle, 2003; McBrien et al., 2000), altered distribution of collagen fibers of varying diameters (Curtin et al., 1979; Curtin & Teng, 1958; McBrien et al., 2001), collagen degradation (Avetisov et al., 1983; Guggenheim & McBrien, 1996; Norton & Rada, 1995; Rada & Brenza, 1995), and modification of biomechanical properties (Avetisov et al., 1983; Phillips et al., 2000; Phillips & McBrien, 1995; Siegwart & Norton, 1999; Wang et al., 2008).

The precise shape of the cornea is governed by the biomechanical properties of its thick, well organized, highly structured stromal layer. Little is known about whether the altered structure and ultrastructure of the sclera (Harper & Summers, 2015; McBrien et al., 2001) in myopic eyes are accompanied by comparable changes in the cornea's biomechanical properties. Nevertheless, there is ample evidence indicating that the corneal *structure* is altered in myopic eyes. First, human myopia is associated with an increased corneal curvature and reduced thickness (Carney et al., 1997; Chang et al., 2001; Grosvenor & Goss, 1998; Leung et al., 2013; Touzeau et al., 2003) (however, see also contradictory findings (Cho & Lam, 1999; Fam et al., 2006; Li et al., 2016)). Second, in animal models, many experimental treatments – form deprivation (FD), optical defocus, constant lighting, spectral composition of the light source, and high illuminant lighting conditions – alter not only the eye's axial dimensions but also the anterior corneal shape (Cohen et al., 2008; Kee & Deng, 2008; Kee et al., 2005; Li et al., 1995; Rucker et al., 2015). These results indicate the involvement of the anterior segment during refractive-error development, and they highlight the importance of understanding whether changes in the biomechanical properties of the cornea underlie its altered shape in myopic eyes.

A high degree of interest in corneal biomechanics has driven the development of multiple measuring devices using innovative approaches. Devices for measuring corneal biomechanical properties have evolved from conventional stress-strain measuring instruments (i.e., strip extensometry (Hoeltzel et al., 1992; Jue & Maurice, 1986; Nyquist, 1968; Shin et al., 1997; Wollensak et al., 2003)) and inflation tests (Boyce et al., 2008; Elsheikh et al., 2008; Smolek, 1993; Woo et al., 1972) to commercially available air-puff systems (i.e., Ocular Response Analyzer, ORA; Reichert, Depew, New York (Luce, 2005); and Corneal Visualization Scheimpflug imaging, Corvis ST; Oculus, Wetzlar, Germany (Bekesi et al., 2016)). Although the strip extensometry is the gold standard in mechanical engineering, measuring corneal biomechanics using this technique is difficult, because the cornea is anisotropic, highly curved, and hydrated; furthermore, measurement along a single axis may not represent corneal biomechanics as a whole, and stretching the cornea during the measurement may disrupt the distribution of its collagen fibrils (Roberts & Liu, 2017; Ruberti et al., 2011). Alternatively, inflation test, a powerful method that can evaluate regional ex-vivo ocular biomechanics by mapping strain distribution as a function of the inflation pressure (IOP), has been widely adopted and provided better understanding of biomechanical characteristics under a wide variety of physiological conditions (Ma et al., 2019; Pavlatos et al., 2018; Whitford et al., 2016). However, determining material properties, such as Young's modulus, is more complicated than strip extensometry, and also in-vivo measurements will be challenging (Ruberti et al., 2011). By contrast, the air-puff systems (i.e., ORA and Corvis ST) are emerging non-contact/non-invasive techniques that measure *in-vivo* corneal biomechanical

properties and provide multiple useful clinical parameters. Nevertheless, air-puff systems having principles of deforming cornea and measuring by image analysis can be confounded by multiple factors, such as corneal geometries and optical distortions (Long et al., 2015; Roberts & Liu, 2017; Rosales & Marcos, 2009). This study applied a system with air-puff to inflate the cornea but adopted a different imaging technique (optical coherence tomography; OCT). OCT was introduced in 1991 (Huang et al., 1991) with the use of an interferometry-based imaging method, it is a widely used technology in ophthalmology nowadays. There were several successful attempts to integrate OCT to air-puff system for quantifying corneal biomechanics in humans (Alonso-Caneiro et al., 2011; Maczynska et al., 2019); however, since these systems were built for human eyes, its applicability to quantifying corneal biomechanical properties in small animals' eyes is limited. The custom-made OCT air-jet system (Chao et al., 2013; Huang et al., 2009) used in this study, therefore, was designed for the small animal, chicks, by miniaturizing the nozzle of AJ-OCT to calculate corneal stiffness coefficient (CS) as the change in corneal deformation depth under controlled air pressure.

Using the custom-made AJ-OCT, this study aimed to explore: 1) applicability of AJ-OCT system for CS measurements on chicks, and 2) identifying CS changes in highly myopic chicks while intraocular pressure was controlled since it was one of the influential factors for corneal biomechanics (Kling & Marcos, 2013; Lu, Chong, Leung, & Lam, 2019).

Methods

Animal Husbandry

Nineteen White Leghorn chicks (*Gallus gallus domesticus*) were hatched and raised in the Centralized Animal Facility of The Hong Kong Polytechnic University. The animal facilities had an average luminance of 150 lux at the chicks' eye level (12h:12h light-dark cycle) with temperature-controlled at 25 °C. Food and water were provided *ad libitum*. All experiments were conducted in accordance with the ARVO Statement for the Use of Animals in Ophthalmic and Vision Research, and the protocols were approved by the Animal Subject Experiment Subcommittee of the Hong Kong Polytechnic University (ASESC 14-15/28).

Treatment

To induce form-deprivation myopia (FDM), thirteen chicks underwent visual manipulation monocularly (right eye) by diffuser for a week from day 5 post-hatching. The diffusers were produced (Figure 2.1) by stamping a heated metal ball on a translucent polystyrene sheet (thickness= 0.5 mm, diameter= 12 mm, average light transmission= 30 %) and glued to a Velcro ring (Chu et al., 2012). They were attached to the matching Velcro rings glued around the feathers of the chick's orbit and removed daily for cleansing using cotton buds with 70 % isopropyl alcohol. Their left eyes served as untreated controls. Another 6 age-matched chicks without any visual manipulations served as a normal group.

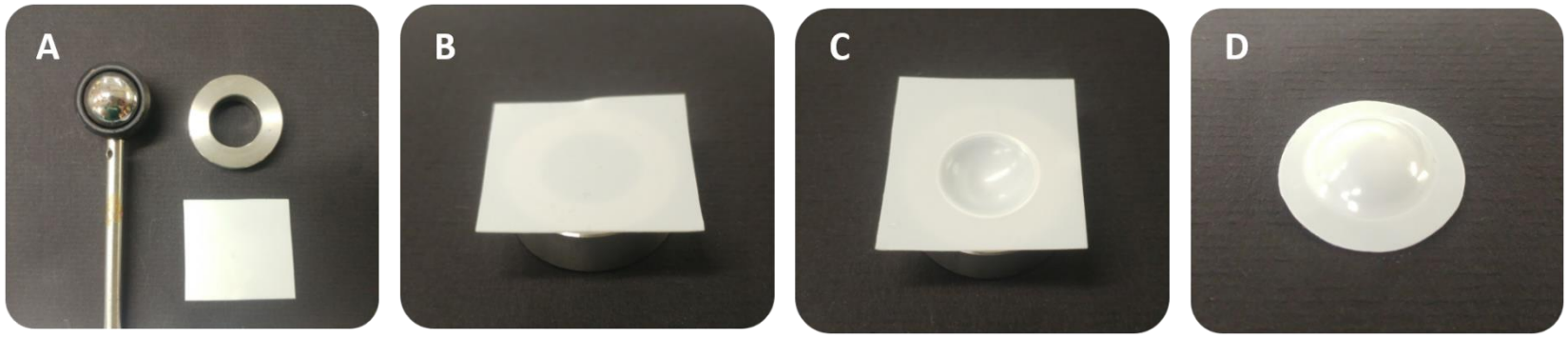

Figure 2.1. Translucent diffuser manufacturing procedures. (A) A metal ball, a platform with a hole, and a piece of translucent polystyrene sheet. (B) Placing the sheet on the platform. (C) Stamping the heated metal ball on the sheet. (D) A diffuser after trimming the edge.

Refractometry

Refractive errors were measured by a modified Hartinger coincidence refractometer (Figure 2.2A), an instrument that has been validated to refract chicks eyes with good repeatability (Chu et al., 2012; Kee & Deng, 2008; Wallman & Adams, 1987) (Model 110, Carl Zeiss Meditec, Germany). Refractometry was performed at the end of the 1-week treatment period (P12). To prevent corneal and lenticular accommodation from confounding the measurements in chicks (Chu et al., 2014; Glasser et al., 1995; Schaeffel & Howland, 1987), Isoflurane inhalation anesthesia (1-1.5 % with oxygen flow rate of 1.5 L/min) was used as a means of cycloplegia (Wallman & Adams, 1987) prior to refraction. While chicks were anesthetized, palpebral commissures were horizontally aligned and a custom-made speculum was used to gently open the eyelids. The stainless steel speculum was custom made, designed to deliver minimal tension to eyelids with negligible refractive power changes (Kee & Deng, 2008; Schmid & Wildsoet, 1997). To ensure that the measurements were performed along the pupillary axis, a ring of 39 LEDs concentric with the refractometer's optical axis was projected on the chick's cornea to align with the center of pupil (Figure 2.2B). Three repeated measurements were made per eye and the average refractive error was calculated using power vector analyses (Thibos et al., 1997). The refractive status in this study was expressed as spherical equivalent (SE). All measurements were conducted at the same time of the day (10:00-11:00 a.m.) to avoid the potential variation in refraction due to circadian rhythm (Campbell et al., 2012; Johnson et al., 2004).

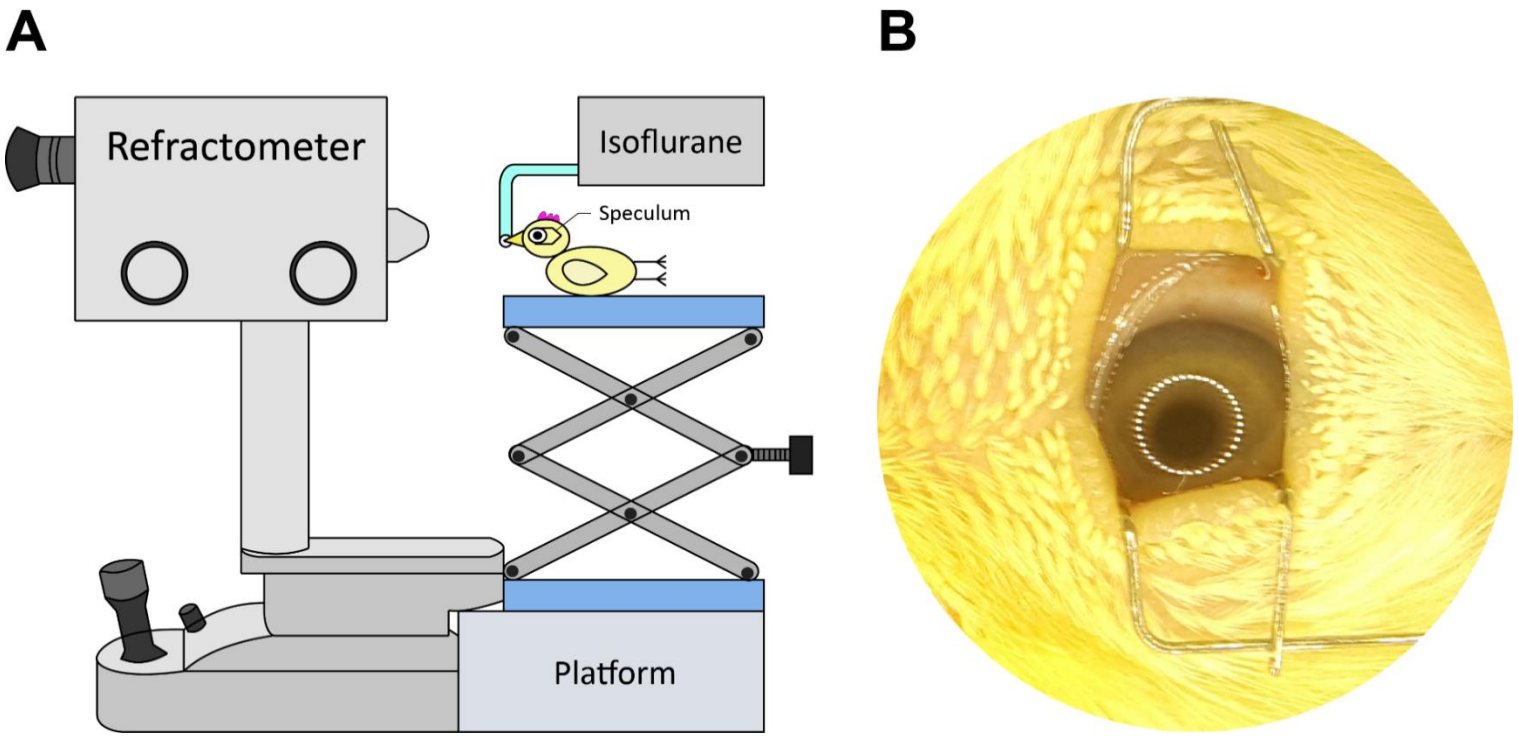

Figure 2.2. (A) Schematic diagram of a refractometer and refractive error measurements. (B) Circle-shaped reflected light dots around pupil are used to align the pupillary axis with optical axis of the refractometer.

Air-jet Optical Coherence Tomography (AJ-OCT)

A customized air-jet optical coherence tomography system (AJ-OCT) (Chao et al., 2013; Huang et al., 2009) was used to measure *in-situ* corneal stiffness coefficient (CS). The system consisted of a custom-made fiber optic-based time-domain OCT, an air-jet probe, and data acquisition module parts (Figure 2.3). The optical beam from the probe was generated by a 1310 nm superluminescent diode (SLD) light source (Dense-Light, DL-CS3055 A, Singapore) with an output power of 5 mW, and a 3-dB bandwidth of 50 nm. A 5-mm diameter and 2-mm length orifice was connected to the air-jet bubbler to deliver uniform air-jet to the corneal surface. The air pressure (1.06 to 1.14 N) was controlled automatically by an air regulator (IR1000-01, SMC Corporation, Japan), and was monitored by a calibrated pressure sensor (PMP 1400, General Electric Company, U.S.) installed behind the bubbler. To detect the central cornea where the indentation mainly occurred, a visible red-light beam with an OCT A-scan mode with a rate of approximately 3.1 Hz was used. A custom-written Labview (National Instrument, U.S.) algorithm was used for collecting the OCT signals and air pressures. These two data were cross-correlated using a custom-made MATLAB algorithm (MATLAB R2007b, Version 7.5.0, The MathWorks, U.S.) to extract the corneal displacement (in units, mm) under the corresponding air pressures (in units, N). The corneal stiffness coefficient (in units, N/mm) was then produced from a regression line of the displacement curve and air pressures. This corneal stiffness coefficient was considered as the stiffness of the cornea under investigation.

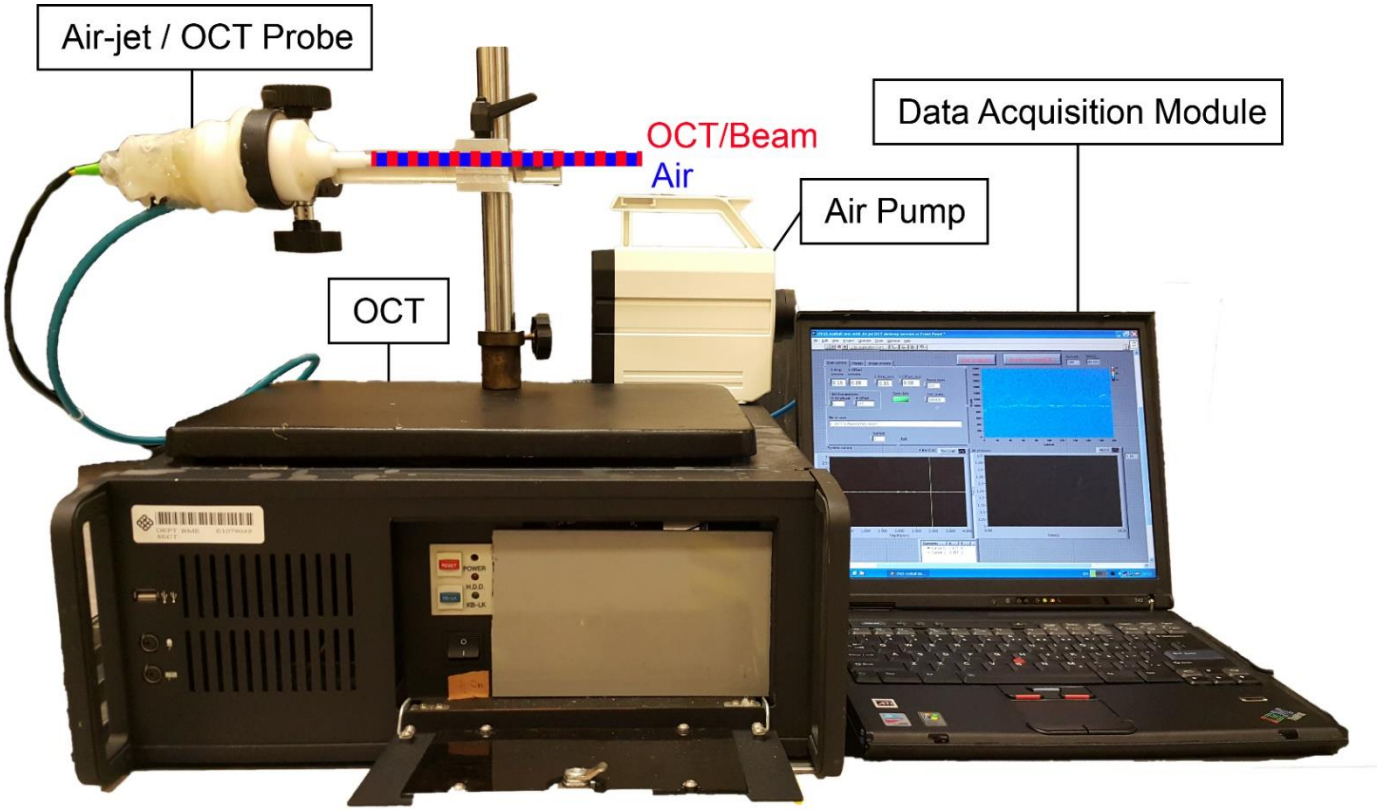

Figure 2.3. The customized air-jet optical coherence tomography (AJ-OCT) imaging system. The directions of the air-jet and OCT probe were aligned (blue solid line and red dotted line, respectively).

Corneal Stiffness Coefficient (CS) Measurements

Because preliminary observation showed that the nictitating membrane of alert chicks showed instantaneous reflexive response when an air jet was applied on the cornea, chicks were euthanized by carbon dioxide asphyxiation for *in-situ* CS measurements. Chicks were moved to a custom-made platform and their heads were affixed while their eyelids were gently opened with a speculum. To perform *in-situ* CS measurements under controlled intraocular pressures (IOP), a 3-way stopcock was used to connect a custom-made hydrostatic manometer, a digital pressure transducer (BP transducer, Harvard Apparatus, U.S.), and a needle (see Figure 2.4). A winged infusion set (Terumo, Belgium) with a 30 G needle (BD Precise Glide, U.S.) was prepared to cannulate the eye through the superior sclera and fixed in the vitreous chamber. This set-up allowed the control of IOP from 0-50 mmHg without leakage of aqueous humor from the site of cannulation, ensuring that *in-situ* CS measurements were performed under a stable condition. The agreement of the IOP measurements between the two instruments (the manometer and digital pressure transducer) was determined by recording the heights of the reservoir filled with 0.9 % sodium chloride (Sigma-Aldrich, Germany) when the pressure transducer read 0, 10, 20, 30, 40, and 50 mmHg. Recorded heights were then transformed to pressure using the equation:

$$p = \rho \, g \, h \tag{2.1}$$

where p is pressure, ρ is density of 0.9 % saline (1.0046), g is acceleration of gravity (9.81 m/s^2), and h is height (in units, m). Figure 2.5A showed the linear regression fit of the IOPs measured by the two instruments (y= 0.972x + 1.301, r^2=

0.999), this formula was then used to convert the pressure transducer's readings to intended IOP levels when measuring the *in-situ* CS.

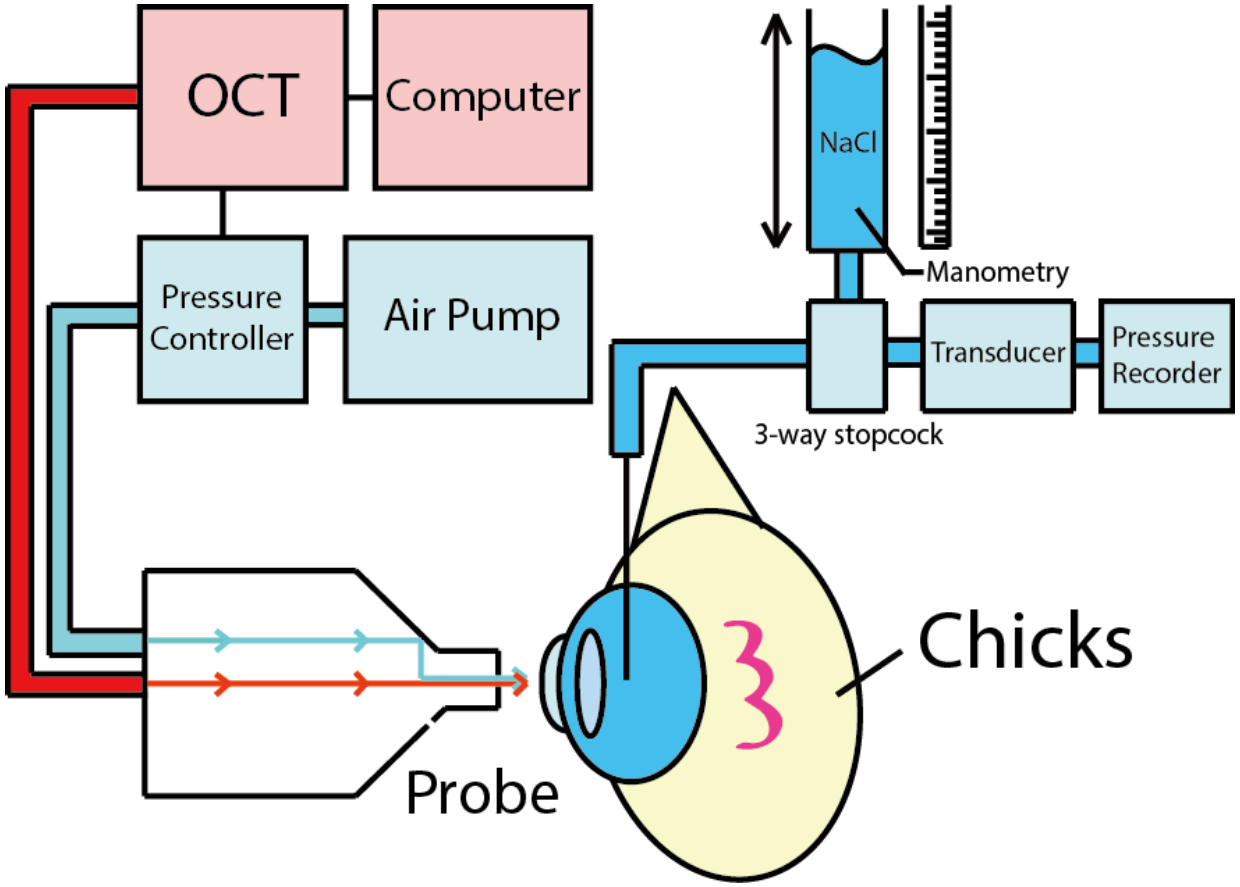

Figure 2.4. The schematic diagram of corneal stiffness coefficient measurements.

Bland-Altman plot in Figure 2.5B showed a good agreement between two methods (mean difference= –0.246, 95 % limits of agreement= –1.331 to 0.841). To determine the impacts of IOP on CS measurements, we set the IOP levels at 0, 5, and 10 mmHg. Note that these IOP levels were lower than the physiological IOP (about 12 to 22 mmHg) in alert chicks (Nickla et al., 1998). Although we had tried to measure CS at IOP >10 mmHg, the corneal deformation was undetectable with the default air pressure (1.06 to 1.14 N) in the current setting. Because the primary goal of this study was to determine the effects of highly myopic eye growth on corneal stiffness coefficient under controlled IOPs, we only measured CS at these three IOP levels. At each IOP level, an air-jet probe was first aligned with the central cornea by positioning a visible red-light beam on the central cornea. When OCT A-scan signals of the anterior cornea, posterior cornea, and anterior crystalline lens reached maximum amplitudes (Figure 2.6A vs. 6B), three sets of CS measurements were obtained consecutively, without re-alignment. A drop of 0.9 % saline solution was instilled to moisturize the eye before each CS measurement. Each CS measurement consisted of 5 cycles of loading and unloading air pressures varied continuously from 1.06 to 1.14 N. The collected data were analyzed by a custom-made MATLAB algorithm (see “AJ-OCT” above for detail). The sequence of CS measurements for the two eyes was randomized, and measurements for each eye were completed within 10 minutes.

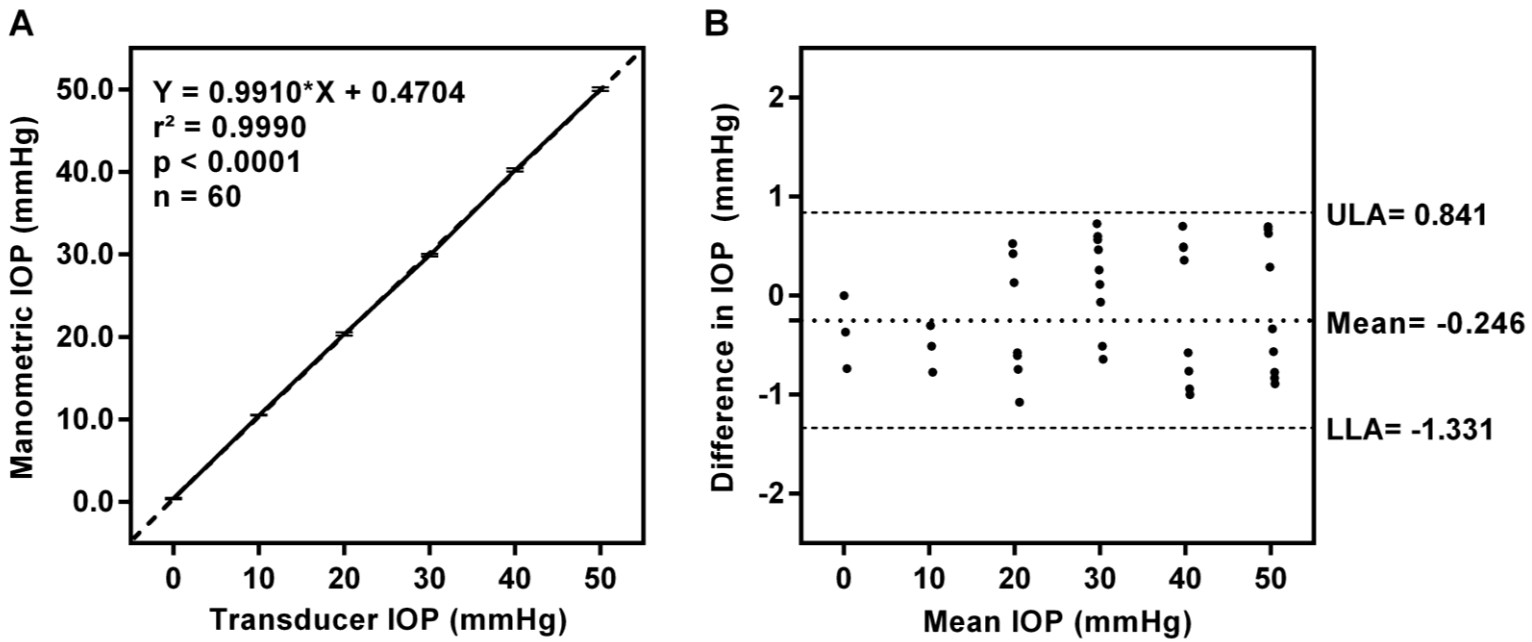

Figure 2.5. Validation of the IOP controller. (A) Linear regression fit of IOPs measured by a hydrostatic manometer and the pressure transducer. (B) Bland-Altman plot of the IOP readings calculated from a hydrostatic manometer and those collected from the pressure transducer. The mean difference and 95 % limits of agreement are represented by a dotted line and dashed lines, respectively. ULA, upper limit agreement; LLA, lower limit agreement. The symbols represent mean±SEM.

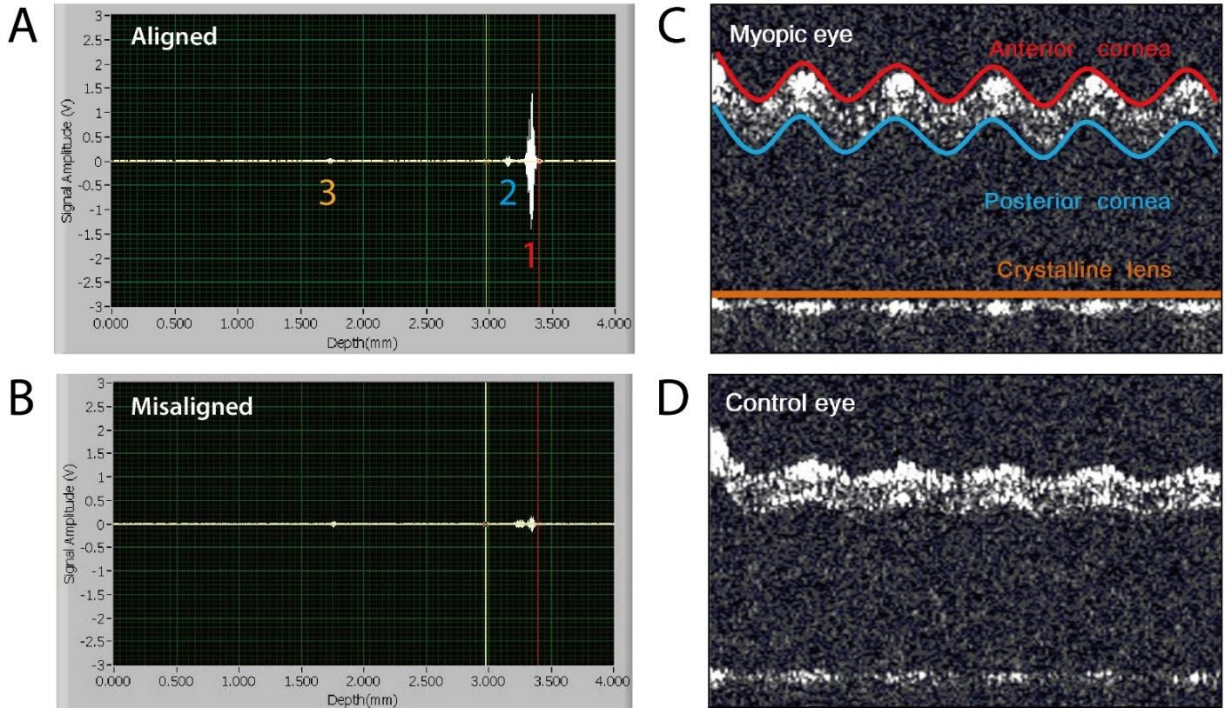

Figure 2.6. (A) Maximal OCT signals acquired with proper alignment, signals identified as anterior corneal ("1"), posterior corneal ("2"), and crystalline lens surfaces ("3") (B) Poor alignment with minimal signals. (C&D) Images acquired from a myopic eye (C) and the fellow control eye (D) showing the changes in the locations of the three surfaces over time. Note that with the same five cycles of air jets, the myopic cornea showed a bigger magnitude of change, indicating a softer cornea.

Statistical Analyses

IBM SPSS (version 21.0.0, IBM, U.S.) or GraphPad Prism (Version 6.01, GraphPad Software, U.S.) were used for statistical analysis. Shapiro-Wilk test was first conducted to verify the normality of data. Based on this, either paired *t*-test or Wilcoxon signed-rank test was used to test the difference in refractive status between the treated (or right) and contralateral (or left) eyes. A mixed two-way ANOVA with Bonferroni-corrected *post-hoc* tests was performed to test the effect of myopia development and IOP on corneal stiffness coefficient when data passed Levene's test and Mauchly's test for homogeneity of variance and sphericity of variance, respectively. If sphericity was violated, either Greenhouse-Geisser (if $\varepsilon>0.75$) or Huynh-Feldt (if $\varepsilon<0.75$) corrections were applied. Intergroup differences in CS were tested by independent *t*-tests. Correlations between CS and IOP were tested at each IOP level using Pearson's correlation analysis. The significance level for all tests was set at 95 %.

Results

Refractive Development

As shown in Figure 2.7A, wearing diffusers for 7 days induced a significantly higher degree of myopia in treated eyes compared to fellow eyes (mean±SEM: SE= –24.85 ± 1.80 D vs. –1.42 ± 0.54 D; paired-*t*-test, p<0.001), whereas the spherical-equivalent refractive error in the right and left eyes were not statistically different in the normal group (mean±SEM: SE= –1.56 ± 0.49 D vs. –1.82 ± 0.40 D; paired-*t*-test, p= 0.63). Compared to the normal group, the treated group also showed a significantly higher magnitude of interocular difference in SE (Figure 2.7B, mean±SEM: SE= –23.43 ± 1.76 D vs. 0.25 ± 0.49 D; independent-*t*-test, p<0.001).

Corneal Biomechanical Changes

The myopic eyes had significantly reduced CS compared to contralateral fellow eyes (mixed two-way ANOVA; main effect of myopia treatment: F (1, 24) = 17.13, p<0.001). As shown in Figure 2.8A, a decreased CS was observed at all IOP levels (paired *t*-test, all p<0.05). Increasing IOP levels also increased CS in both treated and contralateral eyes (main effect of IOP increment: F (1.60, 38.52) = 54.02, p<0.001). Bonferroni corrected *post-hoc* tests showed that the CS in treated eyes at 10mmHg was significantly higher than CSs at both 0 and 5 mmHg (both p<0.001). Also, CS in treated eyes measured under 0 and 5 mmHg were not statistically different (p= 0.055). CS of the fellow untreated eyes had no such difference from

those of right or left eyes in the age-matched normal chicks at all IOPs (Kruskal-Wallis H test, $p>0.05$). There was no interaction effect between visual manipulation and IOP (F (1.60, 38.52)= 0.74, p= 0.89). When CS was expressed as the percentage of interocular difference [(treated eye – fellow eye)/fellow eye*100 %], ninety-two percent of treated eyes showed a reduction in CS at 0 mmHg (range= –9.60 % to –49.76 %), while 77 % (range= –5.75 % to –60.27 %) and 85 % (range= –5.86 % to –74.52 %) had reduced CS at 5 mmHg and 10 mmHg respectively (Figure 2.8B). When data from treated eyes and right eyes of age-matched normal chicks were pooled for correlation analyses (Figure 2.9), SE were moderately correlated with CS when IOP was set at 0 mmHg (r= +0.66, $p<0.01$), but not at 5 mmHg (r= +0.32, p= 0.17) or 10 mmHg (r= +0.08, p= 0.71).

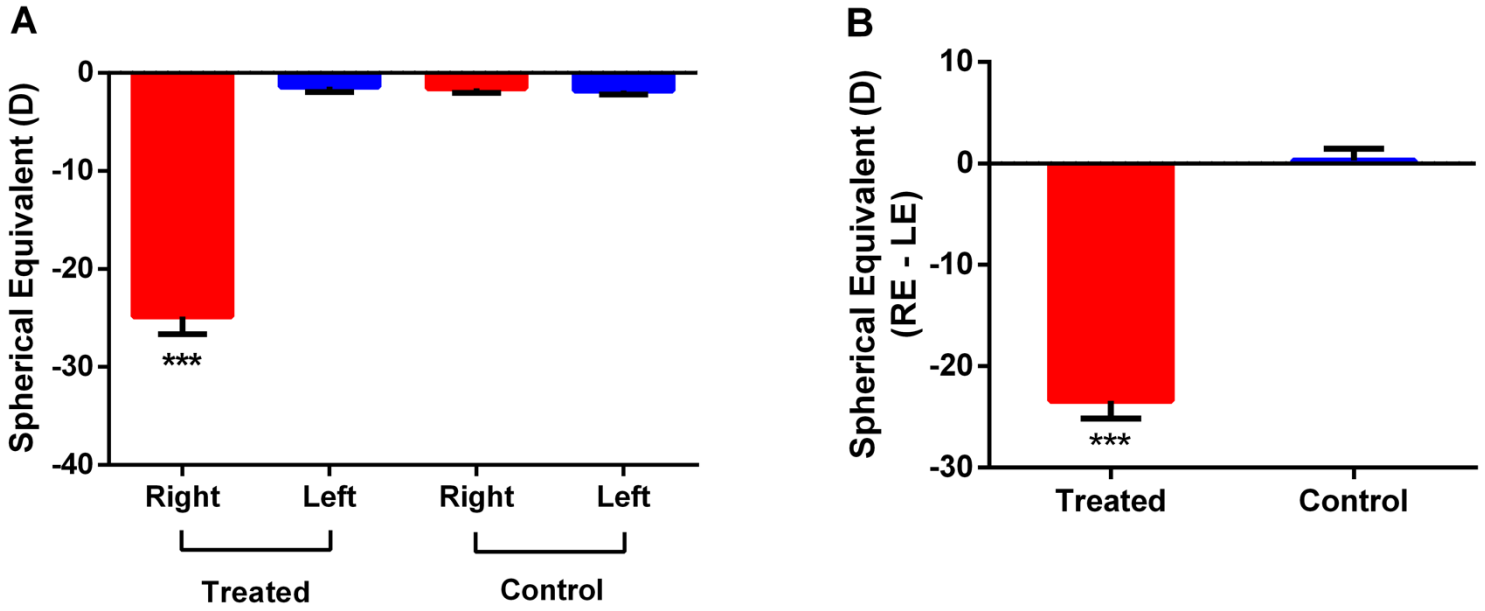

Figure 2.7. (A) After 7 days of form deprivation (P5-P12), treated/right eye in the treated group developed significant myopia compared to fellow/left eye. No difference in refractive status was found in the fellow eyes of the treatment and control groups. (B) A significant difference ($p<0.001$***) was found between the treated and control groups in terms of interocular differences (treated/right - fellow/left) in spherical-equivalent refractive errors. Bars represent mean±SEM.

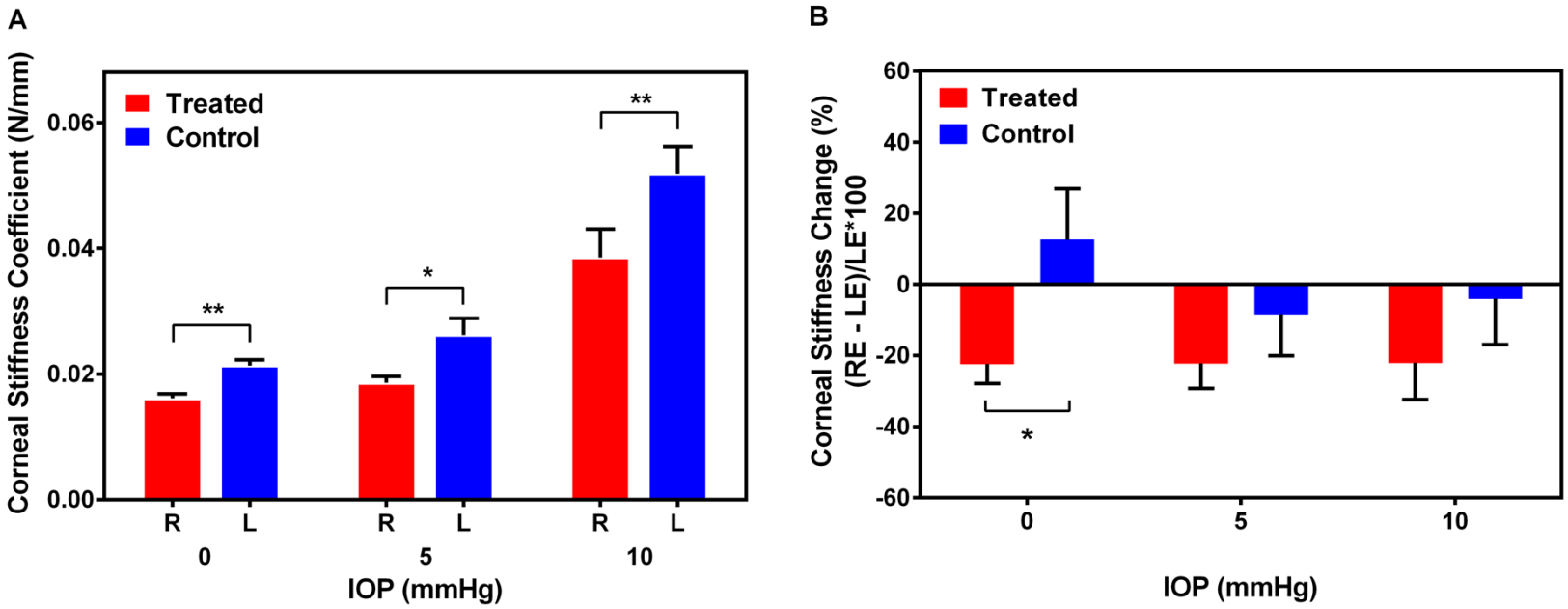

Figure 2.8. (A) Corneal stiffness coefficient (CS) measured under different IOPs at P12 in the treated group. Form-deprived highly myopic eyes had a significant decrease in CS compared to contralateral control eyes measured at all IOP levels. (B) A significant interocular difference in CS [(treated eye – fellow eye)/fellow eye*100 %] was found under 0 mmHg between treated and control groups. Mann-Whitney U test, *p<0.05. Bars represent mean±SEM.

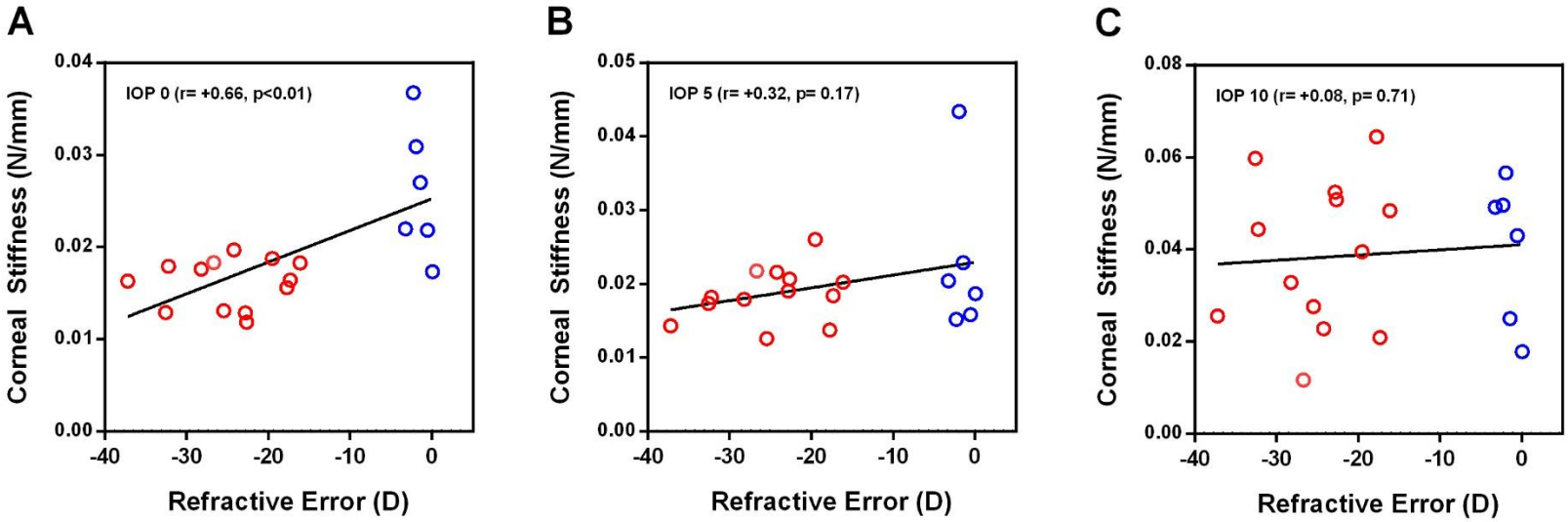

Figure 2.9. Pearson correlations between spherical-equivalent refractive error and corneal stiffness. Red and blue symbols represent treated and normal chicks respectively.

Discussion

It was found that there was a significant reduction in CS in experimentally induced highly myopic eyes. At all tested IOPs, myopic corneas were more deformed compared to their fellow eyes; in other words, they became softer (less stiff). CS was positively correlated with SE when IOP was controlled at 0 mmHg ($r = +0.66$, $p<0.01$), indicating that a more myopic eye was associated with a softer cornea. These results are in agreement with most studies using ORA in the human myopic cornea (Bueno-Gimeno et al., 2014; Chang et al., 2010; Jiang et al., 2011; Shen et al., 2008; Song et al., 2008; Wong & Lam, 2015), although some contradictory results were also reported (Lim et al., 2008; Radhakrishnan et al., 2012). While ORA has generated interest in myopia research, the use of corneal hysteresis (CH) in characterizing the corneal biochemical properties may have several limitations: First, it is unclear how CH is related to corneal stiffness/rigidity, a biomechanical property more extensively studied and described using Young's modulus. Although many researchers have used CH and corneal stiffness interchangeably, these two terms are not the same: CH represents the energy dissipation during the loading-unloading cycle, while stiffness refers to the resistance to deformation in response to a force. The fact that only negligible changes in CH were found in stiffened corneas by corneal-crosslinking (CXL) (Gkika et al., 2012; Goldich et al., 2009; Sedaghat et al., 2010) also indicates the need to carefully interpret CH as a biomechanical property. Second, CH might be sensitive to changes in IOP (Kaushik et al., 2012; Touboul et al., 2008). Since highly myopic

subjects are known to have altered IOP (David et al., 1985; Detry-Morel, 2011; Mitchell et al., 1999; Wong et al., 2003), it is necessary to consider the impact of IOP when measuring CH. In this respect, the finding of reduced CS under controlled IOP conditions in highly myopic eyes provides strong evidence that the biomechanical properties of the eye's anterior coat can be influenced by myopia development.

Similar to the sclera, the cornea is comprised of collagenous extracellular matrix and proteoglycans (Daxer et al., 1998). Previous studies on myopic sclera of tree shrews indicated that the scleral biomechanical changes were attributable to a thinned fibrous sclera (McBrien et al., 2001; Phillips et al., 2000; Phillips & McBrien, 1995) probably due to a combination of the loss of collagen tissue and proteoglycans (McBrien et al., 1999; McBrien et al., 2000; Norton & Rada, 1995), the reduction of type1 collagen (Gentle et al., 2003; Gentle et al., 2002; Siegwart & Norton, 2002), and the up-regulation of active collagen-degrading enzymes (Guggenheim & McBrien, 1996; Rada & Brenza, 1995). In chicks, changes in the fibrous sclera resemble those reported in tree shrews: reduced scleral thickness (Gottlieb et al., 1990; Marzani & Wallman, 1997); decreased proteoglycan synthesis (Marzani & Wallman, 1997; Rada et al., 1998); and increased gelatinase activities (Rada et al., 1999). Whether the cornea also undergoes similar structural and molecular changes during abnormal ametropic development remains unclear, but it is a question of clinical significance. Further studies are needed to determine the influence of abnormal ametropic development on corneal biomechanical properties. It is equally important to understand whether the changes in the cornea are a passive by-product of abnormal eye growth or is actively regulated by

a signaling pathway.

While these results provide strong evidence of significant corneal changes in highly myopic eyes, there are several methodological limitations that should be improved for a better understanding of the role of corneal biomechanics. First, the current AJ-OCT system ignored the slight ocular displacement due to air-jet indentation. It was observed that some eyeballs were displaced slightly backward by the air jet during indentation, probably due to the combination of a stiffer cornea and/or the increased IOPs. This backward ocular displacement could confound the CS measurements, which was supported by larger standard deviations of CS measured at 5 and 10 mmHg. This limitation may be overcome by determining the corneal deformation using a reference plane from an internal ocular surface, such as anterior/posterior surface of the crystalline lens. Second, the current AJ-OCT system deformed the corneal surface with force varying from 1.06 to 1.14 N. This range did not seem to work for a stiffer cornea or when the IOP was higher than 5 mmHg; consequently, the shallow indentation might be difficult to detect during image analysis, leading to poor repeatability. This technical limitation also restricts the application of this system for *in-vivo* corneal biomechanical measurements in chicks under normal physiological IOP range (12 to 22 mmHg) (Nickla et al., 1998). Third, corneal dehydration can be a critical issue when applying the air-jet based system on euthanized chicks. Although we applied saline to moisturize the cornea before each measurement, it was obvious that significant corneal dehydration occurred after 5 cycles of air puffs. The cornea primarily consists of water (about 80 %) and its hydration state could significantly affect corneal biomechanical properties (Hatami-Marbini, 2014; Hatami-Marbini &

Etebu, 2013; Hennighausen et al., 1998; Kling & Marcos, 2013); thus, an alternative method without using air puffs or reducing the measurement cycle may improve the measurement. Fourth, a motor-driven IOP manipulator is needed to replace the manometer. In some cases, apparently erroneous IOPs (lower than expected) were noted even after extended time was given for the manometer to achieve equilibrium after cannulation. Lastly, the corneal biomechanical properties in this study did not take into account the potential impacts of corneal biometric parameters. As previously reported, myopia development in chicks induced noticeable corneal structural changes including altered shape (astigmatism) (Irving et al., 1992; Kee & Deng, 2008) and curvature (Gottlieb et al., 1987; Troilo et al., 1995). Thus, whether the reduced CS found in myopic chicks was confounded by altered corneal parameters needs further confirmation.

In summary, a significant reduction in corneal stiffness was observed in highly myopic chicks. However, further investigation with improved methodology is needed to confirm this important finding.

Chapter 3

High Myopia Induced by Form Deprivation Alters Corneal Biomechanical Properties in Chicks.

Abstract

Purpose: To investigate whether the development of high myopia has an impact on corneal biomechanical properties in relation to other biometric parameters**.**

Methods: Right eyes of twelve chicks were monocularly occluded from day 5 to 12 to induce form-deprivation (FD) myopia, while four age-matched chicks served as a normal control group. At the end of treatment, the corneal radius of curvature, ocular axial dimensions, and spherical-equivalent refractive error were measured by videokeratography, A-scan ultrasonography, and Hartinger refractometer, respectively. After chicks were sacrificed, a custom-made optical-coherence-tomography-indentation probe system was applied to measure *in-situ* corneal tangent modulus (TM) and stiffness coefficient (CS), while maintaining intraocular pressure (IOP) at three levels (5, 15, and 25 mmHg), which cover the physiological IOP range. For data analysis, MATLAB algorithm integrated with a cross-correlation analysis was applied to calculate TM and CS from recorded corneal displacement

and corresponding force.

Results: Compared to the fellow untreated eyes, FD-treated eyes developed significantly high myopia (–26.75 ± 10.16 D vs. –0.34 ± 0.84 D; paired t-test, $p<0.001$), steeply curved corneas (2.91 ± 0.14 mm vs. 3.08 ± 0.13 mm; paired t-test, $p<0.01$), reduced corneal thickness (185.0 ± 13.2 μm vs. 192.7 ± 8.8 μm; paired t-test, $p<0.05$), and decreased TM&CS at all IOP levels (mixed two-way ANOVA, all $p<0.01$). When data from right eyes of treated and control groups were pooled for Pearson's correlation analysis, spherical equivalent had moderate positive correlations with TM (all $r> +0.52$, $p<0.05$) and CS (all $r> +0.59$, $p<0.05$) at all IOPs, and vitreous chamber depth had negative correlations with corneal biomechanical properties at most IOP levels (TM at all IOPs: $r> –0.61$, $p<0.05$; CS at 15 and 25 mmHg: $r> –0.70$, $p<0.01$).

Conclusions: Form-deprivation induced high myopia with notable changes in corneal structural and biomechanical properties. Significant correlations with posterior ocular dimensions imply that the cornea may be involved in refractive error development.

Introduction

In Chapter 2, the potential impacts of high myopia on corneal biomechanical properties were investigated using a custom-made air-jet optical coherence tomography (OCT) system. While the findings of corneal softening in highly myopic chicks were striking and resembled similar changes in humans (He et al., 2017; Hon et al., 2017), there were a few technological limitations associated with the air-jet OCT system. Specifically: 1) the air-jet force was not strong enough to deform chicks' corneas beyond a certain stiffness level; 2) air-jet produced severe corneal dehydration; 3) eyeballs were displaced inwardly during the corneal indentation by air-jet; and 4) corneal biometric parameters were not included to derive intrinsic biomechanical properties; these limitations could contribute to measurement errors. To overcome these limitations, optical coherence tomography (Chao et al., 2013; Huang et al., 2009) was incorporated into the indentation system(Wang et al., 2016), and this novel OCT-indentation system applied to determine the impact of FD-induced high myopia on *in-situ* corneal biomechanical properties (CB), while IOP was maintained at one of three constant, physiological levels. This system was designed by taking into account the anatomical features of the target animal model, the chicken; specifically: 1) the indenter probe was miniaturized (1 mm diameter) to accommodate the steep corneal curvature in small animals; 2) the crystalline lens surface was used as a reference (see details in Methods), to avoid confounding error due to eyeball movement during the corneal indentation (Ko et al., 2013); and 3) time-domain OCT (TD-OCT) was incorporated to provide a fast, high-

resolution tracking of corneal and crystalline lens surfaces during indentation at different IOPs. TD-OCT was chosen as the first approach, because its reference arm allows an extended depth of detection, and because it is less expensive than the frequency-domain OCT (FD-OCT). By integrating essential corneal geometrical parameters (corneal thickness and curvature) measured with other instruments, data were used to calculate the corneal tangent modulus (Ko et al., 2013; Wang et al., 2016; Young et al., 2002). As shown in the results, the novel system provided high sensitivity to measure small, but significant changes in corneal biomechanical properties in highly myopic eyes.

Methods

Animal Husbandry

Sixteen White Leghorn chicks (*Gallus gallus domesticus*) were obtained from the Centralized Animal Facility of The Hong Kong Polytechnic University. Three batches of 5-6 chicks each were raised in a cage (75 cm x 45 cm) illuminated by fluorescent tubes (150 lux at chicks' eye level, 12h:12h light-dark cycle with lights on from 0700 to 1900) in a temperature-controlled (25 °C) room. Food and water were provided *ad libitum*. All experiments were conducted in accordance with the ARVO Statement for the Use of Animals in Ophthalmic and Vision Research, and the protocols were approved by the Animal Subject Experiment Subcommittee of the Hong Kong Polytechnic University (ASESC 14-15/28).

Form-deprivation Myopia (FDM)

To induce FDM, a Velcro ring was glued to the feathers around the right orbit of 12 chicks on post-hatching day 5 (P5), and matching Velcro rings with plastic-molded translucent diffusers (thickness= 0.5 mm, diameter= 12 mm, average light transmission= 30 %) were attached. In the subsequent one-week treatment period, the diffusers were removed daily for cleaning. The left eyes served as untreated control eyes. Four age-matched chicks without any treatment served as the age-matched normal group.

Ocular Biometric Measurements

Refractive status, corneal parameters, and ocular axial dimensions of chicks were measured at P12 by a modified Hartinger refractometer (Kee & Deng, 2008), a custom-made videokeratography system (VKS) (Chu et al., 2014), and a high-resolution A-scan ultrasonography system (Nickla et al., 1998), respectively. The measurements always started with VKS at 07:00-08:00 when chicks were alert, followed by refractions and A-scan ultrasonography when chicks were anesthetized. The three measurements were completed by 11:00. The protocols for these methods have been described in detail elsewhere (Chu et al., 2014; Kee & Deng, 2008; Nickla et al., 1998), and a brief description of each method follows.

Videokeratography System (VKS)

After the pupillary center was aligned (concentric) with the Placido rings projected on the cornea, a consecutive series of 500-800 frames were captured via a multiple-shot mode, using a CCD camera for image analysis. Four or more images per eye were selected manually for image processing, on the basis of objective criteria described elsewhere (Chu et al., 2014) (viz., a minimum of 15 sharply focused Placido rings, with maximal ring-to-ring width). Mean corneal curvatures (average of the two principal power meridians) were calculated from these images through a custom-written MATLAB algorithm and averaged using power vector analysis (Thibos et al., 1997).

Hartinger Refractometer (see also Chapter 2)

Refractive status was measured along the pupillary axis, using a modified Hartinger refractometer (Kee & Deng, 2008), while chicks were anesthetized by isoflurane inhalation (1.5 % in O_2, with an oxygen flow rate of 1.5 L/min). Three measurements per eye were made and averaged for the spherical equivalent, using power vector analysis (Thibos et al., 1997).

A-scan Ultrasonography

Ocular axial dimensions were measured using an A-scan ultrasonographer (GE Panametrics, U.S.) integrated with a 50 MHz focused high-frequency polymer transducer (PVDF; PI50-2-R0.50; GE Panametrics, U.S.). A-scan ultrasonography has been verified as an effective tool for measuring the axial dimensions of chicks' ocular components (Nickla et al., 1998) and is widely used in this field. After the chick was anesthetized, a drop of artificial tears (Lacryvisc; Alcon, France) was applied to the cornea, to minimize irritation by the ultrasound-interfacing gel (Aquasonic; Parker Laboratories, U.S.). Fifty data sets per eye were collected by a data-collection card, installed in a computer, at a sampling rate of 500 MHz. These data were later analyzed, using a custom-written algorithm to identify peaks representing the borders between the ocular components (Nickla et al., 1998), and averaged.

Optical-coherence-tomography-indentation Probe System

Applying the principle of an ultrasound-indentation system (Wang et al., 2016), a customized optical-coherence-tomography-indentation (OCT-indentation) system was developed, validated (see below), and used it to measure *in-situ* corneal tangent modulus (TM) and corneal stiffness (CS). The OCT-indentation system consisted of a fiber-optic based time-domain OCT, an indenter of 1 mm diameter, a CCD camera, and data acquisition modules (see Figure 3.1. for the dimensions of the system). The infrared beam was generated by a 1310 nm super-luminescent diode (SLD) light source (Dense-Light, DL-CS3055 A, Singapore) with an output power of 5 mW and a 3 dB bandwidth of 50 nm. To aid in alignment with the central cornea, a visible light source providing red light (Figure 3.2A) and a CCD camera were coupled into the system. The scanning depth was set at approximately 8 mm, with a fast-scanning delay line. Light scattered and reflected from the anterior ocular components (Figure 3.2B) was detected using the OCT A-scan mode and transformed into digital images via a data-acquisition module. The maximum indentation depth was set to 1 mm, with a speed of 0.57 mm/s (vs. 0.83mm/s of the strain rate of strip test). The indentation depth and the corresponding force (shown as red boxes in Figure 3.2C and D), recorded by a force sensor (Model JLBS-M2-10N, Bengbu Sensor System Engineering Co. Ltd. China), were displayed in real-time during measurements. A custom-written algorithm (Labview, version 12, National Instrument, U.S.) was developed to control the OCT indentation system and record data. For data analysis, a MATLAB algorithm (MATLAB R2007b, Version 7.5.0, The MathWorks, U.S.) with a cross-correlation method was used to track corneal displacement (units: mm) under the corresponding indentation force.

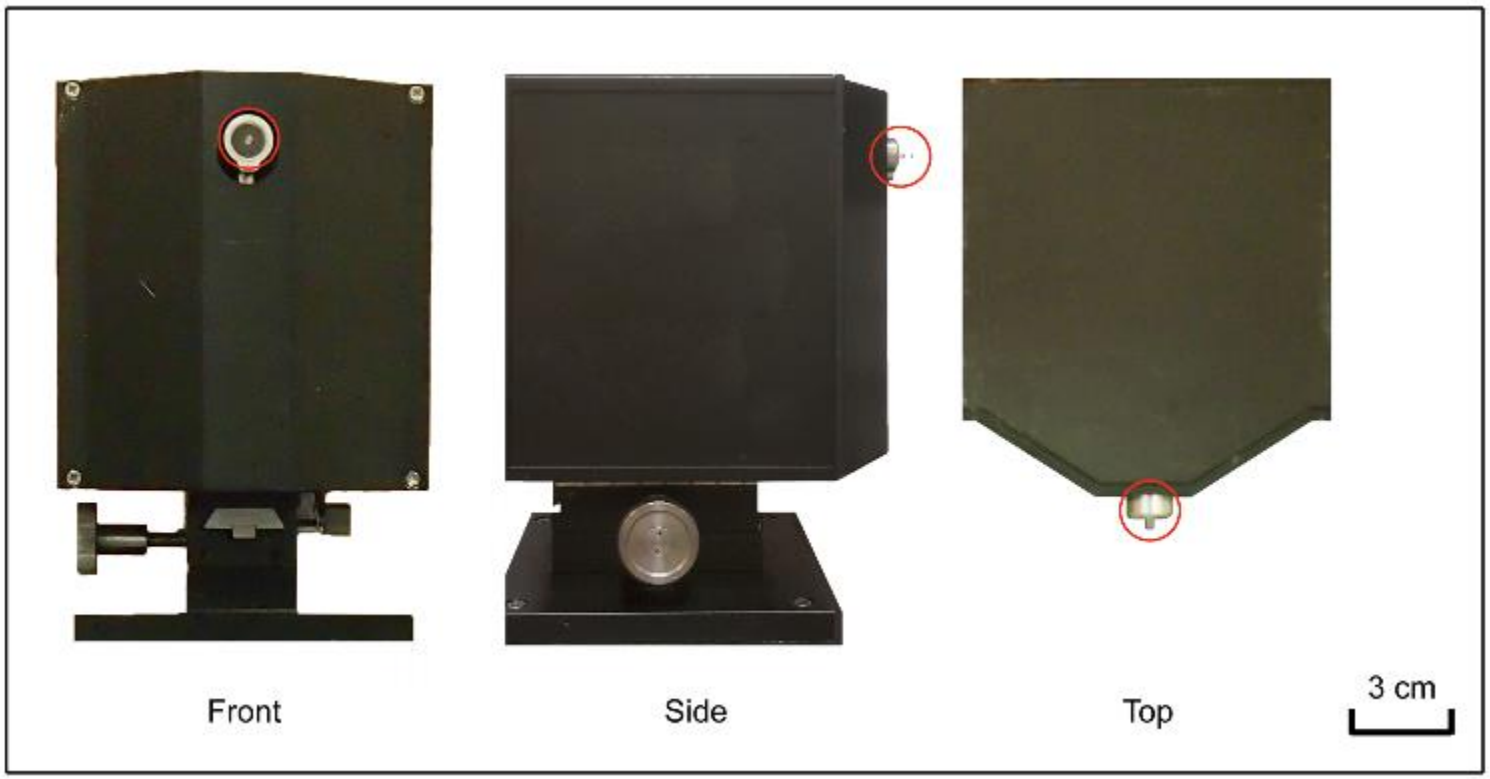

Figure 3.1. Different dimensional views of the OCT-indentation probe system. The probe is highlighted with red circles.

The corneal stiffness coefficient (units: mN/mm) was then derived from the regression line of indentation force vs. corneal displacement. The corneal tangent modulus (units: MPa) was calculated by taking into account the individual corneal radius of curvature and thickness, collected from VKS and A-scan ultrasonography, respectively (Ko et al., 2013; Wang et al., 2016; Young et al., 2002) (see Figure 3.3 and 3.4). Corneal tangent modulus (TM) describes the tangent modulus of elasticity (E) at a given IOP (instantaneous slope of the stress-strain curve at specific stress or strain), taking into account the contributions of corneal thickness and corneal radius of curvature. The equation used to derive TM was adopted from previous studies (Ko et al., 2013; Roark & Young, 1989; Wang et al., 2016):

$$E|_{IOP} = \frac{a(R_c - t\ /\ 2)\sqrt{1 - v^2}}{t^2} \frac{dF}{d\delta}\Big|_{IOP} \tag{3.1}$$

where *Rc* is the radius of corneal curvature, *t* is the corneal thickness, *v* is the Poisson's ratio (0.45) (Wang et al., 2016), *dF* is the differential force, *dδ* is the displacement interval, and *a* is a geometrical constant derived from μ:

$$\mu = r_0 \left[\frac{12(1 - v^2)}{(R_c - t\ /\ 2)^2 t^2}\right]^{1/4} \tag{3.2}$$

where r_0 is the radius of the full-contact area between the flat-surface indentation probe and the cornea. Thus, *a* is determined by interpolating the values from the relationship between *a* and μ (Roark & Young, 1989).

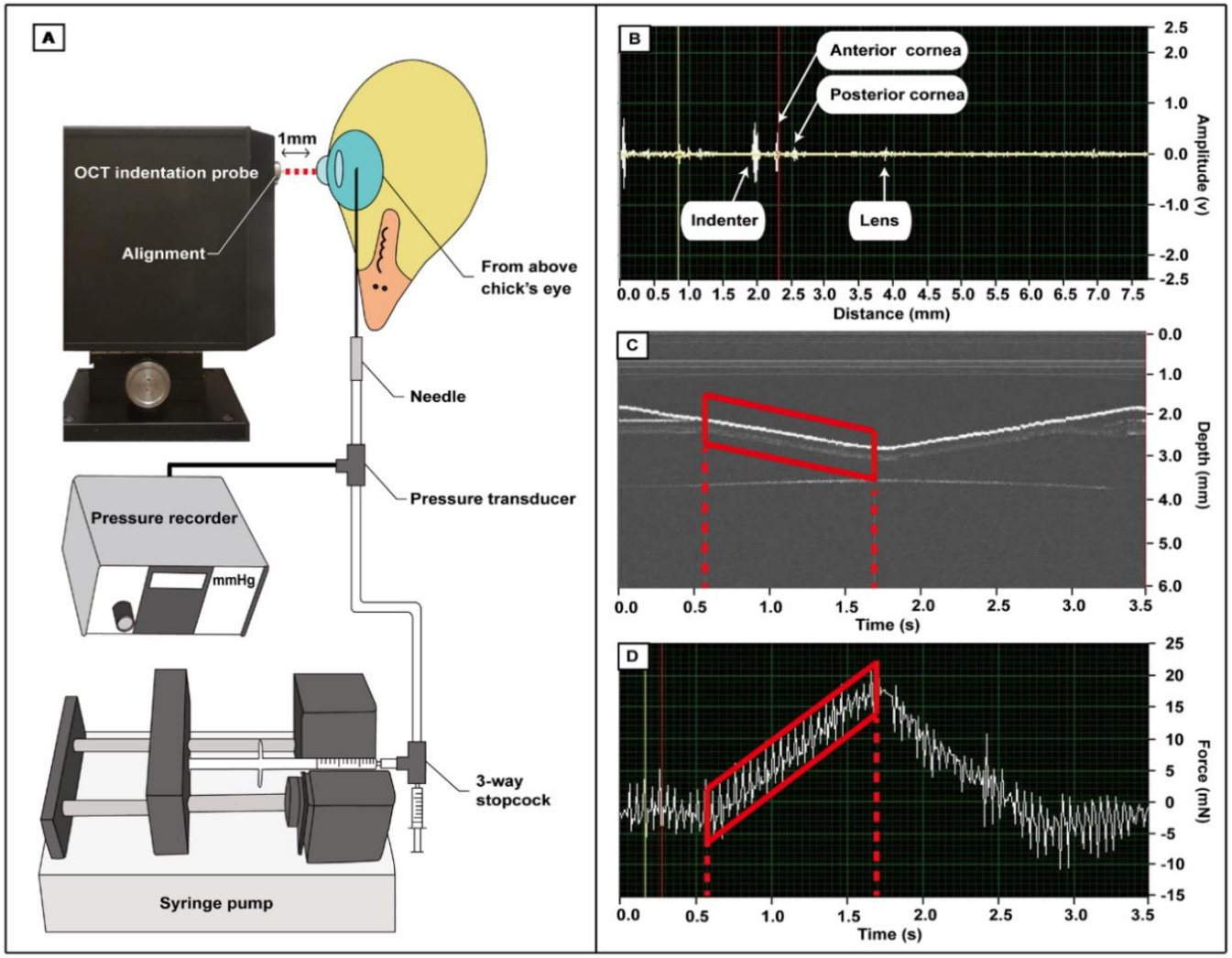
A
1mm
OCT indentation probe
Alignment
From above chick's eye
Needle
Pressure transducer
Pressure recorder
mmHg
3-way stopcock
Syringe pump
B
Anterior cornea
Posterior cornea
Indenter
Lens
Amplitude (v)
Distance (mm)
C
Depth (mm)
Time (s)
D
Force (mN)
Time (s)

Figure 3.2. Overview of OCT-indentation probe system. (A) Schematic diagram of the set-up for OCT-indentation probe with an IOP controller. The central cornea of the chick was aligned with a visible light source emitted from the OCT-indentation probe (red dashed line). Before measurements, a digitally-controlled syringe pump with a pressure recorder was connected with the eye through a needle, to hold the IOP at one of three levels. (B) To ensure axial alignment of the indentation probe with the eye, measurements started only after the operator obtained the maximal signals from the three anterior ocular surfaces (anterior cornea, posterior cornea, and anterior lens). (C & D) After each 1-mm indentation was completed (red outlines), the deformation depth (C) and corresponding force (D) over time were cross-correlated to calculate the corneal tangent modulus (TM) and corneal stiffness coefficient (CS). The oscillations in (D) were due to motor vibration and were removed before further data analyses (see also Figure 3.3).

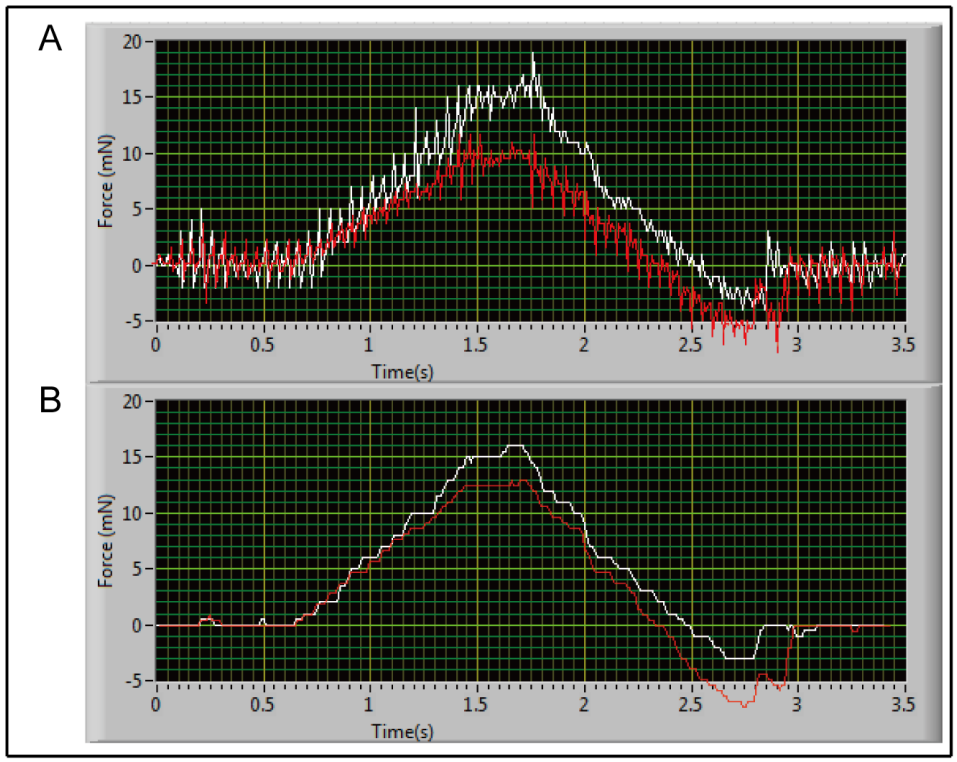

Figure 3.3. Raw data for a complete cycle of indentation obtained from the OCT-indentation probe system. Data from a highly myopic eye (red) and the fellow control eye (white) were superimposed here to illustrate the difference. The oscillations due to the motor's vibrations (A) were smoothened (B) using a custom written analysis module in Labview before further analysis.

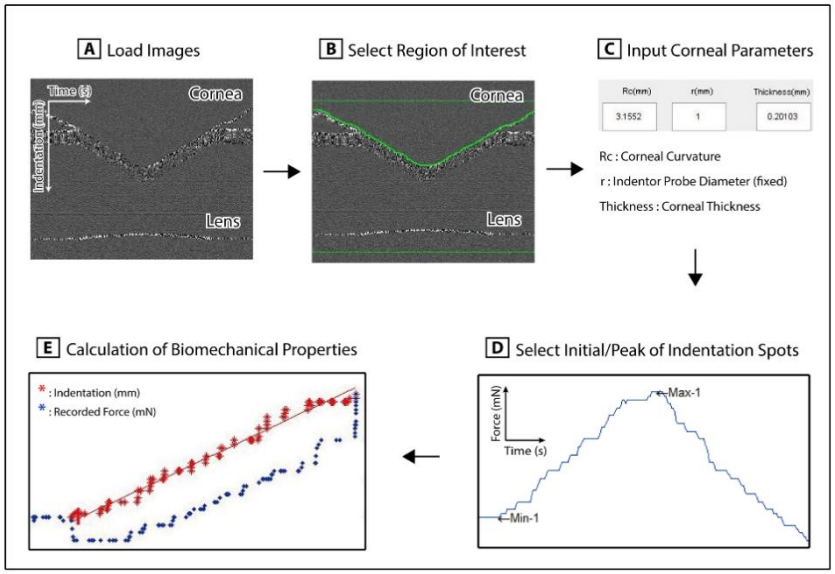

Figure 3.4. The process of quantifying the raw data of corneal deformation over time. (A) Time-dependent changes in corneal interface due to the indentation probe, recorded by the OCT A-scan mode. The raw data were loaded into a custom-written MATLAB algorithm for TM/CS calculations. (B) A region of interest (the corneal interface) was selected. (C) Corneal biometric parameters (thickness and curvature) from individual birds were entered for the calculation of TM. (D) The initial and peak indentation points were selected. (E) Cross-correlation analysis was performed to compute corneal biomechanical properties (TM and CS).

Validation and Repeatability of OCT-indentation Probe

To validate the OCT-indentation probe system, its accuracy in measuring tangent modulus of seven silicone corneal phantoms made with a range of Young's modulus (0.05 to 0.64 MPa) that covered the TM values of chicks (0.12 to 0.52 MPa) was first determined as revealed in a pilot experiment. The mean TM values (average of three measurements) of the seven corneal phantoms were then compared with the tensile modulus (Wang et al., 2016) measured with an extensometer (Electro Force 3600, TA Instruments, U.S.) for the corresponding corneal strips. Note that tangent modulus and tensile modulus are two distinctly different indices, derived by different methods and formulae; viz.: while tangent modulus reflects the stress-strain relationship along with the deformation depth and surface, the tensile modulus is derived by biaxial stress-strain relationship. The tensile modulus measurement was chosen as an external validity test because it is known to most investigators. The corneal phantoms and strips were made by 7 sets of RT2 silicone (Zheng et al., 2014) (E600~635A/B, Hong Ye Jie Technology, China). All corneal phantoms were designed to mimic the corneal central thickness of normal chicks (200 μm), a radius of curvature (3 mm), and white-to-white diameter (5 mm). Each corneal phantom was mounted on an artificial anterior chamber, using a previously established set-up (Wang et al., 2016), and two sets of three OCT-indentation measurements were collected at 5 mmHg IOP. The silicone strip was first fixed by two jaws on an extensometer, and then a 20 mN pre-stress was applied to the strip with an initial length of 8mm, followed by an elongation of 6mm with a velocity of 50 mm/min. Because of the viscoelastic property of the silicone strip, regression analysis between stress and strain was performed, and the strain from

25 % to 35 % on the linear slope was selected for the calculation of tensile modulus. The tangent modulus and tensile modulus, collected respectively by the OCT-indentation probe system and extensometer, were analyzed by a regression analysis.

The reliability and repeatability of the OCT-indentation probe system for measuring the tangent modulus were tested on three silicone corneal phantoms (Tensile modulus; A= 0.053 MPa, B= 0.266 MPa, C= 0.507 MPa). Similar settings as described above were employed, and two sets of three measurements were made for each of the four IOP levels (0, 5, 15, 25 mmHg) that cover the chicks' physiological IOP range (Nickla et al., 1998) (12 to 22 mmHg). Intra-class correlation coefficients (ICC) were assessed.

Measurement of Corneal Biomechanical Properties in Chicks' Eyes

After the completion of ocular biometric measurements, the chicks were euthanized by carbon dioxide asphyxiation to prevent the reflexive response of the nictitating membrane from interfering with the movement of the probe during indentation. While the head was maintained in an erect posture on an adjustable platform, the eyelids were held apart gently with a speculum. A computer-programmed syringe pump (NE-1000, New Era Pump, U.S.) was used to control IOP during the indentation process. This pump was connected with a 1mL syringe filled with 0.9% saline, with its infusion rate set as 0.2 mL/hr. The apparatus was handled with special care to remove any trapped air bubbles, which would degrade the accuracy of IOP increments. To measure and monitor the pressure in the eye, a 30G

needle (BD Precise Glide, U.S.) was used to cannulate the eye through the superior sclera, to a depth of approximately 5 mm (around the middle of the vitreous chamber). This set-up allowed the IOP to be maintained at a pressure of up to 50 mmHg without leakage of aqueous humor. The needle was connected with a pressure transducer (BP transducer, Harvard Apparatus, U.S.) and the syringe pump through a 3-way stopcock. To determine the effects of IOP on corneal biomechanical measurements, three IOP levels (5, 15, and 25 mmHg) were chosen to cover the normal physiological range of IOP (12 to 22 mmHg) in alert chicks (Nickla et al., 1998). The indentation probe was controlled by a high-precision linear stage (Figure 3.1), by which it was moved towards the corneal surface and set at about 0.2~0.3 mm in front of the corneal apex (Figure 3.2B). The CCD camera was used to align the primary location of the probe with the central cornea, using a visible light source. Three sets of measurements were then collected, allowing maximal signals from the anterior cornea, posterior cornea, and crystalline lens to be clearly identified from the real-time OCT images (Fig 3.2B). The sequence for measuring corneal biomechanical properties in the two eyes was randomized, and the measurements for each eye were completed within 10 minutes.

Statistical Analyses

All statistical analyses were conducted using either IBM SPSS (version 21.0.0, IBM, U.S.) or GraphPad Prism (Version 6.01, GraphPad Software, U.S.). Normality of distribution of variables was first verified by the Shapiro-Wilk test. As the data for refraction were normally distributed, paired *t*-tests were used to test

the differences in refractive status between the treated (or right) and contralateral (or left) eyes. The comparison between right and left eyes in the normal control group was tested by Mann Whitney U-test, because of the small sample size (n = 4). A mixed two-way ANOVA was performed when both normalities by Shapiro-Wilk test and homogeneity of variance by Levene's test were not violated. Depending on the result of Mauchly's test, either Greenhouse-Geisser (if $\varepsilon>0.75$) or Huynh-Feldt (if $\varepsilon<0.75$) corrections were applied when sphericity of variance was violated. To test the main treatment effects of form deprivation and IOP levels on corneal biomechanics, *post-hoc* Bonferroni tests were used. Independent *t*-tests were conducted to test the intergroup differences in corneal biomechanics. Correlations between IOP and corneal biomechanics at different IOP levels were tested using Pearson's correlation analysis. Multiple regression analysis was performed to determine the contribution of ocular biometric parameters to corneal biomechanics. To prevent multi-collinearity, the minimum cutoffs for tolerance and variance inflation factor (VIF) were set as 0.1 and 5.0 respectively. Dependent variables showing a non-linear relationship with independent variables were excluded. The significance level for all tests was set at 5 %.

Results

The OCT-indentation probe system showed high external validity when comparing the tangent modulus (TM) measurements of this system with the tensile modulus measured by an extensometer (Figure 3.5A, y= 2.078x–0.0691, r^2= 0.96, p<0.001). The system also showed low intra-session variability (mean coefficient of variance (CV)= 8.53 %) and good inter-session repeatability from two sets of three consecutive TM measurements performed on seven corneal phantoms (intraclass correlation coefficient (ICC)= 0.992; 95 % confidence intervals (CI)= 0.982 to 0.997, p<0.001; see also Figure 3.5B for a Bland-Altman plot). When applying the system to measure TM of three corneal phantoms of different tensile modulus (0.053, 0.266, and 0.507 MPa) at four IOP levels (0, 5, 15, and 25 mmHg), the system also showed low intra-session variability (mean CV= 4.98 %) and a high degree of inter-session repeatability (ICC= 0.994, 95% CI= 0.988 to 0.997, p<0.001; see also Figure 3.6B for a Bland-Altman plot) from two sets of three TM measurements collected at the four IOPs.

Table 3.1 summarizes the ocular biometric parameters (SE: Spherical Equivalent; CRC: Corneal Radius of Curvature; CCT: Central Corneal Thickness; ACD: Anterior Chamber Depth; LT: Lens Thickness; VCD: Vitreous Chamber Depth; RT: Retinal Thickness; CT: Choroidal Thickness; ST: Scleral Thickness) and corneal biomechanical properties (TM, Tangent Modulus and CS, Corneal Stiffness coefficient) measured at P12 (post-hatching day 12) in both eyes of chicks in the FD-treated and age-matched normal groups. There was no evidence of any

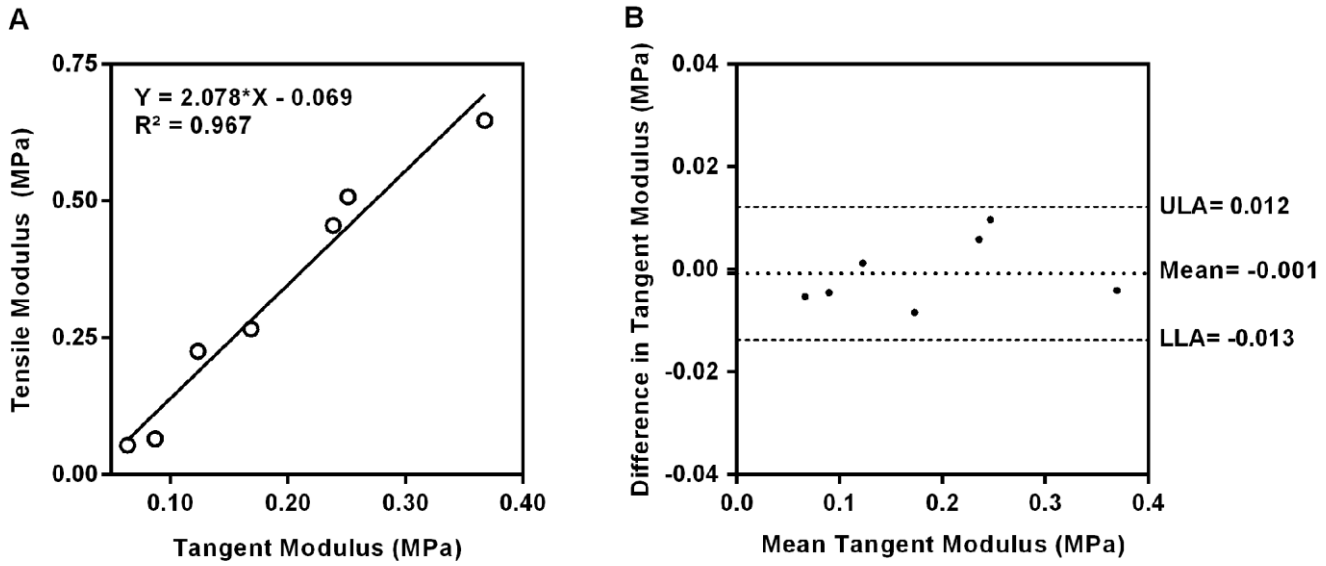

Figure 3.5. Validation of measurements using OCT-indentation probe. (A) External validation by examining the linear regression between the tangent modulus of the corneal phantom (by the probe) and the tensile modulus of the silicone strips from corresponding corneal phantoms (by extensometer). (B) Inter-session repeatability of the tangent-modulus measurement, by Bland-Altman plot. The mean difference and 95 % limits of agreement are represented by a dotted line and dashed lines, respectively. ULA, upper limit agreement; LLA, lower limit agreement.

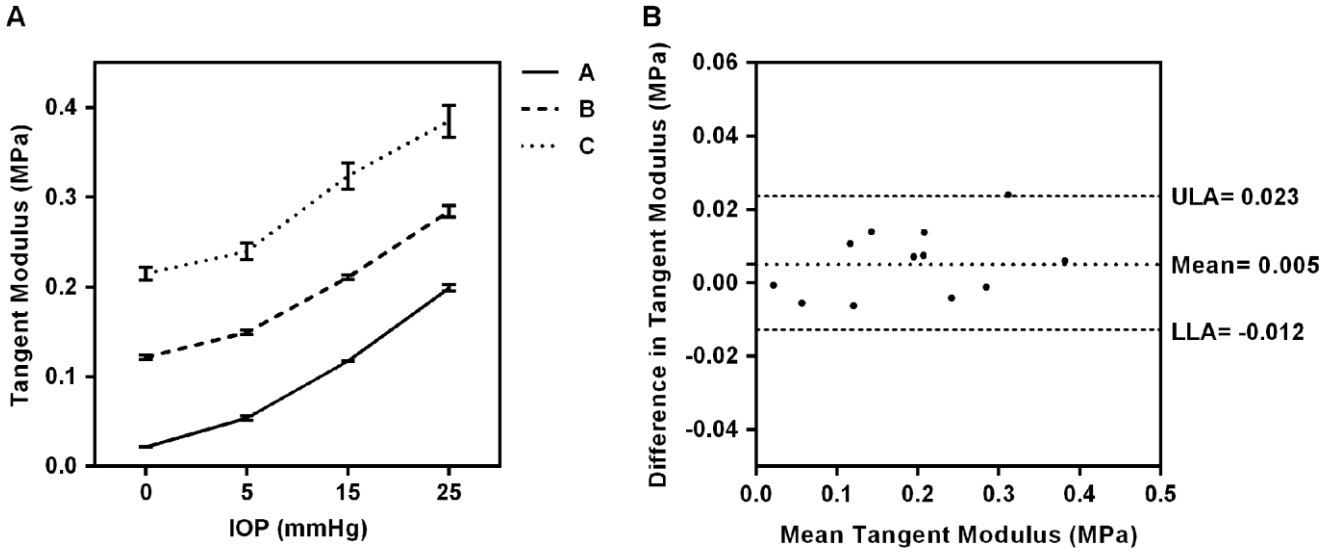

Figure 3.6. Reliability and repeatability of tangent modulus measurements performed on 3 corneal phantoms at 4 IOP levels using OCT-indentation probe. (A) Changes in tangent modulus of three different corneal phantoms (A= 0.053 MPa, B= 0.266 MPa, C= 0.507 MPa) under four IOP levels. (B) Bland-Altman plot of the two sets of repeated measurements of tangent-modulus under four IOP levels. The mean difference and 95 % limits of agreement are represented by a dotted line and dashed lines, respectively. ULA, upper limit agreement; LLA, lower limit agreement. The symbols represent mean ± SEM.

Table 3.1. Summary of ocular biometric data and corneal biomechanical properties.

		FD-treatment Group (n= 12)			Age-matched Normal Group (n= 4)		
Parameters	**Unit**	**RE (Treated)**	**LE (Untreated)**	**p**	**RE**	**LE**	**P**
SE	D	-26.75±10.16	-0.34±0.84	<0.001	0.03±0.72	0.37±0.89	0.886
CRC	mm	3.07±0.10	3.19±0.09	0.001	3.17±0.07	3.19±0.06	1.000
CCT	µm	185.0±13.2	192.7±8.8	0.032	194.9±6.7	195.8±6.4	0.886
ACD	µm	1412.9±150.6	1249.1±51.0	0.004	1228.5±138.4	1323.5±173.8	0.486
LT	µm	2224.3±164.8	2074.8±86.7	0.008	2198.5±236.8	2073.4±147.3	0.686
VCD	µm	5968.5±329.4	5149±165.5	<0.001	5232.7±137.2	5225.4±192.5	0.886
RT	µm	205.3±16.9	230.6±18.6	0.020	210.4±12.5	191.5±62.8	0.686
CT	µm	167.5±44.3	223.7±32.8	0.010	233.1±39.4	263.6±17.0	0.343
ST	µm	107.8±26.5	111.9±17.7	0.661	114.9±32.9	124.1±42.7	0.886
TM @ IOP 5	MPa	0.12±0.013	0.15±0.014	<0.001	0.14±0.007	0.15±0.007	0.343
TM @ IOP 15	MPa	0.28±0.048	0.35±0.045	0.002	0.32±0.026	0.32±0.024	1.000
TM @ IOP 25	MPa	0.42±0.061	0.52±0.071	0.001	0.49±0.061	0.50±0.051	0.886
CS @ IOP 5	mN/mm	10.52±0.98	12.28±1.47	0.001	12.26±0.47	12.43±1.14	0.886
CS @ IOP 15	mN/mm	24.02±3.20	28.56±3.37	0.011	27.13±2.83	26.67±2.79	1.000
CS @ IOP 25	mN/mm	35.99±3.37	41.90±4.33	0.002	40.90±5.66	41.72±6.21	0.886

Abbreviations: SE, spherical equivalent; CRC, corneal radius of curvature; CCT, central corneal thickness; ACD, anterior chamber depth; LT, lens thickness; VCD, vitreous chamber depth; RT, retinal thickness; CT, choroidal thickness; ST, scleral thickness; TM, tangent modulus; CS, corneal stiffness coefficient. Data are mean ± SD, paired-*t*-tests in the treated group and Mann-Whitney U-tests in the normal group.

Table 3.2. Pearson's correlation analysis between ocular biometric parameters and corneal biomechanical properties.

	SE	CRC	CCT	ACD	LT	VCD	RT	CT	ST
TM @ IOP5	.571*	.463	-.062	-.477	.000	-.612*	-.080	.600*	.044
TM @ IOP10	.603*	.438	-.096	-.372	-.203	-.759**	.293	.224	.068
TM @ IOP15	.603*	.438	-.096	-.372	-.203	-.759**	.293	.224	.068
CS @ IOP5	.523*	.423	-.185	-.285	-.130	-.684**	.292	.199	-.015
CS @ IOP10	.594*	-.077	.119	-.604*	.155	-.487	-.295	.546*	.027
CS @ IOP15	.703**	.068	.094	-.539*	-.131	-.761**	.159	.153	.087

Note: * $p<0.05$. ** $p<0.01$.

Abbreviations: Abbreviations: SE, spherical equivalent; CRC, corneal radius of curvature; CCT, central corneal thickness; ACD, anterior chamber depth; LT, lens thickness; VCD, vitreous chamber depth; RT, retinal thickness; CT, choroidal thickness; ST, scleral thickness; TM, tangent modulus; CS, corneal stiffness coefficient.

significant difference in ocular parameters and corneal biomechanical properties (TM and CS), between the fellow untreated (left) eyes of the FD-treated group and the right and left eyes of the normal group (Mann-Whitney U-tests, all $p>0.05$). Furthermore, the effect sizes (G*Power, version 3.1.9.3, Universität Düsseldorf, Germany) for comparing TM of the right and left eyes of normal birds (n= 4) were all <0.29 at three IOPs – indicating low variability and negligible interocular differences, even with small sample size. One week of form-deprivation induced significantly higher myopia, and a steeper and thinner cornea, in treated eyes than in the fellow untreated eyes (Table 3.1, paired-*t*-test, all $p<0.05$).

There were no significant differences in TM or CS, between the right and left eyes of chicks in the age-matched normal group, at any of the three IOP levels; in contrast, there were significant reductions in both TM and CS in FD-treated eyes compared to fellow untreated eyes at all three IOP levels (mixed two-way ANOVAs, all $p<0.01$, Table 3.1). However, TM and CS were found to increase as the IOP increased, in both normal and treatment groups (mixed two-way ANOVAs, all $p<0.001$). Figure 3.7 shows the percentage difference in TM and CS between the treated and control eyes [100 %*(treated eye – fellow eye)/fellow eye] in treated versus normal groups. TM and CS of treated eyes were smaller than those of normal control eyes at all three IOP levels (Table 3.1), with statistically significant differences at 5 and 15 mmHg (Mann-Whitney U-tests, all $p<0.05$), but not at 25 mmHg (Mann-Whitney U-test, $p>0.05$). In terms of percentage of eyes showing interocular differences in TM, eleven (92 %) treated eyes showed a reduction in TM at 5 mmHg (range= −4.27 % to −36.56 %) and 15 mmHg (range= −2.34 % to −41.44 %), while ten (83 %) treated eyes had lower TM at 25 mmHg (range= −4.86 %

to −36.81 %).

Pearson correlation analyses were conducted to determine the relationship between ocular biometric parameters and corneal biomechanical properties at different IOP levels (Table 3.2 and Fig 3.8). SE was moderately correlated with TM (all $r>+0.52$, $p<0.05$) and CS (all $r>+0.59$, $p<0.05$) at all IOPs, and even higher correlations were found between VCD and corneal biomechanical properties at most IOPs (TM at all IOPs: $r>-0.61$, $p<0.05$; CS at 15 and 25 mmHg: $r>-0.70$, $p<0.01$). Lastly, ACD showed moderate correlations with CS at 5 and 15 mmHg ($r>-0.54$, $p<0.05$), but was not correlated with TM ($r>-0.28$, $p\geq0.06$). CRC, CCT, ST did not show any significant correlations with TM or CS.

To evaluate which ocular biometric parameters (except AL, because it was the sum of individual axial dimensions) play a major role in corneal biomechanics, multiple linear regression analyses were performed. Variables showing non-linearity (by using scatterplot) with corneal biomechanics, or multicollinearity with VCD, were excluded from the analyses, leaving four parameters (CRC, CCT, ACD, and VCD) for further analyses. Results (Table 3.3 and 3.4) showed that VCD was the only variable strongly associated with TM and with CS; this was the case under all IOP levels except 5 mmHg IOP, at which none of the tested variables showed significant associations.

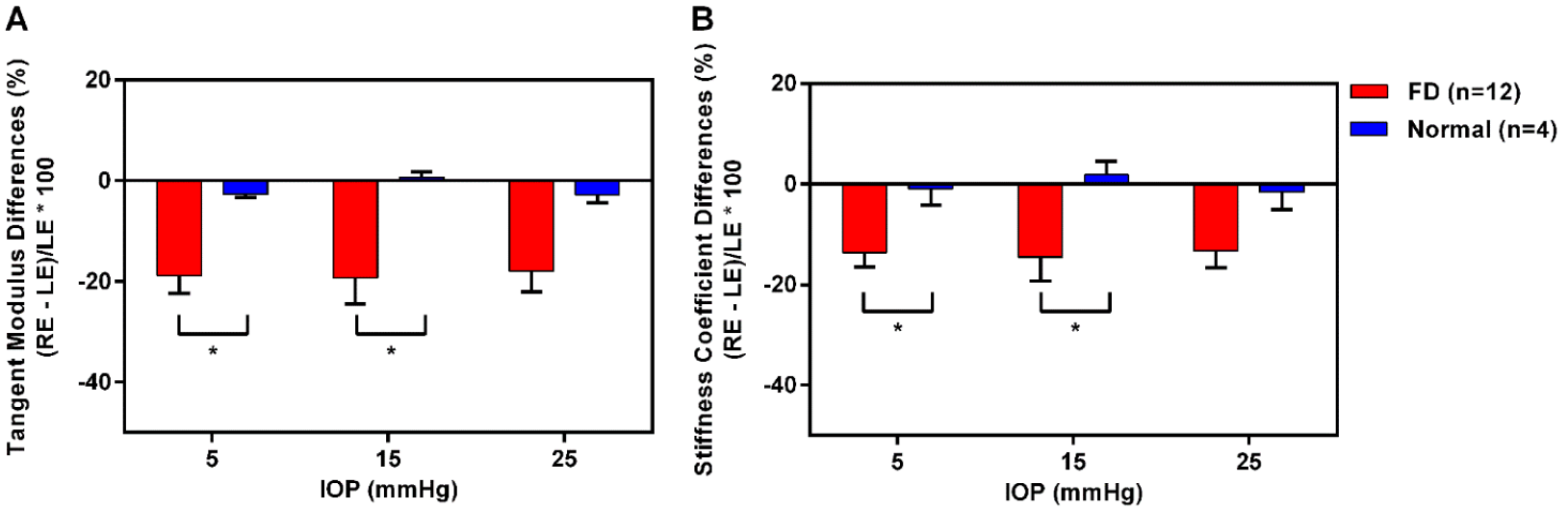

Figure 3.7. Effects of form-deprivation (FD)-induced high myopia, on corneal biomechanical properties. Significant interocular differences (100 %*(RE [treated eye] – LE [fellow eye])/LE [fellow eye]) in (A) TM and (B) CS were found at 5 and 15 mmHg between the treated and normal groups. Mann-Whitney U-tests, *$p<0.05$. Bars represent mean ± SEM.

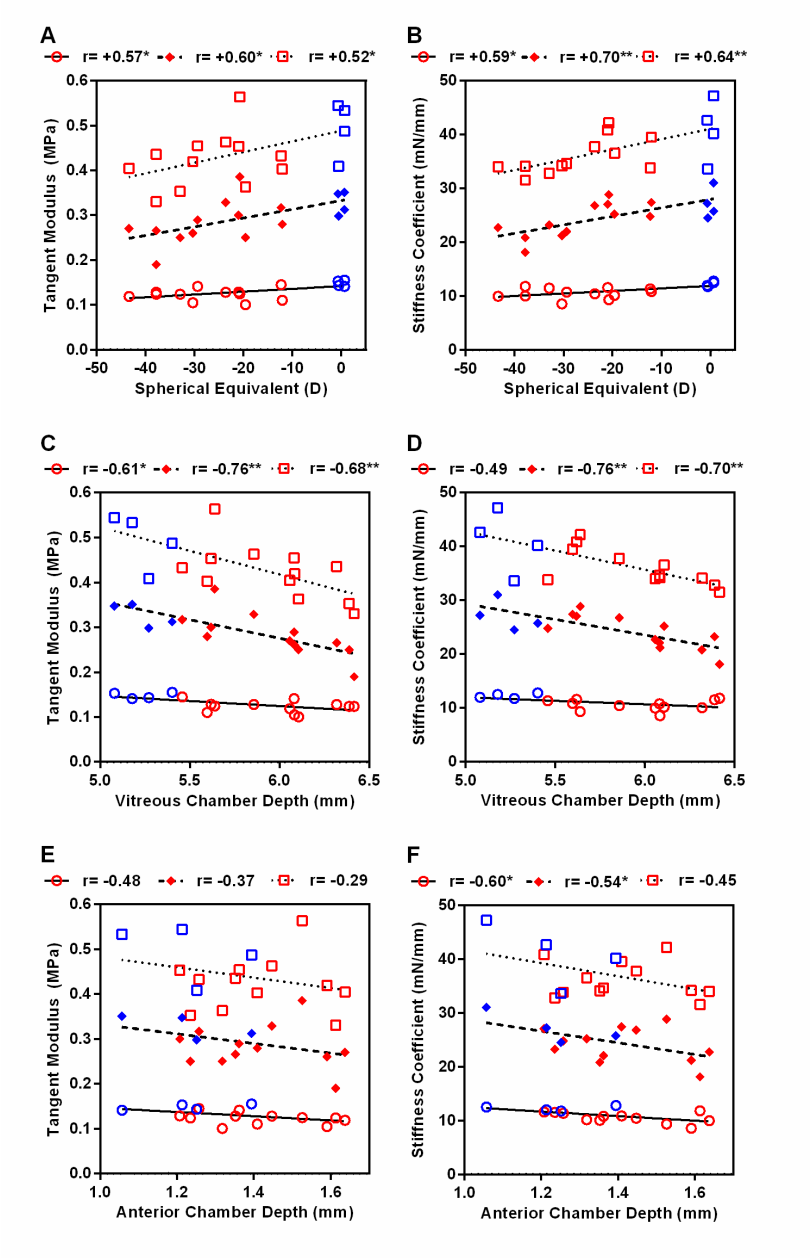

Figure 3.8. Pearson correlations between biometric parameters (spherical-equivalent refractive errors, vitreous chamber depth, and anterior chamber depth) and TM and CS. Red and blue symbols represent treated and normal chicks respectively. ○: IOP 5 mmHg, ◇: IOP 15 mmHg, □: IOP 25 mmHg. *p<0.05, **p<0.01 (for correlation analyses).

Table 3.3. Results of the multiple regression analysis for corneal tangent modulus (independent variable) at different IOPs.

	Unstandardized coefficient		Standardized coefficient	t	*p*	*F*	95% CI	Adjusted R^2
	B	SE	β					
5 mmHg	—	—	—	—	—	4.740*	—	.499
CCT	-.001	.000	-.482	-2.188	.051	—	-.001 to .000	—
CRC	.076	.034	.505	2.260	.045*	—	.002 to .151	—
ACD	-.000	.000	-.380	-1.662	.125	—	.000 to .000	—
VCD	-.000	.000	-.307	-1.326	.211	—	.000 to .000	—
15 mmHg	—	—	—	—	—	7.377**	—	.630
CCT	-.002	.001	-.423	-2.231	.047*	—	-.003 to .000	—
CRC	.172	.086	.385	2.005	.070	—	-.017 to .360	—
ACD	-.000	.000	-.105	-.536	.604	—	.000 to .000	—
VCD	-.000	.000	-.632	-3.174	.009**	—	.000 to .000	—
25 mmHg	—	—	—	—	—	6.244**	—	.583
CCT	-.003	.001	-.518	-2.576	.026*	—	-.005 to .000	—
CRC	.279	.128	.444	2.177	.052	—	-.003 to .561	—
ACD	-.000	.000	-.071	-.342	.739	—	.000 to .000	—
VCD	-.000	.000	-.570	-2.700	.021*	—	.000 to .000	—

Abbreviations: CCT, central corneal thickness; CRC, corneal radius of curvature; ACD, anterior chamber depth; VCD, vitreous chamber depth; CI, confidence interval; R^2, adjusted coefficient of determination. *p<0.05, **p<0.01

Table 3.4. Results of the multiple regression analysis for corneal stiffness coefficient (independent variable) at different IOPs.

	Unstandardized coefficient		Standardized coefficient	t	*p*	*F*	95% CI	Adjusted R^2
	B	SE	β					
5 mmHg	—	—	—	—	—	2.554	—	.293
CCT	.005	.024	.059	.223	.827	—	-.048 to .059	—
CRC	-3.540	2.894	-.325	-1.224	.247	—	-9.909 to 2.828	—
ACD	-.003	.002	-.459	-1.691	.119	—	-.007 to .001	—
VCD	-.001	.001	-.353	-1.285	.225	—	-.003 to .001	—
15 mmHg	—	—	—	—	—	5.290*	—	.534
CCT	-.008	.056	.030	.139	.892	—	-.116 to .132	—
CRC	-8.135	6.711	-.261	-1.212	.251	—	-22.907 to 6.636	—
ACD	-.004	.004	-.177	-.801	.440	—	-.013 to .006	—
VCD	-.006	.002	-.759	-3.397	.006**	—	-.010 to -.002	—
25 mmHg	—	—	—	—	—	3.787*	—	.426
CCT	-.024	.083	-.067	-.284	.782	—	-.206 to .159	—
CRC	-10.627	9.901	-.257	-1.073	.306	—	-32.419 to 11.166	—
ACD	-.004	.007	-.133	-.545	.597	—	-.018 to .011	—
VCD	-.007	.003	-.740	-2.985	.012*	—	-.013 to -.002	—

Abbreviations: CCT, central corneal thickness; CRC, corneal radius of curvature; ACD, anterior chamber depth; VCD, vitreous chamber depth; CI, confidence interval; R^2, adjusted coefficient of determination. *p<0.05, **p<0.01

Discussion

This study showed that in chicks: the novel OCT-indentation probe provided reliable and repeatable *in-situ* corneal biomechanical measurements; form-deprivation produced significant reductions in corneal tangent modulus and stiffness when IOP levels were controlled at physiological levels; and the two corneal biomechanical indices were significantly correlated with elongation of the vitreous chamber in highly myopic eyes.

Using an OCT-indentation device, created by adopting the operating principle of a recently-developed ultrasound indentation probe (Wang et al., 2016), significant reductions in both TM and CS in highly myopic eyes were observed under all three IOP levels tested (Table 3.1). The method and approach used are novel in several respects. *First*, because the cornea is the anterior-most ocular tissue, contributing to both optical quality and mechanical stability of the eye, its roles in ocular rigidity (Friedenwald, 1937) and stress-strain behavior (Hoeltzel et al., 1992) have been studied widely. However, common clinical devices (ORA and Corvis ST) cannot provide corneal biomechanics parameters in terms of standard engineering terminology (stress-strain behavior); therefore, interpretation of biomechanical indices (e.g., corneal hysteresis) is not straightforward (Hon & Lam, 2013; McMonnies, 2012). In this study, the corneal tangent modulus – Young's modulus, derived by integrating the data within the linear portion of the stress-strain curve (Ko et al., 2013; Wang et al., 2016; Young et al., 2002) was measured to investigate corneal biomechanical changes in an animal model widely used for

studying refractive development. The biomechanical indices measured showed internal and external validity. *Second*, both corneal tangent modulus and corneal stiffness coefficient were measured, rather than relying only on measurements that do not take into account the corneal curvature and thickness (Hoeltzel et al., 1992). Nevertheless, the findings that CS was only weakly correlated with corneal curvature (at all IOPs; $r<-0.08$, $p>0.77$) and thickness (at all IOPs; $r<+0.12$, $p>0.66$), and that CS was highly correlated with TM (at all IOPs; $r>+0.71$, $p<0.01$), suggest that CS can substitute for TM as a valuable metric for representing corneal biomechanical properties in chicks. *Third*, the corneal biomechanical measurements were performed at three IOP levels covering the normal physiological range in chicks. IOP has been identified as one of the key factors influencing corneal biomechanical properties (Kling & Marcos, 2013), and an elevated IOP has been reported in some myopic eyes (Mitchell et al., 1999; Nomura et al., 2004). As revealed in Table 3.1 and Figure 3.8, the TM measurements using the OCT-indentation probe were sensitive to both the IOP level and the degree of myopia. Thus, performing the measurements without controlling for IOP could have masked a potential impact of myopia on corneal biomechanics. *Fourth*, because conventional methods of assessing biomechanical properties in isolated tissue samples (*in vitro*) may cause measurement artifacts, corneal biomechanical properties were measured *in situ*. Lengthy preparation steps, as required for extensometry and inflation testing, increase the risk of structural disruption (Ruberti et al., 2011) and dehydration (Kling & Marcos, 2013) of samples, which could adversely affect their biomechanical properties. In this study, the cornea was exposed to the air only during the 10-minute measurement interval, while the

fellow eye was protected from desiccation by the closed eyelid. Furthermore, the sequence of measurements (treated eye vs. control eye) was randomized. Consequently, the *in-situ* OCT-indentation measurement should provide an assessment of the tissue's biomechanical status under conditions very close to those of the normal cornea *in vivo*.

The two reduced corneal biomechanical indices were associated with myopia and posterior segment depth (Figure 3.8). Ten of the twelve treated eyes showed reductions in corneal tangent modulus relative to that of the fellow eyes, at all three IOP levels, with the differences varying from 2 % to 41 %. These results – together with the growing evidence of a softer cornea in myopic eyes using different methods and animal models (Wang et al., 2008) underscore the importance of understanding the relationship between corneal biomechanical properties and myopia development (Hon et al., 2017). In this study, while the highly myopic eyes developed significant corneal thinning and steepening, along with deepening of the ACD and VCD (Table 3.1), VCD stood out as the key biometric parameter associated with TM and CS (Figure 3.8 and Table 3.2 ~ 4). Corneal thinning (Chang et al., 2001; Touzeau et al., 2003) and steepening (Carney et al., 1997; Grosvenor & Goss, 1998) have been reported in human myopes, but not in all studies (Cho & Lam, 1999; Fam et al., 2006; Li et al., 2016). In animal models of myopia, corneal steepening was found in myopic chicks (Gottlieb et al., 1987; Troilo et al., 1995), macaque monkeys (Qiao-Grider et al., 2004) and guinea pigs (Howlett & McFadden, 2006), but not in tree shrews (Guggenheim & McBrien, 1996; McBrien et al., 2001). It appears that corneal thinning has not previously been reported in any animal models of myopia. Although it should be noted that chicken

cornea has collagen structure and organization that may contribute to different corneal biometric and biomechanical properties from other species (e.g., radially oriented collagen fibrils and a ring of bones which may be associated with ciliary musculature for corneal accommodation (Boote et al., 2008; Boote et al., 2009; Murphy et al., 1995; Pardue & Sivak, 1997)), their corneas share many similar features such as layer structure and extracellular matrix with humans (Fowler et al., 2004). Therefore, chicks could serve as a useful model for studying biomechanical changes of the cornea during myopia development. In further studies, it would be of interest to examine how corneal biomechanical properties altered in eyes developing myopia, and to determine whether other treatment paradigms – such as lens-induced defocus – lead to comparable biomechanical changes to the cornea.

How might corneal biomechanical properties be involved in form-deprivation myopia (FDM) development? It should be noted that the biometric and biomechanical changes of the myopic cornea in this study resemble those reported in the sclera of myopes in previous studies. Specifically, in tree shrews, FDM has been shown to reduce scleral thickness at the posterior pole (Phillips et al., 2000) and increase the creep rate of the sclera at both the posterior pole and equatorial region (Phillips et al., 2000; Siegwart & Norton, 1999). FDM in chicks also increased the creep rate of the posterior and equatorial sclera, but it had no significant effects on scleral thickness or secant elastic modulus (Phillips et al., 2000), probably in part because the chick sclera includes an inner cartilaginous layer, in addition to an outer fibrous layer that is homologous to the sclera of tree shrews and other mammals, and in part because of differential molecular changes in these tissue layers during myopia development (Marzani & Wallman, 1997; Rada & Brenza,

1995). Because changes in creep rate in tree shrew were significantly associated with both vitreous chamber elongation and myopia severity, but not with changes in scleral thickness, it is possible that the axial elongation during myopia progression is related to extracellular molecular changes (Guggenheim & McBrien, 1996; McBrien et al., 2001; Phillips et al., 2000; Siegwart & Norton, 1999) that might alter the creep rates in mammalian sclera (Phillips et al., 2000; Siegwart & Norton, 1999). Given the results in tree shrews (Phillips et al., 2000; Siegwart & Norton, 1999) and the lack of significant change in scleral thickness in this study (Table 3.1, mean difference between treated and fellow untreated eye (mean ± SD)= –4.02 ± 30.89 μm; $t(11)= -0.45$, p= 0.66), it is less likely that scleral thinning *per se* causes a significant reduction in scleral biomechanical properties. Nevertheless, the thinning and deformation of the cornea (Table 3.1) in the highly myopic chick eyes, and the significant associations between the two corneal biomechanical indices and the essential structural (vitreous chamber depth) and refractive components (spherical-equivalent refractive error), indicate that corneal biomechanical properties are sensitive to myopia development in chicks. In light of the results from tree shrews, which showed a significant association between scleral biomechanics and axial elongation rate, but not axial length per se (Grytz & Siegwart, 2015; Siegwart & Norton, 1999), further studies are needed to determine the relationships (e.g., time course of change) of scleral and corneal biomechanical properties, to one another, as well as to the underlying molecular mechanisms.

Although the application of the novel OCT-indentation probe system on a myopia model provides new insights into the association between individual ocular component dimensions vs. corneal biomechanics, several improvements in

methodology may be considered in future experiments. *First*, at the 1 mm-depth maximal indentation, it was observed that the deformed central corneal area could be as wide as approximately 2.5 mm in diameter. Because the corneal thickness and curvature change gradually from center to periphery, the biomechanical properties measured might be affected by the variability of these biometric properties with a location in the deformed area. Whether a probe of smaller diameter might provide more accurate measurements needs to be investigated; using our current device to measure the biomechanical properties of a species with a still smaller cornea – which is likely to have greater regional structural variation – would make this potential source of bias even more important. *Second*, the corneal thickness parameter used to calculate the tangent modulus was acquired by A-scan ultrasonography one day before the biomechanical measurement. While this delay after A-scan was designed to prevent any adverse influence of corneal hydration (due to the application of ultrasound gel) by allowing a day for complete recovery after ultrasonography, the possibility remains that corneal thickness might have changed during that interval, or might vary during the biomechanical measurement. Real-time measurement of corneal thickness may be achieved in the future, by analyzing the two peaks representing the anterior and posterior corneal surfaces in the OCT image (see Figure 3.2B). *Third*, tissue-mimicking corneal phantom cannot fully represent the viscoelastic nature of real cornea which has highly organized complex structure of collagen fibrils (Meek & Boote, 2004; Meek & Knupp, 2015). Additional validation experiments of measuring Young's modulus of real corneal tissues by the extensometry instead of corneal phantom will be necessary to ensure whether the improved OCT-indentation probe can accurately

derive the corneal biomechanical properties in the future experiments. *Fourth*, holding IOP near the physiological limit in chicks might have influenced the measurements of corneal biomechanical properties. Unlike the 5 mmHg and 15 mmHg conditions, the maximal indentation under 25 mmHg conditions led to an instantaneous increase of IOP by about 2 to 3 mmHg, as recorded by the pressure transducer. Because such a sudden increment in IOP has been associated with reduced CCT (Park et al., 2013) and decreased ACD (He et al., 2012), in mammalian animal models, this might be the reason why higher standard deviations of TM and CS were noted at 25 mmHg.

In conclusion, significantly lower corneal tangent modulus and stiffness coefficient were demonstrated in the thinner, steeper cornea of highly myopic chicks.

Chapter 4*

Corneal proteome and differentially expressed corneal proteins in highly myopic chicks using a label-free SWATH-MS quantification approach

(*Part of the content of this chapter is reproduced with permission from: Kang, B. S., Lam, T. C., Cheung, J. K. W., Li, K. K., & Kee, C. S. (2019). Data on corneal proteome and differentially expressed corneal proteins in highly myopic chicks using a data independent quantification approach. Data in brief, 26, 104478. A revised version of this chapter has been submitted for review.)

Abstract

Purpose: To establish chicken corneal proteome and identify differentially expressed corneal proteins during high myopia development.

Methods: Monocular form-deprivation (FD) myopia was induced in the right eyes of eight chicks from day 5 to 12 while the left untreated eyes served as fellow-contralateral controls. At the end of the treatment, ocular biometric measurements (refractive error, ocular axial dimensions, and corneal radius of curvature) were performed, and three chicks were screened and euthanized for corneal tissues

collection. After protein/peptide extractions, samples were fractionated by offline high-pH reversed-phase peptide fractionation technique to increase the corneal proteome. Then, mass spectrometry integrated with information dependent acquisition (IDA) and data independent acquisition (DIA; SWATH-MS) were performed to identify and screen differentially expressed proteins, respectively.

Results: Significantly high myopia was induced in FD-treated eyes compared to untreated fellow-contralateral eyes (mean±SD: –24.91 ± 4.66 D vs. 0.79 ± 1.15 D; paired t-test, $p<0.001$). Similar to the previous study, several ocular biometric changes were found in the treated eyes: higher corneal power (mean±SD: 118.02 ± 2.54 D vs. 112.05 ± 2.96 D; paired t-test, $p<0.001$), deeper anterior chamber depth (mean±SD: 1479.56 ± 138.60 µm vs. 1281.71 ± 52.52 µm; paired t-test, $p<0.01$), and reduced corneal thickness (mean±SD: 188.24 ± 6.08 µm vs. 196.78 ± 9.41 µm; Mann-Whitney U-test, $p<0.05$). As a result of IDA analysis, a total of 2096 unique proteins (13081 peptides) were discovered at 1 % global FDR. This spectral library was further used for SWATH-MS analysis to identify eight corneal proteins (Reactive intermediate imine deaminase A homolog, Cadherin-1, RuvB-like helicase, Fibrinogen alpha chain, Fibrinogen beta chain, Fibrinogen gamma chain, Alpha-2-macroglobulin-like 4, and Chromobox 3 protein) that might be significantly and differentially expressed in high myopia.

Conclusions: This study comprised the first chicken corneal proteome investigation combined with identification of differentially expressed corneal proteins in highly

myopic eyes by applying state-of-the-art bioinformatics analysis. Results suggested that molecular activities might be involved during the structural changes of the cornea during myopia development.

Introduction

The cornea is a transparent, curved shaped structure that occupies one-third of the eye shell and accounts for the majority of the refractive power of the eye. Approximately 80 % of mass and volume of the cornea consists of a dense, interwoven collagen tissue – the stroma. The highly organized collagen fibrils spacing with a homogenous diameter within the stroma ensures the clearness of light refraction and geometrical properties (Meek, 2009). The primary focus of cornea research has been either managing disrupted collagen distributions caused by pathologies (Zhou et al., 2017) or refractive surgeries (Farah et al., 1998) to restore visual clarity, there has been little interest in the understanding of corneal changes during refractive development. Despite the increasing myopia prevalence (Holden et al., 2016) and potential ocular complications arising from high myopia development (Saw et al., 2005), few studies have investigated the relationship between corneal geometries and the degree of refractive errors in humans (Carney et al., 1997; Grosvenor, 1988; Grosvenor & Goss, 1998; Horner et al., 2000; Leung et al., 2013).

While genomics has extended the understanding of etiology of diseases, it possesses a critical limitation that mRNA levels may not fully reflect the level of final products (Lundberg et al., 2010; Vogel et al., 2011), proteins, mainly because of alternative splicing and post-translation modification (PTM) (Cho, 2007; Manzoni et al., 2018). This led a natural movement from genomics to proteomics; however, highly sensitive and reproducible analytical methods are required as proteins

cannot be amplified like DNA (by polymerase chain reaction), making less abundant proteins difficult to detect (Cho, 2007). Compared to classic proteomics methods (e.g, gel electrophoresis) with restriction in low throughput and specificity, mass spectrometry (MS) effectively facilitates the investigation of complex protein mixtures. Among several types of MS available (Bantscheff et al., 2012; El-Aneed et al., 2009), this study applied a hybrid quadrupole time-of-flight MS analytical proteomic technique (Andrews et al., 2011; Shan et al., 2018) integrated with the novel sequential windowed acquisition of all theoretical mass spectra (SWATH-MS) (Gillet et al., 2012; Shan et al., 2018). In this approach, ionized peptides within the given range of the entire mass to charge ratio (m/z) are fragmented and recorded systematically in an unbiased fashion (data independent acquisition; DIA) (Ludwig et al., 2018; Shan et al., 2018). Protein/peptide identification and quantification are performed in a targeted approach based on the prerequisite ion spectral libraries collected by information dependent acquisition (IDA), which contain intensities, m/z, and retention time of all precursors and their corresponding ion fragments (Schubert et al., 2015). Since proteins that are not listed in the ion spectral libraries cannot be analyzed and quantified, generating a comprehensive library that covers the extensive range of protein pools is crucial (Frederick & Ciborowski, 2016). There have been successful investigations of the human corneal proteome (Dyrlund et al., 2012; Karring et al., 2005; Meade et al., 2009), but the chicken corneal proteome was not available because their corneas have not been used for proteomics-based research, unlike other ocular tissues such as the retina and vitreous (Lam et al., 2006; Yu et al., 2017). In a pilot study, a total of 1214 corneal proteins were identified (unpublished) as an ion library from untreated chicken eyes. However,

this ion spectral library had fundamental limitations: 1) the corneal proteins that appeared exclusively in myopic eyes were unquantifiable as they were not listed; and 2) low-abundant proteins might have been masked by plentiful proteins (e.g., collagens). To overcome these limitations, this experiment included corneas from highly myopic eyes as well as untreated control eyes for generating an in-depth ion spectral library using offline peptide fractionation technique (Scientific, 2016). By integrating the generated library, differentially expressed corneal proteins in myopic eyes could be screened by applying SWATH-MS coupled to bioinformatics (Kang et al., 2019).

Several animal models are used for myopia research (Mcfadden & Wallman, 1995; Schaeffel et al., 2004; Sherman et al., 1977; Troilo et al., 2019; Verolino et al., 1999; Wiesel & Raviola, 1977), but chicken is a particularly effective model for corneal studies (Wisely et al., 2017). First, the chicken cornea is composed of five distinct layers similar to those in the human cornea, while other animals, such as rabbits and rodents lack the Bowman's layer (Fowler et al., 2004; Ritchey et al., 2011). Second, although chicken has a slightly thinner cornea than the human, the relative thickness ratio is very similar (Ritchey et al., 2011). In addition to similarity of anatomical features, the corneal morphology of chickens is responsive to various visual experiences (Kee & Deng, 2008; Kee et al., 2005; Lauber & Oishi, 1987) and lighting conditions (Cohen et al., 2008; Rucker et al., 2015), which support the use of chicken corneas over those of other species.

Methods

Animals

Eight White Leghorn chicks (*Gallus gallus domesticus*) were raised in the Centralized Animal Facility of The Hong Kong Polytechnic University. During the experimental period, chicks were given food and water *ad libitum*. The luminance of the animal room was maintained at 150 lux at chicks' eyes level with a 12 hr:12 hr light-dark cycle. All experiments were conducted in accordance with the ARVO Statement for the Use of Animals in Ophthalmic and Vision Research and approved by the university's Animal Subjects Ethics Sub-Committee (ASESC 16-17/22).

Treatments

Form deprivation (FD) paradigm was used to induce high myopia from day 5 post-hatching (P5) by gluing detachable plastic-molded translucent diffusers (mean light transmission= 30 %) onto a Velcro ring over the feathers of right orbit. Left eyes were untreated and served as contralateral controls. During the 7-day treatment period, the diffusers were cleaned regularly to prevent dust and moisture from reducing light transmittance.

Ocular Biometric Measurements

At the end of treatment period (P12), biometric measurements, including corneal videokeratography, ocular axial dimensions, and refractive status were performed as described in the previous study (Kang et al., 2018). Briefly, a custom made videokeratography system (VKS) was used to measure corneal astigmatism and corneal power (Chu et al., 2014). Approximately 600 consecutive corneal images were captured by a CCD camera with a frame rate of 60 frames per second (Guppy GF 046B, Allied Vision, Germany) after aligning the pupillary center with the Placido rings. The distance between adjacent reflected concentric rings was used to exclude images of accommodated cornea (constricted Placido rings), and around four to five images per eye were manually chosen for image analysis using a custom-written MATLAB algorithm. The corneal radii of curvature and astigmatic components (J0 and J45, calculated by Power vector analysis) derived from these images were averaged (Thibos et al., 1997). In order to screen eyes with similar biometric changes (see details in Tissue Collection), chicks were then anesthetized with isoflurane inhalation (1.5 % to 2.0 % with oxygen) to collect ocular axial dimensions measured by a high-frequency A-scan ultrasonographer (GE Panametrics, U.S.). Three measurements per eye, each measurement consisting of 30 data sets were conducted and averaged after manually identifying peaks representing the inner ocular surfaces (Nickla et al., 1998). Then, a minimum of three refractive error measurements was carried out per eye using a modified Hartinger refractometer (Kee & Deng, 2008) and averaged for spherical equivalent, J0, and J45 astigmatic components.

Tissue Collection

Entire procedures of sample preparation for proteomic analysis has been described in the previous study (Kang et al., 2019). FD treatment typically induces high myopia with high inter-subject variability. To minimize the potential effects due to this variability on proteomics analysis, only three out of the eight chicks having high myopia (> 20 D) with similar interocular changes in the corneal radius of curvature (< –7 %) and axial length (> +9 %) were selected. After the chicks were sacrificed by carbon dioxide asphyxiation, both eyes were enucleated and placed in chilled-PBS. Eyes were hemisected along the ora serrata using a razor blade. The ciliary body and crystalline lens were discarded gently, and the anterior segments were washed briefly in chilled-PBS to remove aqueous humor. Corneal tissue samples of 4-mm diameter were collected using sterilized Biopsy Punches (Integra™, Miltex, U.S.). Collected tissues were rinsed again with chilled-PBS and snap-frozen in liquid nitrogen.

Homogenization

Each corneal tissue sample was loaded to a homogenizer (Precellys Evolution, Bertin Instrument, France) with 100 µL of a customized lysis buffer [30 mM tris-HCl (pH 8.5), 7 M urea, 2 M thiourea, 2 % (v/v) CHAPS, 1 % (v/v) ASB14 with a protease inhibitor cocktail (cOmplete™, Roche Molecular Systems, U.S.)]. Samples were homogenized with two cycles of 30 seconds at 6800 RPM under cool

conditions. After lysates were collected, they were centrifuged for 25 minutes at 6800 RPM individually before clear supernatants were collected. The concentration of lysed protein was then quantified using a 2-D Quant Kit (GE Healthcare, U.S.) following the manufacturer's instructions.

Sample Preparation

Based on the protein concentration, samples were diluted with the same lysis buffer to achieve equal concentration and volume (25 µL; 2.5 µg/µL) for faster sample preparation procedures. The identical amount of proteins from each sample was extracted and equally pooled for the purpose of building an IDA spectral library. For protein reduction, 0.1 M dithiothreitol (DTT) was added (final concentration= 10 mM DTT) and the mixture incubated for 45 minutes at 37 °C. Following this, 0.2 M iodoacetamide (IAA) was added (final concentration= 20 mM IAA) and the mixture further incubated for 20 minutes in a dark room. Samples were then suspended in 100 % (v/v) acetone (volume= volume of sample x 4) and stored in a –25 °C freezer overnight. The suspended samples were precipitated by 20-minute centrifugation at 4 °C. The supernatant was discarded and samples were re-suspended in 80 % (v/v) acetone, followed by centrifugation. After removing the acetone, the tubes containing the pellets were completely dried at room temperature for 5 hours. Then, 8 M urea dissolved in 0.1 M TEAB was added to tubes. Samples were digested with trypsin (1 µg per 25 µg protein amount), followed by incubation in a temperature-controlled (37 °C) shaking chamber (ThermoMixer, Eppendorf, Germany) for 18 hours. Contaminants in the sample,

including detergent, buffer salts, and organic modifiers (e.g., DTT and urea), which could influence the quality of MS data (Azarkan et al., 2007; Larsen et al., 2002) were then removed using cleanup kits (Oasis® HLB Sorbent Cartridge, Waters, U.S.), and the samples were re-suspended by adding 0.1 % (v/v) formic acid.

Offline High-pH Reversed-phase Peptide Fractionation

The pooled corneal peptide samples (total= 13 µg) were fractionated by using a kit (Pierce™ High-pH Reversed-phase Peptide Fractionation Kit, Thermo Fisher Scientific, U.S.) according to the manufacturer's instructions. Briefly, columns in the kit were centrifuged to remove the solution and pack the resin material, followed by adding 300 µL of 100 % (v/v) ACN and 0.1 % (v/v) TFA (trifluoroacetic acid) with centrifugation for column conditioning. For a flow-through fraction, 0.1% TFA was added to each sample and they were loaded into columns for centrifugation. The resins in the columns were then washed by adding water with centrifugation. Retained fractions were eluted by adding step gradient elution solutions with either 12.5 % or 50 % (v/v) ACN dissolved in 0.1 % (v/v) TFA. Collected fractions were dried and re-suspended by adding 0.1 % (v/v) formic acid. After performing a peptide assay using a kit (Pierce™ Quantitative Colorimetric Peptide Assay, Thermo Fisher Scientific, U.S.), samples (2 µg each) were loaded for MS analysis.

LC-MS/MS Configuration

A hybrid TripleTOF® 6600 quadrupole Time-of-Flight mass analyzer (Sciex Framingham, MA) connected to a nano LC415 was applied for proteomic data acquisition. Digested samples (2 µg) were loaded to a trap column (350 µm x 0.5 mm, C18) for 15 minutes with a flow rate of 2 µL·min−1 with loading buffer (2 % (v/v) ACN with 0.1 % (v/v) formic acid). Then, samples were separated on the analytical column (100 µm x 30 cm, C18) in the mixture with a flow rate of 350 µL·min−1 using the gradient: 0-0.5 min: 5 %B, 0.5-90 min: 10 %B, 90-120 min: 20 %B, 120-130 min: 28 %B, 130-135 min: 45 %B, 135-141 min: 80 %B, 141-155 min: 5 % with solvent A (2 % (v/v) ACN with 0.1 % (v/v) formic acid) and B (98 % (v/v) ACN with 0.1 % (v/v) formic acid). Samples were conveyed to TripleTOF 6600 through 10 µm SilcaTip electrospray emitters (New Objective, U.S.). For data acquisition, a high-resolution TOF-MS scan mode with a mass range of 350 to 1500 m/z was set while a 100 to 1800 m/z mass range was set for MS/MS. Intensity (ions greater than 125 cps) was one of the selection criteria for parent ions. Collision-induced dissociation was triggered by rolling collision energy. The ion accumulation time was set to 250 ms (MS) and 80 ms (MS/MS). For data independent acquisition (SWATH-MS), the instrument was set for variable isolation window in a looped mode over the mass range of 100 to 1800 m/z scans of 100 variable windows with an accumulation time of 30 ms.

Protein Identification by IDA

Three types of reference proteome libraries were generated using the same pooled sample with two technical replicates (2 µg each): high-pH reversed-phase fractionated peptide lysates with two different gradients (12.5 % and 50 % v/v ACN; see details in Offline High-pH Reversed-phase Peptide Fractionation) and unfractionated control. For generating a comprehensive library, acquired MS raw data (.wiff) from both the fractionated and unfractionated samples were loaded and digitally integrated in ProteinPilot software (Version 5.0.1, Sciex Framingham, MA) with Paragon Algorithm (Shilov et al., 2007) to form the combined spectral ion library (i.e. comprehensive= fractionated + unfractionated control; fractionated= 12.5 % + 50 % v/v ACN; and unfractionated control). Protein identification was performed based on the Uniprot database (Taxonomy_9031_Gallus gallus) with options available for searching parameters of trypsin digestion, iodoacetamide cysteine alkylation, and thorough search. The protein detection threshold (Unused Protscore) was set to >0.05, equivalent to a confidence level of 10 %, and a false discovery rate (FDR) analysis was also performed. Only screened proteins at 1 % global FDR were considered for protein counts and further bioinformatics analysis.

SWATH-MS

Six samples (3 myopic and 3 contralateral fellows; 2 µg each) were loaded to MS with two technical replicates. The raw data generated (.wiff) were processed with PeakView software (Version 2.1, Sciex Framingham, MA) to extract relevant transitions of each identified peptide/protein. Two reference proteome libraries,

produced from IDA analysis (comprehensive and high-pH reversed-phase fractionated) were used for matching the corresponding peptide fragment peaks. Then, a minimum of 10 peptides with high signal/noise ratio in-between 30 and 130 min of the run was selected for retention time calibration. Following parameters were set before peak extraction: 10 peptides per protein, 6 transitions per peptide, and a 10-min extracted-ion chromatogram (XIC) with 75 ppm width. Peptide confidence and FDR thresholds were given at 95 % and 1 % respectively. Resulting data were exported to MarkerView software (Version 1.3.1, Sciex Framingham, MA) for normalization using most likely ratio (MLR) method (Lambert et al., 2013), followed by statistical analysis (unpaired *t*-test). Raw data generated from IDA analysis and SWATH-MS are available at Peptide Atlas public repository (http://www.peptideatlas.org/PASS/PASS01410) for general release.

Bioinformatics Analysis

Protein IDs from the generated IDA library were categorized by gene ontologies (cellular component, molecular function, and biological process) using the online database Panther Gene Ontology (GO) (http://www.pantherdb.org/) (Mi et al., 2017). Significantly differentially expressed proteins found in SWATH-MS analysis were visualized using a Venn diagram, and the list of proteins shared in multiple libraries was investigated. These proteins were further searched in the UniProt protein database (http://www.uniprot.org/) (UniProt, 2019) to determine their functional information. Additionally, a protein-protein interaction network was analyzed using STRING V11 (online pathway analysis tool; https://string-

db.org/) (Szklarczyk et al., 2019). The outline of the proteomic experiment workflow is summarized in Figure 4.1.

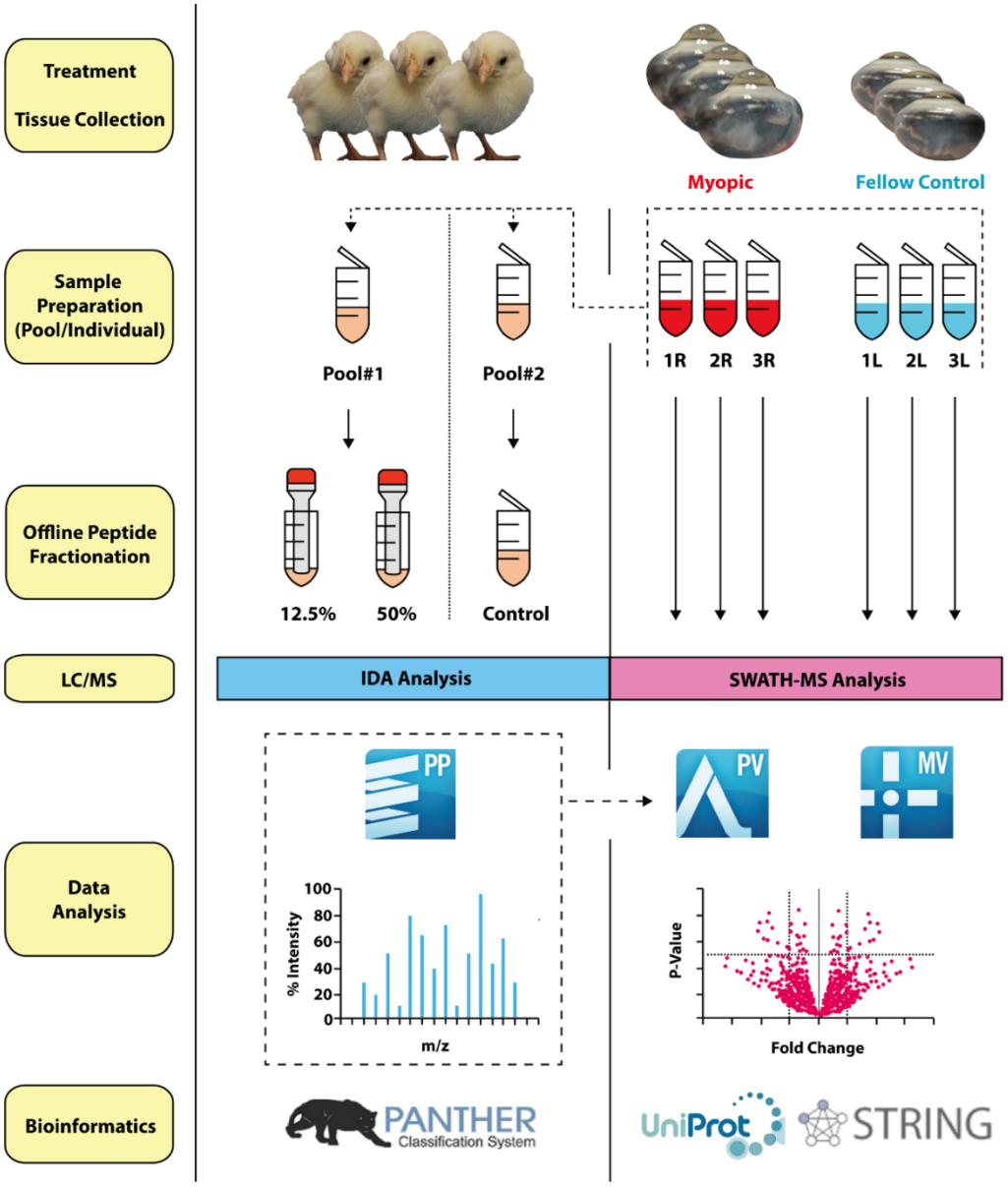

Figure 4.1. A schematic diagram showing the workflow of proteomic analysis. The experiments were divided into two phases: Left) generating ion spectral library using IDA analysis integrated with ProteinPilot (PP), and Right) discovery of differentially expressed proteins via SWATH-MS analysis integrated with PeakView (PV) and MarkerView (MV).

Results

As expected from the previous study (Kang et al., 2018), FD treatment for 7 days induced extremely high myopia (Figure 4.2A, mean±SD: –24.91 ± 4.66 D vs. 0.79 ± 1.15 D; paired t-test, $p<0.001$), accompanied by significant refractive and corneal astigmatisms (Figure 4.3) in right eyes compared to fellow control eyes. Significant anterior ocular biometric changes were observed in the highly myopic eyes: deeper anterior chamber depth (mean±SD: 1479.56 ± 138.60 μm vs. 1281.71 ± 52.52 μm; paired *t*-test, $p<0.01$), stronger corneal power (mean±SD: 118.02 ± 2.54 D vs. 112.05 ± 2.96 D; paired *t*-test, $p<0.001$), and reduced central corneal thickness (mean±SD: 188.24 ± 6.08 μm vs. 196.78 ± 9.41 μm; Mann-Whitney *U*-test, $p<0.05$). Correlation analysis of treated eyes showed that spherical-equivalent refractive error was significantly correlated with anterior segment parameters (Table 4.1): anterior chamber depth (Pearson's $r= -0.629$, $p<0.01$), corneal power ($r= -0.707$, $p<0.01$), and central corneal thickness ($r= +0.513$, $p<0.05$).

To generate a comprehensive proteome spectral library by IDA analysis, corneal tissue samples from both treated and fellow control eyes were pooled and fractionated or served as unfractionated controls. Fractionated samples, which combined two technical replicates, showed distinctive protein numbers and distributions at two gradient levels (1623 at 12.5 % vs. 1396 at 50 %; 817 shared; Figure 4.4A and 4.5A). Compared to the library of the unfractionated control sample, a noticeably larger number of proteins were detected through fractionated samples (2016 vs. 1487), as many as 764 proteins also appeared exclusively after

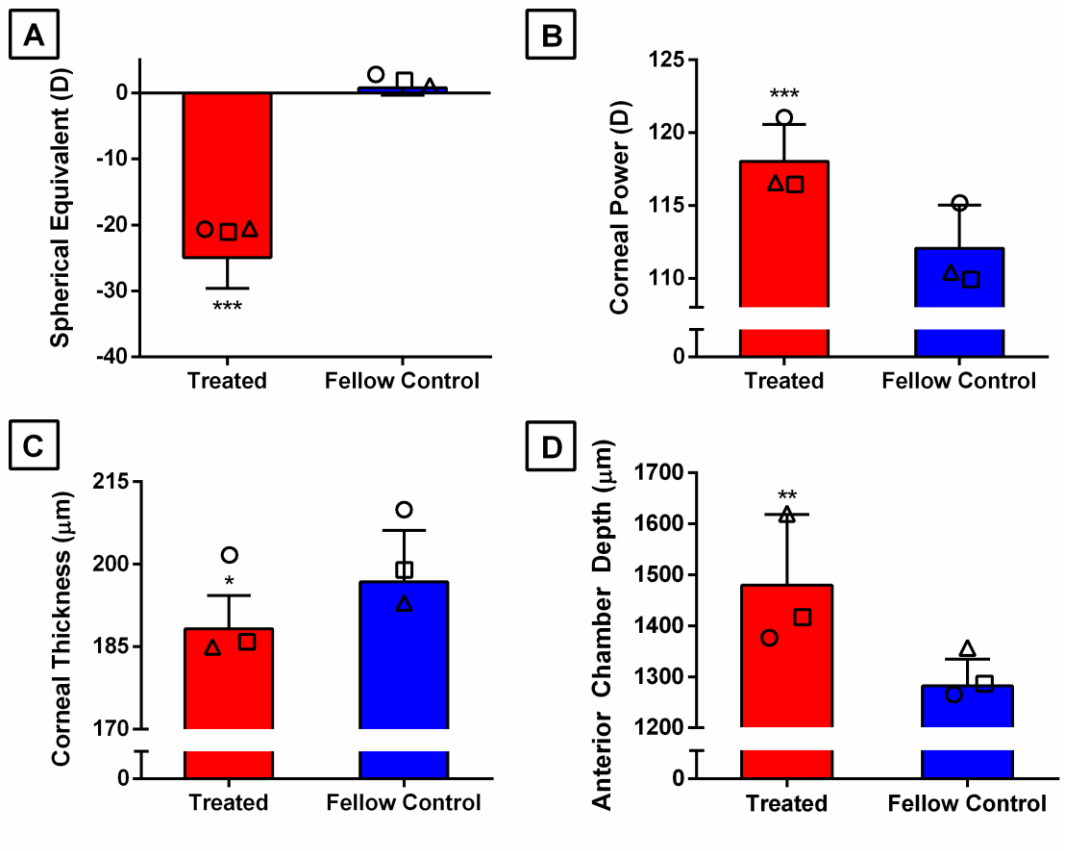

Figure 4.2. Ocular biometric parameters after a week of FD treatment. Treated eyes developed extremely high myopia (A) with a steeper cornea (B), a thinner cornea (C), and a deeper anterior chamber depth (D). Data from the same bird are represented with the same symbol. Paired t-tests were performed on all parameters except central corneal thickness (Mann-Whitney U-test), *p<0.05, **p<0.01, ***p<0.001. Bars represent mean±SD.

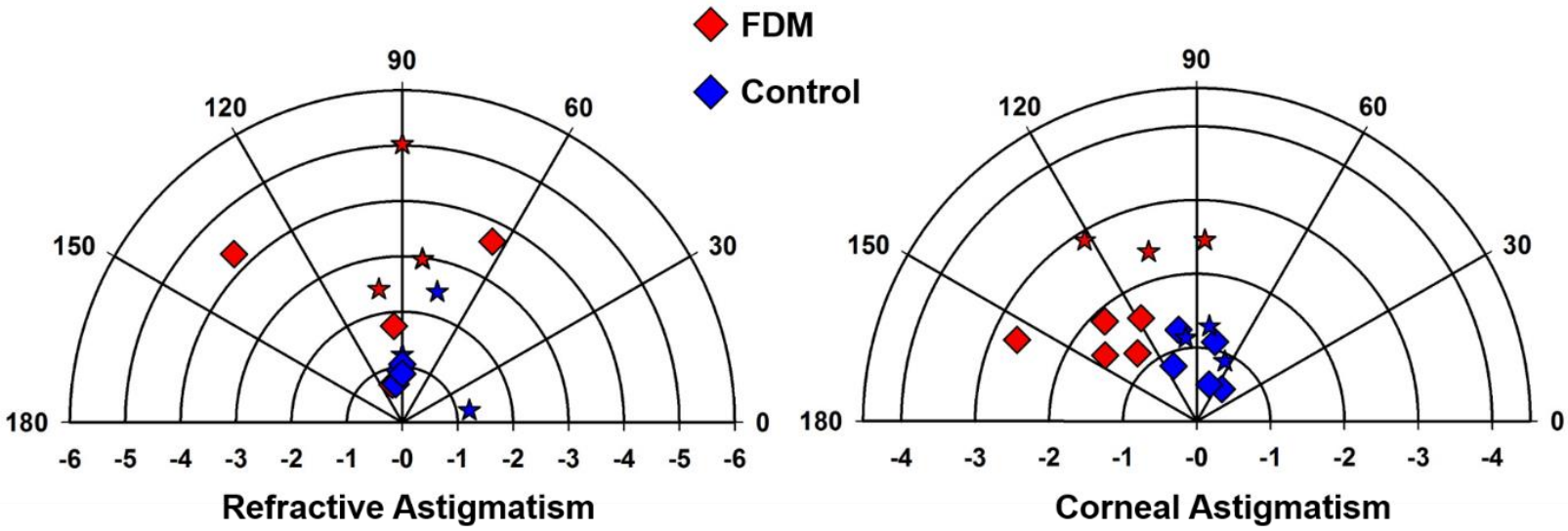

Figure 4.3. The distributions of refractive and corneal astigmatisms in all eight FD-treated chicks. Each symbol in the polar plot represents the magnitude (radius) and axis (angle) of refractive (left) and corneal (right) astigmatism for one bird. Star symbols (★) indicate the eyes used for proteomic analysis.

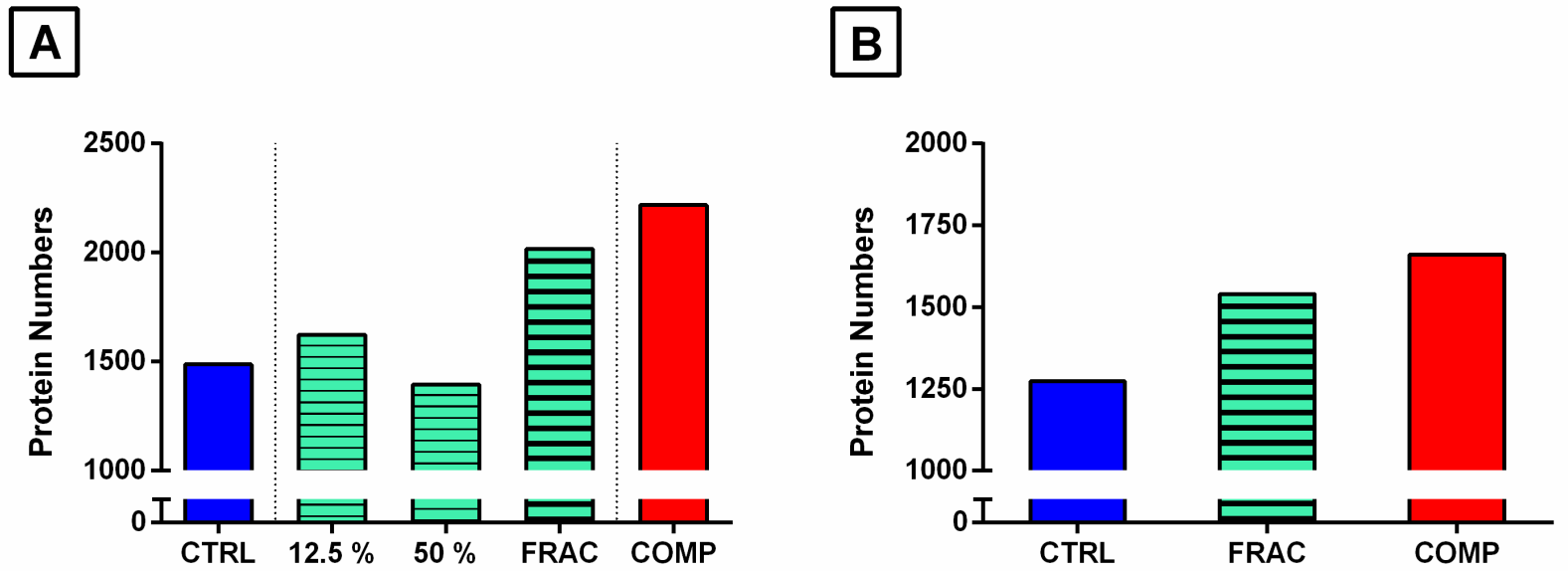

Figure 4.4. (A) number of proteins derived from IDA-based ion spectral libraries with offline peptide fractionation. (B) number of proteins derived by SWATH-MS analysis. Protein identification was performed at 1 % FDR cutoff. CTRL= control library from the unfractionated control sample; 12.5% and 50 %= fractionated libraries from offline peptide fractionated samples in two ACN gradients; FRAC= fractionated library by combining 12.5% and 50 %; COMP= comprehensive library by combining FRAC and CTRL.

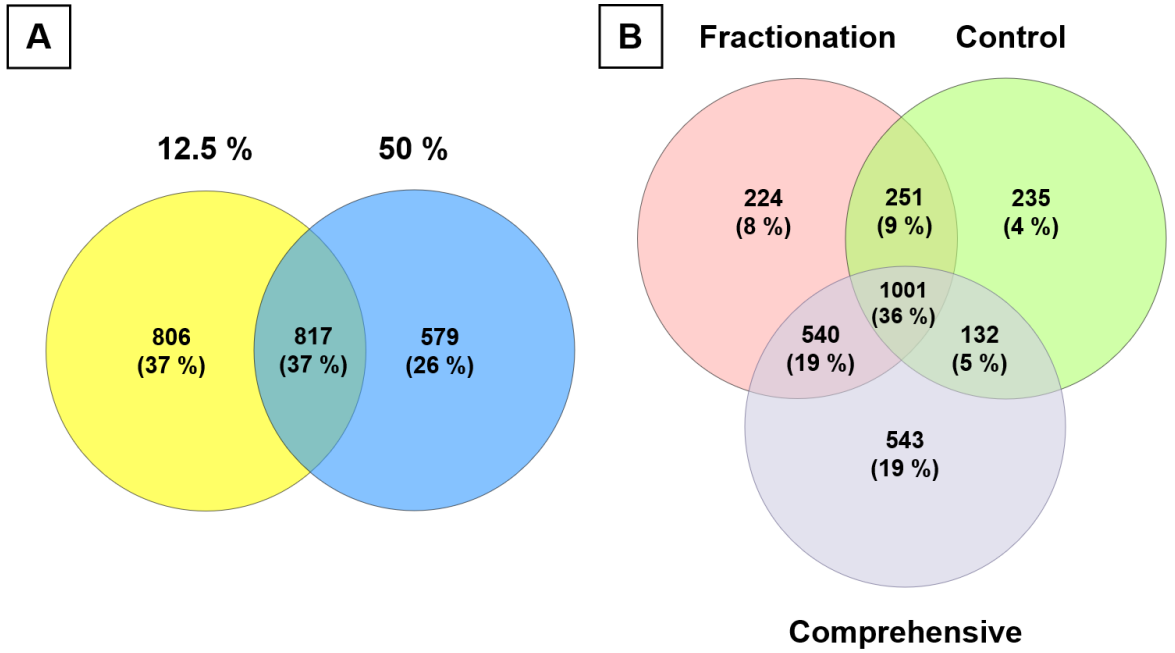

Figure 4.5. Venn-diagrams showing: A) number of proteins detected from two gradient eluting solutions (12.5 % and 50 % ACN) using derived fractionated libraries; B) protein distributions across all libraries. The percentage in parentheses refers to: (number of proteins/total number of proteins) * 100.

Table 4.1. Pearson's correlation analysis between ocular refractive and axial components.

	SE	RA	CP	CA	CCT	ACD	VCD
SE	1	.669**	-.707**	.684**	.513*	-.629**	-.823**
RA		1	-.678**	.688**	0.146	-0.237	-0.282
CP			1	-.601*	-0.394	0.482	0.386
CA				1	0.184	-0.414	-.568*
CCT					1	-.624**	-.502*
ACD						1	.757**
VCD							1

Note: * p<0.05. ** p<0.01.

Abbreviations: SE, spherical equivalent (D); RA, refractive astigmatism (D); CP, corneal power (D); CA, corneal astigmatism (D); CCT, central corneal thickness (µm); ACD, anterior chamber depth (µm); VCD, vitreous chamber depth (µm)

fractionation (Figure 4.4A and 4.5B). When combining fractionated and unfractionated control IDA libraries, a total of 2096 unique proteins (13081 peptides) were discovered at 1 % global FDR, which can serve as a comprehensive library for the chicken cornea (COMP in Figure 4.4A). Approximately 40 % more proteins were found in this in-depth protein pool compared to the single unfractionated control library – suggesting that the coverage of further protein quantification is more effective by adopting the comprehensive library. The list of identified proteins was further classified using Panther GO into several sub-categories, these included "Molecular Function, Biological Function, Cellular Component, and Protein Class". This classification was performed to visualize overall compositions of the comprehensive library, as well as to compare the proportion of proteins derived from peptide fractionation. As a result, 1347 out of 2096 proteins were mapped to Gene IDs for the analysis (see Figure 4.6 for an overview): 1) the major molecular functions were binding (GO:000548; 36.9 %), catalytic activity (GO:0003824; 37.4 %), and structural molecule activity (GO:005198; 9.0 %); 2) biological functions were cellular process (GO:0009987; 34.8 %), metabolic process (GO:0008152; 25.4 %), and localization (GO:0051179; 13.5 %); 3) regarding cellular components, proteins mostly performed their functions at cell (GO:0005623; 47.7 %), organelle (GO:0043226; 27.2 %), and protein-containing complex (GO:0032991; 11.9 %); 4) three abundant protein classes were nucleic acid binding (PC00171; 14.2 %), hydrolase (PC00121; 12.4 %), and enzyme modulator (PC00095; 11.1 %). To compare protein characteristics between the fractionated and unfractionated control samples, 1260 out of 2016 and 913 out of 1487 proteins, respectively, were mapped in Panther GO. As shown

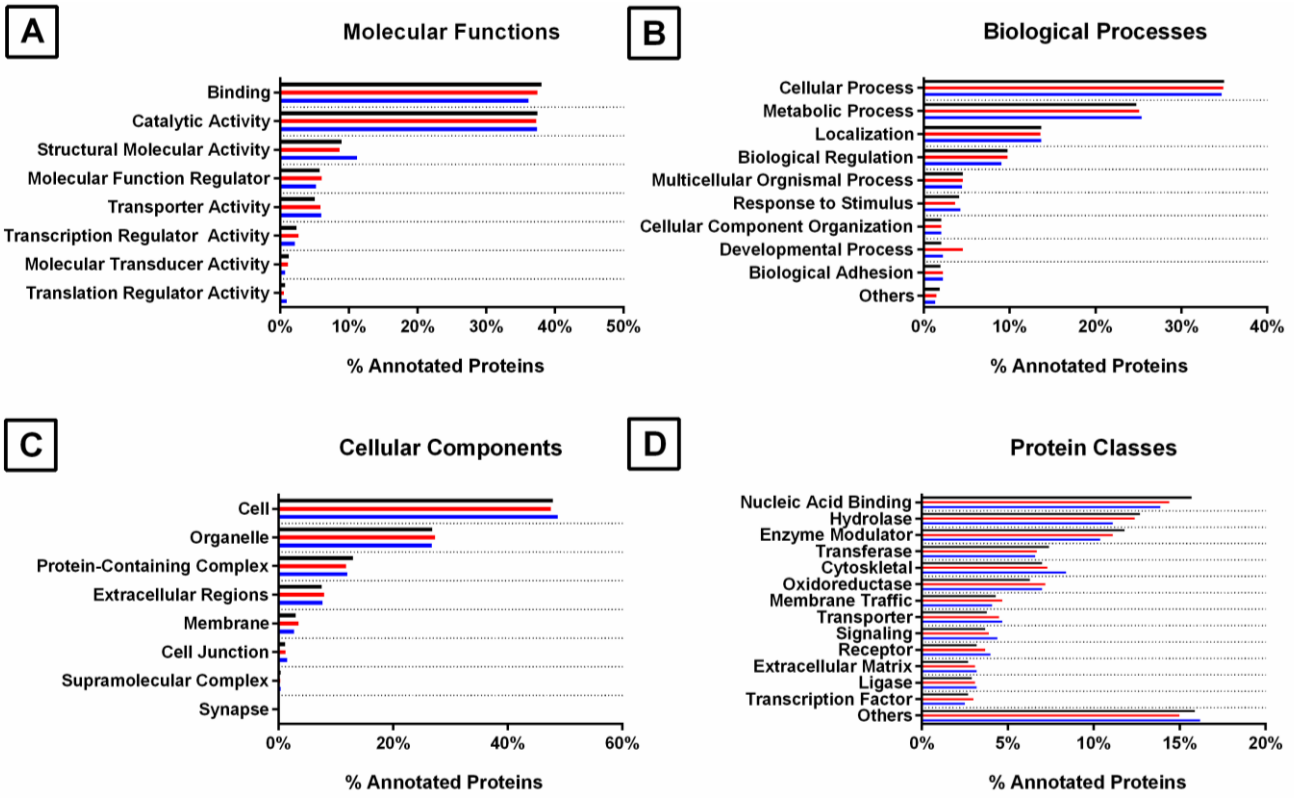

Figure 4.6. The percentage of corneal proteins categorized by molecular functions (A), biological processes (B), cellular components (C), and protein classes (D). Black, red, and blue bars represent comprehensive, fractionated and unfractionated control libraries, respectively.

in Figure 4.4, although the total protein numbers produced by these two methods were quite different, the proportion of proteins in the four GO categories (molecular function, biological process, cellular component, and protein class) were very similar (less than 3 % differences).

Constructed ion-spectral libraries were used for SWATH-MS analysis to screen differentially expressed corneal proteins during high myopia development. The number of quantifiable proteins resulting from integrating different ion spectral libraries is shown in Figure 4.4B, indicating that the coverage of libraries is crucial for increasing analysis depth in SWATH-MS analysis. Proteins IDs in comprehensive (n= 1660) and fractionated (n= 1541) libraries were extracted, and co-expressed proteins in both libraries were filtered. This step increases the reliability of results although the number of quantifiable proteins is reduced (n= 1393). Subsequently, proteins with a minimum of 2 peptides were selected to minimize false-positive findings. Table 4.2 lists and highlights corneal proteins with statistically significant expression in treated eyes compared to fellow control eyes (>1.2-fold differences with statistical significance of $p<0.05$ in both comprehensive and fractionated libraries). After a week of FD treatment, it was found that three proteins were upregulated (RIDA, CDH1, and RUVBL1) and five downregulated (FGG, FGB, FGA, A2ML4, and CBX3) in treated corneas. These eight proteins were then analyzed using the STRING online pathway tool to investigate protein-protein interactions. As a result, Fibrinogen chain proteins (alpha, beta, and gamma) were observed to interact and co-express with Alpha-2-macroglobulin-like 4, while other proteins remained isolated (Figure 4.7).

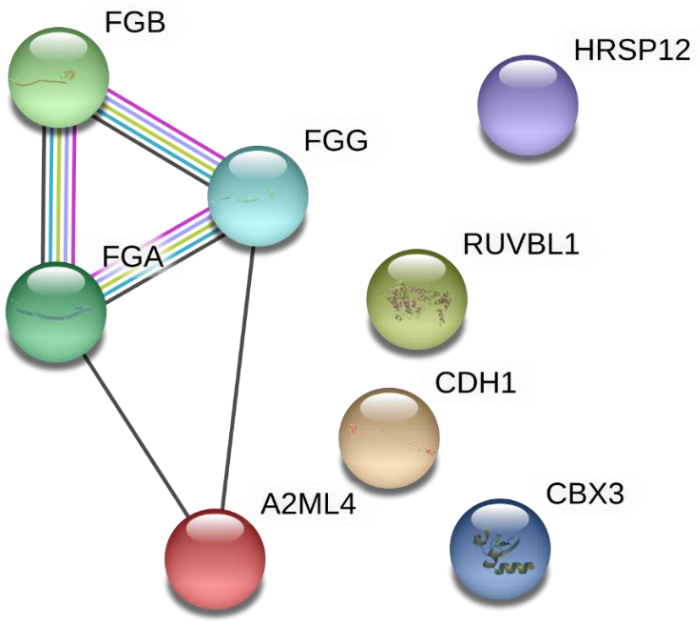

Figure 4.7. A diagram of protein-protein interaction derived from STRING. Fibrinogen chain alpha, beta, and gamma families (FGA, FGB, and FGG) have close interactions with each other and co-express with Alpha-2-macroglobulin-like 4 (A2ML4). Each colored line represents co-expression (black), interaction confirmed from the curated database (cyan), interaction confirmed from the experiment (pink), text mining (yellow), protein homology (light blue). Please refer to Table 4.2 for the abbreviation of annotated proteins.

Table 4.2. Summary of differentially expressed proteins in corneal tissue after FD treatment. SWATH-MS was performed against two sets of in-depth libraries (COMP; comprehensive and FRAC; fractionated). Proteins with significant expression (>1.2-fold differences) were highlighted.

No.	Protein ID	Protein Description	Gene ID	Gene Description	Amino Acid Length	Mass (Da)	Fold changes (COMP)	P-values (COMP)	Fold changes (FRAC)	P-values (FRAC)
1	A0A1L1RZS5	Reactive intermediate imine deaminase A homolog	RIDA	Reactive intermediate imine deaminase A homolog	139	14821	1.3	0.021	1.3	0.013
2	E1C6M9	Cadherin-1	CDH1	Cadherin-1	887	97755	1.2	0.016	1.2	0.041
3	F1N8Z4	RuvB-like helicase	RUVBL1	RuvB-like helicase	456	50180	1.2	0.019	1.2	0.001
4	E1C6J9	Thy-1 membrane glycoprotein	THY1	Thy-1 membrane glycoprotein	161	18173	1.2	0.047	1.1	0.017
5	A0A1L1RIZ2	Calpain small subunit 2	CAPNS2	Calpain small subunit 2	248	27411	1.1	0.031	1.2	0.032
6	A0A1I7Q419	40S ribosomal protein S12	RPS12	40S ribosomal protein S12	121	13529	1.1	0.031	1.2	0.002
7	A0A1D5PKN8	Sulfurtransferase	MPST	Sulfurtransferase	297	33223	1.1	0.002	1.1	0.026
8	F1NHH1	Uncharacterized protein	CSTB	Cystatin B	98	11160	1.1	0.014	1.1	0.039
9	F1P360	Cytoskeleton associated protein 4	N/A	Cytoskeleton associated protein 4	499	56823	1.1	0.043	1.0	0.043
10	R4GL78	Platelet-activating factor acetylhydrolase IB subunit beta	PAFAH1B2	Platelet-activating factor acetylhydrolase IB subunit beta	241	26807	-1.1	0.001	-1.1	0.027
11	F1P2F0	Collagen alpha-3(VI) chain	COL6A3	Collagen alpha-3(VI) chain	3137	339619	-1.1	0.002	-1.1	0.010
12	Q5ZKM2	Elongation factor 1-alpha	RCJMB04_10b5	Elongation factor 1-alpha	462	50139	-1.1	0.029	-1.1	0.002
13	E1C7H6	Serpin family F member 1	SERPINF1	Serpin family F member 1	416	46505	-1.1	0.018	-1.1	0.014
14	Q6QAZ9	Annexin	N/A	Annexin	342	38500	-1.1	0.046	-1.1	0.037
15	F1P4V1	Fibrinogen alpha chain	FGA	Fibrinogen alpha chain	783	87295	-1.2	0.002	-1.2	0.010
16	F1NK40	Uncharacterized protein	A2ML4	Alpha-2-macroglobulin-like 4	1474	163339	-1.2	0.001	-1.2	0.001
17	O93481	Chromobox protein (CHCB2)	CBX3	Chromobox protein (CHCB2)	174	19777	-1.2	0.030	-1.2	0.045
18	F1NUL9	Fibrinogen beta chain	FGB	Fibrinogen beta chain	480	54581	-1.2	0.016	-1.2	0.038
19	E1BV78	Uncharacterized protein	FGG	Fibrinogen gamma chain	438	49955	-1.3	0.008	-1.3	0.005

Discussion

This study yielded three novel findings: 1) chicken corneal proteome was reported for the first time; 2) the most comprehensive corneal proteome pools were successfully generated using IDA analysis with the offline peptide fractionation technique; 3) potential protein biomarkers for high myopia were screened using a novel SWATH-MS integrated with the extensive corneal proteome.

The proteome refers to the set of proteins containing biological information. By knowing and quantifying the proteome in areas of interest (cells, tissues, and organisms), the roles and functions of biomarker proteins in the disease process can be identified. However, although increasing efforts have been devoted to record and establish the complete proteome, there are only a limited number of human corneal proteome studies (Dyrlund et al., 2012; Karring et al., 2005; Meade et al., 2009) with corneal pathologies (Chaerkady et al., 2013; Skeie et al., 2018). Although chicken has been used widely as an effective animal model for eye development and ocular pathologies, its corneal proteome had not been studied (Wisely et al., 2017). This study identified a total of 2096 highly confident proteins in chicken corneas by using state-of-the-art proteomic approaches. This largest proteome database provides an important foundation for future studies using chicken.

Even with the rapid advancement of proteomic analysis methods, understanding the entire proteome is challenging mainly because of the extremely

complex protein structure and the differences in protein abundance. This leads to difficulties in detecting low abundant proteins as they can be masked by a few plentiful proteins (Ly & Wasinger, 2011). Increasing the sensitivity of protein identification by lowering the detection threshold can be a solution; however, the trade-off of false-positive findings inevitably increases. A common alternative to address this limitation is using peptide fractionation strategies. These processes simplify the protein structure in an orthogonal direction and lower the number of proteins per MS analysis by assigning proteins into multiple fractions (Qian et al., 2006) – efficiently enabling the identification of a wide range of proteins. Currently, the majority of proteomic research applies online fractionation methods (Manadas et al., 2010; Smoluch et al., 2016), whereas offline methods are relatively rare, due to the extra manual steps and risk of protein loss during the process. Therefore, in this study, a high-pH reversed-phase peptide fractionation kit was adopted as an extra offline fractionation step (Scientific, 2016), which had the advantage of omitting the desalting step, in which a large amount of protein loss occurs. The detection of 2096 proteins indicates that this extended range of proteins was identified successfully using offline peptide fractionation prior to MS analysis. The current study only applied two ACN levels (12.5 % and 50 %), so it is expected that a larger amount of proteins can be discovered if extra gradient steps are added as described in the manufacturer's instructions.

Ocular tissue biomechanics play an important role in maintaining visual functions (Campbell et al., 2014; Detorakis & Pallikaris, 2013). Instability in biomechanics is frequently associated with various shape-related ocular pathologies. Keratoconus, an abnormal protrusion of corneal shape, is related to

reduced stiffness and altered biomechanics-related microstructures (Romero-Jimenez et al., 2010; Tur et al., 2017). Interestingly, during myopia development, the sclera is known to experience tissue remodeling (weakening) and structural changes (McBrien et al., 2001; Phillips et al., 2000; Siegwart & Norton, 1999) associated with ocular elongation, which is thought to due to remodeling of extracellular matrix (ECM) with molecular changes (Guggenheim & McBrien, 1996; Marzani & Wallman, 1997; McBrien et al., 2001; Moring et al., 2007; Norton & Rada, 1995; Rada & Brenza, 1995; Xi et al., 2017). Both progressive keratoconus (Wollensak et al., 2003) and myopia (Dotan et al., 2014) can be treated by tissue strengthening, supporting the role of ocular biomechanics in eye shape regulation. To date, several myopia-associated corneal biomechanical changes in humans have been reported (Hon et al., 2017; Lee et al., 2016; Radhakrishnan et al., 2012; Shen et al., 2008). However, the underlying mechanism of ocular biomechanics and their relationship with ocular morphologic changes and development are poorly understood. In our recent study (Kang et al., 2018), reduced corneal biomechanics (softening) was accompanied by corneal steepening in experimentally induced highly myopic chicks. Since cornea and sclera are connected anatomically (at microscopic level, collagen fibril bundles are continuous from sclera to cornea) (Boote et al., 2020) and share a similar collagen-dominated structural composition (Meek & Fullwood, 2001), it is reasonable to assume that altered corneal biomechanics may be related to scleral biomechanics, particularly some biomarkers involved in ECM remodeling (e.g., matrix metalloproteinases-2; MMP-2 (Guggenheim & McBrien, 1996; Xi et al., 2017), tissue inhibitor of

metalloproteinases-2; TIMP-2 (Liu et al., 2017; Xi et al., 2017), and transforming growth factor-beta 2; TGF-β2 (Seko et al., 1995; Xi et al., 2017)).

This study applied a non-targeted discovery-based proteomic approach to screen differentially expressed corneal proteins in highly myopic eyes to understand whether ECM remodeling is also involved in corneal structural and biomechanical changes. As a result, eight corneal proteins were found to be expressed differentially (3 upregulated and 5 downregulated) in FD-treated highly myopic eyes. Of note, this list does not include genes previously reported to be involved in ECM remodeling (MMP-2, TIMP-2, and TGF-β2), the expression of these proteins either did not reach statistical significance (MMP-2 and TIMP-2) or was not listed (TGF-β2) in either the comprehensive or fractionated libraries. Nevertheless, it is interesting to note that there was a trend of MMP-2 up-regulation when the interocular comparison was performed on an individual basis (fold changes: bird #1= +1.36; bird 2= +1.13; bird #3= +1.30), indicating that averaging the values across animals might have masked this trend. Also, the increased expression of TIMP-2 (a fold change of +1.36, $p<0.001$) in this study is in agreement with a previous study showing up-regulation of TIMP-2 mRNA expression in FD-treated chick corneas (Xi et al., 2017). Although DIA based SWATH-MS is known to be a stringent, consistent, and reproducible protein quantification tool due to its novel peptide-centric scoring analysis (Ludwig et al., 2018), there should be caution in interpretation of the results as the significantly differential expressions were observed only when comprehensive library for SWATH-MS was applied, probably due to the low abundance of target proteins. Therefore, further targeted proteomic analysis with a capability of detecting changes in low abundant proteins, such as

Multiple Reaction Monitoring High-Resolution (MRM-HR), will be necessary to confirm these findings (Liebler & Zimmerman, 2013; Shan et al., 2018).

The key finding from the eight differentially expressed proteins is the down-regulation of fibrinogen family proteins (FGA, FGB, and FGG). Fibrinogen, a type of glycoprotein, has a series of functions, including blood clotting, fibrinolysis, wound healing, tissue repairing, and inflammatory response (Laurens et al., 2006). It also interacts with several cell types (fibroblast, platelet, and endothelial cell) (Laurens et al., 2006). During the coagulation process after tissue wounding, fibrinogen converts to insoluble fibrin. This fibrin then stabilizes platelets (Fang et al., 2005) and activates the secretion of platelet-derived growth factors, stimulating fibroblasts to produce collagen, glycosaminoglycans, and proteoglycans (Bauer et al., 1985). However, this cascade of molecular events is related to an up-regulation of fibrinogen, in contrast to what was observed in this study (down-regulation) in highly myopic chick corneas. Fibrinogen deficiency could affect normal corneal wound healing (Kao et al., 1998), but it is unclear how down-regulated fibrinogen is associated with myopia. It is possible that the up-regulated MMP-2 trend (see above) is related to down-regulated fibrinogen, based on the recent finding of fibrinogen as an inhibiting factor of MMP-2 (Sarker et al., 2019). Interestingly, another down-regulated protein, alpha-2-macroglobulin-like 4, also inhibits a broad range of proteinases, including the MMP family (Rehman et al., 2013; Rodriguez-Calvo et al., 2015). It is worth noting that cadherin-1 (E-cadherin) was upregulated in the highly myopic chick corneas (Table 4.2). E-cadherin is part of a subfamily of classical cadherins, known for its involvement in cell-cell adhesions, cytoskeleton organization, and cell proliferation suppression (Van Aken et al., 2000).

Deficiency of E-cadherin could promote tumor progression (Bracke et al., 1996), as it inhibits invasion of tumor cells into ECM. In the cornea, E-cadherin is present in the epithelial layer (Mohan et al., 1995) and provides epithelial barrier function by increasing cell to cell interactions (Bardag-Gorce et al., 2016). The weak association between corneal wound healing and E-cadherin expression (Takahashi et al., 1992) suggests that the wound healing process is probably not involved in myopia-associated corneal remodeling. Evidence showing the close relationship between E-cadherin and the MMP family (Nawrocki-Raby et al., 2003) indicates the need to understand the role of E-cadherin in myopia progression. Nevertheless, all these findings support the involvement of MMP-2 in the corneal remodeling process in addition to its involvement in scleral remodeling reported in myopic animals (Guggenheim & McBrien, 1996; Xi et al., 2017).

While this study provided fundamental resources of the chicken corneal proteome, several methodological limitations should be considered for future studies. First, the FD paradigm was employed in this study as a first approach to understand potential molecular changes at protein levels in light of recent findings on altered corneal biomechanical properties in FD treated, highly myopic chicks (Kang et al., 2018). This treatment paradigm induced high myopia and dramatic corneal structural changes within a short period of time but also produced high inter-subject variability (Figures 4.2 and 4.3). This high inter-subject variability could potentially make some proteins with high inter-subject variation undetectable (see MMP-2 discussion above). Mainly because the lens induction paradigm produced much less inter-subject variation compared to FD, applying proteomic analyses on LIM chicks may confirm or even extend the list of

differentially expressed proteins. To date, several proteomic studies using lens-induced myopia (LIM) treatment of chicks have been reported (retina (Lam et al., 2006; Zhou et al., 2018) and vitreous (Yu et al., 2017)) – supporting the efficacy of this treatment paradigm. Second, quantifying protein expression at a single time point has obvious limitations. The time point chosen (one week of FD starting from P5) was based on the significant changes in corneal structural and biomechanical parameters reported recently (Kang et al., 2018). However, caution should be applied when attempting to relate these differential expressions to the cause or effect of the myopia development based on a single time point. A significant knowledge gap remains on the spatial-temporal changes in the molecular pathways regulating myopia development. Thirdly, inadequate sample size may affect the quality of results by restricting the number of technical and biological replicates, which is essential for reliable quantitative analysis. It was observed in the current study that protein concentrations in a single cornea are considerably low compared to other ocular tissues (e.g., retina). Sample pooling could be a possible solution to secure enough samples. However, this could limit the statistical power of biomarker detection by altering mean and standard deviation of analytes (Diz et al., 2009; Molinari et al., 2018).

In conclusion, our study documented, for the first time, the largest corneal proteome of chicken by applying novel bioinformatics analysis with offline peptide fractionation. Differentially expressed corneal proteins in highly myopic eyes using a SWATH-MS strategy suggest that molecular changes at protein level are involved in corneal remodeling at least at this time point. These results provide fundamental

information for future corneal research, especially those using chicken as an animal model for myopia development.

Chapter 5

General Conclusion

Overall, the results presented in previous chapters show: 1) significant changes in anterior ocular biometric and biomechanical parameters in highly myopic chicks; 2) an extensive chicken corneal proteome could be established with an effective paradigm; and 3) highly myopic eyes exhibited differentially expressed corneal proteins.

Because the cornea contributes to a significant amount of eye's refractive power and it is the anterior-most ocular structure, previous studies have investigated whether the cornea is involved during the myopia development. Results of several studies investigating myopia development have been contradictory regarding two representative corneal parameters (radius of curvature and thickness), but the recent introduction of biomechanical indexes have provided new evidence that the cornea may participate in myopia progression. Reduced tissue stiffness is a key indicator when tissue remodeling occurs, including in the sclera; thus, further investigation using an effective animal model is crucial to further our understanding on the mechanistic aspects of myopia development.

The findings presented here add to our current knowledge that not only humans but also chicken corneas can be affected by high myopia development.

Axial elongation, in particular vitreous chamber deepening, is known to be the key structural change in the myopic eye. However, the form-deprived highly myopic chicks not only developed a deeper vitreous chamber, but also significant anterior segment abnormalities (corneal thinning, steeper curvature, and deeper anterior segment), supporting the hypothesis that both posterior and anterior segments are involved in myopia development. Most importantly, these anterior segment changes were associated with altered corneal biomechanical properties and differentially expressed corneal proteins, highlighting the importance of understanding the mechanisms underlying this anterior-most refractive component. Exactly how these multiple biological changes orchestrate myopia development remains unclear. It is possible that the cornea undergoes a similar collagen reconstruction process as those reported in myopic sclera. On the other hand, corneal changes could also be explained by a stretching force driven by posterior ocular segments. Since the cornea is the primary refractive component of the eye and could adversely affect visual quality in myopes, further investigation is crucial to address this mechanism.

There are several limitations in experimental designs of these studies that should be considered for future research in this area. First, all the treatment and measurements were performed at a single time point at which myopia development was already established. This is because our instrument for corneal biomechanics measurements can only be applied to sacrificed chicks. Improving the instrument for longitudinal studies would be helpful to address the causative relationship between corneal changes and myopia, particularly by increasing the speed of probe movement to complete the whole indentation process before

instantaneous reflexive response of nictitating membrane occurs. Second, form-deprivation treatment is an effective way to induce extremely high myopia with dramatic corneal changes but produces high inter-subject variability, which may mask significant biomarkers findings. Applying a lens-induced paradigm could help to confirm these results. Lastly, our studies used a small sample, but statistically significant findings were still observed probably due to the dramatic change in biometric components induced by form-deprivation high myopia. By adopting a lens-induced myopia paradigm in the follow-up study, it may be necessary to use a larger sample size due to smaller changes in biometric components associated with the lower degree of myopia seen in the LIM paradigm.

In conclusion, the results presented in this thesis provide important evidence for anterior segment changes in highly myopic chickens. These structural, biomechanical, and molecular changes can be studied quantitatively with tools now available. With the emerging clinical evidence from human studies that highlight the involvement of anterior segment changes in myopia development, the availability of an effective animal model for studying the underlying mechanism should help address many fundamental research questions related to anterior eye growth.

References

Alonso-Caneiro, Karnowski, Kaluzny, Kowalczyk, & Wojtkowski. (2011). Assessment of corneal dynamics with high-speed swept source Optical Coherence Tomography combined with an air puff system. *Optics Express, 19*(15), 14188-14199.

Altan, Demirel, Azman, Satana, Bozkurt, Demirok, & Yilmaz. (2012). Biomechanical properties of axially myopic cornea. *European Journal of Ophthalmology, 22 Suppl 7*, S24-28.

Andrews, Simons, Young, Hawkridge, & Muddiman. (2011). Performance characteristics of a new hybrid quadrupole time-of-flight tandem mass spectrometer (TripleTOF 5600). *Analytical Chemistry, 83*(13), 5442-5446.

Asaoka, Nakakura, Tabuchi, Murata, Nakao, Ihara, . . . Kiuchi. (2015). The relationship between corvis ST tonometry measured corneal parameters and intraocular pressure, corneal thickness and corneal curvature. *Plos One, 10*(10), e0140385.

Avetisov, Savitskaya, Vinetskaya, & Iomdina. (1983). A study of biochemical and biomechanical qualities of normal and myopic eye sclera in humans of different age-groups. *Metabolic Pediatric and Systemic Ophthalmology, 7*(4), 183-188.

Azarkan, Huet, Baeyens-Volant, Looze, & Vandenbussche. (2007). Affinity chromatography: a useful tool in proteomics studies. *Journal of Chromatography B, 849*(1-2), 81-90.

Bantscheff, Lemeer, Savitski, & Kuster. (2012). Quantitative mass spectrometry in proteomics: critical review update from 2007 to the present. *Analytical and Bioanalytical Chemistry, 404*(4), 939-965.

Bao, Geraghty, Wang, & Elsheikh. (2016). Consideration of corneal biomechanics in the diagnosis and management of keratoconus: is it important? *Eye and Vision, 3*.

Bardag-Gorce, Hoft, Wood, Oliva, Niihara, Makalinao, . . . Niihara. (2016). The role of E-Cadherin in maintaining the barrier function of corneal epithelium after treatment with cultured autologous oral mucosa epithelial cell sheet grafts for limbal ttem deficiency. *Journal of Ophthalmology, 2016*, 4805986.

Bauer, Cooper, Huang, Altman, & Deuel. (1985). Stimulation of in vitro human skin collagenase expression by platelet-derived growth factor. *Proceedings of the National Academy of Sciences of the United States of America, 82*(12), 4132-4136.

Bekesi, Dorronsoro, de la Hoz, & Marcos. (2016). Material properties from air puff corneal deformation by numerical simulations on model corneas. *Plos One, 11*(10), e0165669.

Berman. (2013). *Biochemistry of the Eye*: Springer Science & Business Media.
Blackburn, Jenkins, Rollins, & Dupps. (2019). A review of structural and biomechanical changes in the cornea in aging, disease, and photochemical crosslinking. *Frontiers in Bioengineering and Biotechnology, 7*.
Boote, Dennis, Huang, Quantock, & Meek. (2005). Lamellar orientation in human cornea in relation to mechanical properties. *Journal of Structural Biology, 149*(1), 1-6.
Boote, Hayes, Abahussin, & Meek. (2006). Mapping collagen organization in the human cornea: Left and right eyes are structurally distinct. *Investigative Ophthalmology & Visual Science, 47*(3), 901-908.
Boote, Hayes, Jones, Quantock, Hocking, Inglehearn, . . . Meek. (2008). Collagen organization in the chicken cornea and structural alterations in the retinopathy, globe enlarged (rge) phenotype - An X-ray diffraction study. *Journal of Structural Biology, 161*(1), 1-8.
Boote, Hayes, Young, Kamma-Lorger, Hocking, Elsheikh, . . . Meek. (2009). Ultrastructural changes in the retinopathy, globe enlarged (rge) chick cornea. *Journal of Structural Biology, 166*(2), 195-204.
Boote, Sigal, Grytz, Hua, Nguyen, & Girard. (2020). Scleral structure and biomechanics. *Progress in Retinal and Eye Research, 74*.
Boyce, Grazier, Jones, & Nguyen. (2008). Full-field deformation of bovine cornea under constrained inflation conditions. *Biomaterials, 29*(28), 3896-3904.
Bracke, Van Roy, & Mareel. (1996). The E-cadherin/catenin complex in invasion and metastasis. *Current Topics in Microbiology and Immunology, 213 (Pt 1)*, 123-161.
Bueno-Gimeno, Espana-Gregori, Gene-Sampedro, Lanzagorta-Aresti, & Pinero-Llorens. (2014). Relationship among corneal biomechanics, refractive error, and axial length. *Optometry and Vision Science, 91*(5), 507-513.
Campbell, Bunghardt, Kisilak, & Irving. (2012). Diurnal rhythms of spherical refractive error, optical axial length, and power in the chick. *Investigative Ophthalmology & Visual Science, 53*(10), 6245-6253.
Campbell, Coudrillier, & Ethier. (2014). Biomechanics of the posterior eye: A critical role in health and disease. *Journal of biomechanical engineering, 136*(2).
Caporossi, Mazzotta, Baiocchi, & Caporossi. (2010). Long-term results of riboflavin ultraviolet a corneal collagen cross-linking for keratoconus in Italy: the Siena eye cross study. *American Journal of Ophthalmology, 149*(4), 585-593.
Carney, Mainstone, & Henderson. (1997). Corneal topography and myopia. A cross-sectional study. *Investigative Ophthalmology & Visual Science, 38*(2), 311-320.
Celorio, & Pruett. (1991). Prevalence of lattice degeneration and its relation to axial length in severe myopia. *American Journal of Ophthalmology, 111*(1), 20-23.
Chaerkady, Shao, Scott, Pandey, Jun, & Chakravarti. (2013). The keratoconus

corneal proteome: Loss of epithelial integrity and stromal degeneration. *Journal of Proteomics, 87*, 122-131.

Chambers, Lawrie, Cash, & Murray. (2000). Proteomics: a new approach to the study of disease. *Journal of Pathology, 192*(3), 280-288.

Chang, Chang, & Wang. (2010). Assessment of corneal biomechanical properties and intraocular pressure with the Ocular Response Analyzer in childhood myopia. *British Journal of Ophthalmology, 94*(7), 877-881.

Chang, Tsai, Hu, Lin, & Shih. (2001). The cornea in young myopic adults. *British Journal of Ophthalmology, 85*(8), 916-920.

Chao, Ng, Cheung, Zheng, Wang, & Cheing. (2013). In vivo and ex vivo approaches to studying the biomechanical properties of healing wounds in rat skin. *Journal of biomechanical engineering, 135*(10), 101009.

Cho. (2007). Proteomics technologies and challenges. *Genomics Proteomics Bioinformatics, 5*(2), 77-85.

Cho, & Lam. (1999). Factors affecting the central corneal thickness of Hong Kong-Chinese. *Current eye research, 18*(5), 368-374.

Chu, Deng, & Kee. (2012). Effects of hemiretinal form deprivation on central refractive development and posterior eye shape in chicks. *Vision Research, 55*, 24-31.

Chu, Zhou, Zheng, & Kee. (2014). Bi-directional corneal accommodation in alert chicks with experimentally-induced astigmatism. *Vision Research, 98*, 26-34.

Cohen, Belkin, Yehezkel, Avni, & Polat. (2008). Light intensity modulates corneal power and refraction in the chick eye exposed to continuous light. *Vision Research, 48*(21), 2329-2335.

Curtin. (1985). *The myopias : basic science and clinical management*: Philadelphia (Pa.) : Harper and Row.

Curtin, Iwamoto, & Renaldo. (1979). Normal and staphylomatous sclera of high myopia - electron-microscopic study. *Archives of Ophthalmology, 97*(5), 912-915.

Curtin, & Teng. (1958). Scleral changes in pathological myopia. *Transactions - American Academy of Ophthalmology and Otolaryngology, 62*(6), 777-788; discussion 788-790.

David, Zangwill, Tessler, & Yassur. (1985). The correlation between intraocular-pressure and refractive status. *Archives of Ophthalmology, 103*(12), 1812-1815.

Dawson, Grossniklaus, McCarey, & Edelhauser. (2008). Biomechanical and wound healing characteristics of corneas after excimer laser keratorefractive surgery: Is there a difference between advanced surface ablation and sub-Bowman's keratomileusis? *Journal of Refractive Surgery, 24*(1), 90-96.

Dawson, Randleman, Grossniklaus, O'Brien, Dubovy, Schmack, . . . Edelhauser. (2008). Corneal ectasia after Excimer laser keratorefractive surgery:

histopathology, ultrastructure, and pathophysiology. *Ophthalmology, 115*(12), 2181-2191.

Daxer, & Fratzl. (1997). Collagen fibril orientation in the human corneal stroma and its implication in keratoconus. *Investigative Ophthalmology & Visual Science, 38*(1), 121-129.

Daxer, Misof, Grabner, Ettl, & Fratzl. (1998). Collagen fibrils in the human corneal stroma: structure and aging. *Investigative Ophthalmology & Visual Science, 39*(3), 644-648.

Detorakis, & Pallikaris. (2013). Ocular rigidity: biomechanical role, in vivo measurements and clinical significance. *Clinical and Experimental Ophthalmology, 41*(1), 73-81.

Detry-Morel. (2011). Is myopia a risk factor for glaucoma? *Journal Francais D Ophtalmologie, 34*(6), 392-395.

Ding, Shih, Lin, Hsiao, & Wang. (2017). Myopia among schoolchildren in East Asia and Singapore. *Survey of Ophthalmology, 62*(5), 677-697.

Diz, Truebano, & Skibinski. (2009). The consequences of sample pooling in proteomics: an empirical study. *Electrophoresis, 30*(17), 2967-2975.

Dolgin. (2015). The myopia boom. *Nature, 519*(7543), 276-278.

Dotan, Kremer, Livnat, Zigler, Weinberger, & Bourla. (2014). Scleral cross-linking using riboflavin and ultraviolet-A radiation for prevention of progressive myopia in a rabbit model. *Experimental eye research, 127*, 190-195.

Dupps, & Wilson. (2006). Biomechanics and wound healing in the cornea. *Experimental eye research, 83*(4), 709-720.

Dyrlund, Poulsen, Scavenius, Nikolajsen, Thogersen, Vorum, & Enghild. (2012). Human cornea proteome: identification and quantitation of the proteins of the three main layers including epithelium, stroma, and endothelium. *Journal of Proteome Research, 11*(8), 4231-4239.

Edwards, & Lam. (2004). The epidemiology of myopia in Hong Kong. *Annals Academy of Medicine Singapore, 33*(1), 34-38.

Ehlers, & Hjortdal. (2005). The cornea: epithelium and stroma. *10*, 83-111.

El-Aneed, Cohen, & Banoub. (2009). Mass spectrometry, review of the basics: Electrospray, MALDI, and commonly used mass analyzers. *Applied Spectroscopy Reviews, 44*(3), 210-230.

Elham, Jafarzadehpur, Hashemi, Amanzadeh, Shokrollahzadeh, Yekta, & Khabazkhoob. (2017). Keratoconus diagnosis using Corvis ST measured biomechanical parameters. *Journal of Current Ophthalmology, 29*(3), 175-181.

Elsheikh, Alhasso, & Rama. (2008). Biomechanical properties of human and porcine corneas. *Experimental eye research, 86*(5), 783-790.

Fam, How, Baskaran, Lim, Chan, & Aung. (2006). Central corneal thickness and its relationship to myopia in Chinese adults. *British Journal of Ophthalmology,*

90(12), 1451-1453.
Fang, Hodivala-Dilke, Johnson, Du, Hynes, White, & Wilcox. (2005). Therapeutic expression of the platelet-specific integrin, alphaIIbbeta3, in a murine model for Glanzmann thrombasthenia. *Blood, 106*(8), 2671-2679.
Farah, Azar, Gurdal, & Wong. (1998). Laser in situ keratomileusis: literature review of a developing technique. *Journal of Cataract & Refractive Surgery, 24*(7), 989-1006.
Fischbarg, & Maurice. (2004). An update on corneal hydration control. *Experimental eye research, 78*(3), 537-541.
Forrester, Dick, McMenamin, Roberts, & Pearlman. (2015). *The eye e-book: basic sciences in practice*: Elsevier Health Sciences.
Fowler, Chang, Roberts, Zarovnaya, & Proia. (2004). A new paradigm for corneal wound healing research: The white leghorn chicken (Gallus gallus domesticus). *Current eye research, 28*(4), 241-250.
Frederick, & Ciborowski. (2016). 9 - SWATH-MS: Data acquisition and analysis. In Ciborowski & Silberring (Eds.), *Proteomic Profiling and Analytical Chemistry (Second Edition)* (pp. 161-173). Boston: Elsevier.
Friedenwald. (1937). Contribution to the theory and practice of tonometry. *American Journal of Ophthalmology, 20*(10), 985-1024.
Frings, Linke, Bauer, Druchkiv, Katz, & Steinberg. (2015). Effects of laser in situ keratomileusis (LASIK) on corneal biomechanical measurements with the Corvis ST tonometer. *Clinical Ophthalmology, 9*, 305-311.
Gentle, Liu, Martin, Conti, & McBrien. (2003). Collagen gene expression and the altered accumulation of scleral collagen during the development of high myopia. *Journal of Biological Chemistry, 278*(19), 16587-16594.
Gentle, Martin, & McBrien. (2002). Differential expression of collagen types I, III and V in the sclera of myopic eyes: A precursor to fibril diameter changes? *Investigative Ophthalmology & Visual Science, 43*(13), 2449-2449.
Gillet, Navarro, Tate, Rost, Selevsek, Reiter, . . . Aebersold. (2012). Targeted data extraction of the MS/MS spectra generated by data-independent acquisition: a new concept for consistent and accurate proteome analysis. *Molecular & Cellular Proteomics, 11*(6), O111 016717.
Gkika, Labiris, Giarmoukakis, Koutsogianni, & Kozobolis. (2012). Evaluation of corneal hysteresis and corneal resistance factor after corneal cross-linking for keratoconus. *Graefes Archive for Clinical and Experimental Ophthalmology, 250*(4), 565-573.
Glasser, Murphy, Troilo, & Howland. (1995). The mechanism of lenticular accommodation in chicks. *Vision Research, 35*(11), 1525-1540.
Glasser, Troilo, & Howland. (1994). The mechanism of corneal accommodation in chicks. *Vision Research, 34*(12), 1549-1566.
Goldich, Barkana, Morad, Hartstein, Avni, & Zadok. (2009). Can we measure corneal

biomechanical changes after collagen cross-linking in eyes with keratoconus? A pilot study. *Cornea, 28*(5), 498-502.
Gottlieb, Fugate-Wentzek, & Wallman. (1987). Different visual deprivations produce different ametropias and different eye shapes. *Investigative Ophthalmology & Visual Science, 28*(8), 1225-1235.
Gottlieb, Joshi, & Nickla. (1990). Scleral changes in chicks with form-deprivation myopia. *Current eye research, 9*(12), 1157-1165.
Graham, & Judge. (1999). The effects of spectacle wear in infancy on eye growth and refractive error in the marmoset (Callithrix jacchus). *Vision Research, 39*(2), 189-206.
Grosvenor. (1988). High axial length corneal radius ratio as a risk factor in the development of myopia. *American Journal of Optometry and Physiological Optics, 65*(9), 689-696.
Grosvenor, & Goss. (1998). Role of the cornea in emmetropia and myopia. *Optometry & Vision Science, 75*(2), 132-145.
Grytz, & Siegwart. (2015). Changing material properties of the tree shrew sclera during minus lens compensation and recovery. *Investigative Ophthalmology & Visual Science, 56*(3), 2065-2078.
Guggenheim, & McBrien. (1996). Form-deprivation myopia induces activation of scleral matrix metalloproteinase-2 in tree shrew. *Investigative Ophthalmology & Visual Science, 37*(7), 1380-1395.
Hamilton, & Pye. (2008). Young's modulus in normal corneas and the effect on applanation tonometry. *Optometry and Vision Science, 85*(6), 445-450.
Hanash. (2003). Disease proteomics. *Nature, 422*(6928), 226-232.
Harper, & Summers. (2015). The dynamic sclera: Extracellular matrix remodeling in normal ocular growth and myopia development. *Experimental eye research, 133*, 100-111.
Hatami-Marbini. (2014). Hydration dependent viscoelastic tensile behavior of cornea. *Annals of Biomedical Engineering, 42*(8), 1740-1748.
Hatami-Marbini, & Etebu. (2013). Hydration dependent biomechanical properties of the corneal stroma. *Experimental eye research, 116*, 47-54.
Hayashi, Kawahara, Manabe, & Hirata. (2015). Changes in irregular corneal astigmatism with age in eyes with and without cataract surgery. *Investigative Ophthalmology & Visual Science, 56*(13), 7988-7998.
Hayashi, Osawa, & Tohyama. (2002). Comparative observations on corneas, with special reference to Bowman's layer and Descemet's membrane in mammals and amphibians. *Journal of Morphology, 254*(3), 247-258.
Hayes, Fitzke, Hodos, & Holden. (1986). A morphological analysis of experimental myopia in young chickens. *Investigative Ophthalmology & Visual Science, 27*(6), 981-991.
He, Wang, Ding, & Zhong. (2017). Corneal biomechanical properties in high myopia

measured by dynamic Scheimpflug imaging technology. *Optometry & Vision Science, 94*(12), 1074-1080.

He, Wendt, & Glasser. (2012). Manipulation of intraocular pressure for studying the effects on accommodation. *Experimental eye research, 102*, 76-84.

He, Zeng, Liu, Xu, Pokharel, & Ellwein. (2004). Refractive error and visual impairment in urban children in southern China. *Investigative Ophthalmology & Visual Science, 45*(3), 793-799.

Hennighausen, Feldman, Bille, & McCulloch. (1998). Anterior-posterior strain variation in normally hydrated and swollen rabbit cornea. *Investigative ophthalmology & visual science, 39*(2), 253-262.

Henriquez, Izquierdo, Bernilla, Zakrzewski, & Mannis. (2011). Riboflavin/Ultraviolet A corneal collagen cross-linking for the treatment of keratoconus: visual outcomes and Scheimpflug analysis. *Cornea, 30*(3), 281-286.

Hoeltzel, Altman, Buzard, & Choe. (1992). Strip extensiometry for comparison of the mechanical response of bovine, rabbit, and human corneas. *Journal of biomechanical engineering, 114*(2), 202-215.

Holden, Fricke, Wilson, Jong, Naidoo, Sankaridurg, . . . Resnikoff. (2016). Global prevalence of myopia and high myopia and temporal trends from 2000 through 2050. *Ophthalmology, 123*(5), 1036-1042.

Hon, Chen, Lu, Lam, & Lam. (2017). High myopes have lower normalised corneal tangent moduli (less 'stiff' corneas) than low myopes. *Ophthalmic and Physiological Optics, 37*(1), 42-50.

Hon, & Lam. (2013). Corneal Deformation Measurement Using Scheimpflug Noncontact Tonometry. *Optometry and Vision Science, 90*(1), E1-E8.

Horner, Soni, Vyas, & Himebaugh. (2000). Longitudinal changes in corneal asphericity in myopia. *Optometry & Vision Science, 77*(4), 198-203.

Howlett, & McFadden. (2006). Form-deprivation myopia in the guinea pig (Cavia porcellus). *Vision Research, 46*(1-2), 267-283.

Huang, Swanson, Lin, Schuman, Stinson, Chang, . . . Puliafito. (1991). Optical coherence tomography. *Science, 254*(5035), 1178-1181.

Huang, Tseng, Shih, & Chen. (2002). Effect of artificial tears on corneal surface regularity, contrast sensitivity, and glare disability in dry eyes. *Ophthalmology, 109*(10), 1934-1940.

Huang, Zheng, Wang, Chen, Huang, & He. (2009). An optical coherence tomography (OCT)-based air jet indentation system for measuring the mechanical properties of soft tissues. *Measurement science and technology, 20*(1), 1-11.

Hull, Green, & Laughter. (1984). Cornea Endothelial Rose-Bengal Photosensitization - Effect on Permeability, Sodium Flux, and Ultrastructure. *Investigative Ophthalmology & Visual Science, 25*(4), 455-460.

Irving, Sivak, & Callender. (1992). Refractive plasticity of the developing chick eye.

Ophthalmic and Physiological Optics, 12(4), 448-456.
Jiang, Kurihara, Kunimi, Miyauchi, Ikeda, Mori, . . . Tsubota. (2018). A highly efficient murine model of experimental myopia. *Scientific Reports, 8*(1), 2026.
Jiang, Shen, Mao, Chen, Wang, Qu, & Lu. (2011). Association between corneal biomechanical properties and myopia in Chinese subjects. *Eye, 25*(8), 1083-1089.
Johnson, Lytle, Troillo, & Nickla. (2004). Chick eyes show a diurnal rhythm in refractive error. *Investigative Ophthalmology & Visual Science, 45*, U416-U416.
Jue, & Maurice. (1986). The Mechanical-Properties of the Rabbit and Human Cornea. *Journal of Biomechanics, 19*(10), 847-853.
Jung, Lee, Kakizaki, & Jee. (2012). Prevalence of myopia and its association with body stature and educational level in 19-year-old male conscripts in Seoul, South Korea. *Investigative Ophthalmology & Visual Science, 53*(9), 5579-5583.
Kamiya, Shimizu, & Ohmoto. (2009). Comparison of the changes in corneal biomechanical properties after photorefractive keratectomy and laser in situ keratomileusis. *Cornea, 28*(7), 765-769.
Kang, Lam, Cheung, Li, & Kee. (2019). Data on corneal proteome and differentially expressed corneal proteins in highly myopic chicks using a data independent quantification approach. *Data Brief, 26*, 104478.
Kang, Wang, Zheng, Guggenheim, Stell, & Kee. (2018). High myopia induced by form deprivation is associated with altered corneal biomechanical properties in chicks. *Plos One, 13*(11).
Kao, Kao, Kaufman, Kombrinck, Converse, Good, . . . Degen. (1998). Healing of corneal epithelial defects in plasminogen- and fibrinogen-deficient mice. *Investigative Ophthalmology & Visual Science, 39*(3), 502-508.
Karring, Thogersen, Klintworth, Moller-Pedersen, & Enghild. (2005). A dataset of human cornea proteins identified by Peptide mass fingerprinting and tandem mass spectrometry. *Molecular & Cellular Proteomics, 4*(9), 1406-1408.
Kaushik, Pandav, Banger, Aggarwal, & Gupta. (2012). Relationship between corneal biomechanical properties, central corneal thickness, and intraocular pressure across the spectrum of glaucoma. *American Journal of Ophthalmology, 153*(5), 840-849. e842.
Kee, & Deng. (2008). Astigmatism associated with experimentally induced myopia or hyperopia in chickens. *Investigative Ophthalmology & Visual Science, 49*(3), 858-867.
Kee, Hung, Qiao-Grider, Ramamirtham, & Smith. (2005). Astigmatism in monkeys with experimentally induced myopia or hyperopia. *Optometry and Vision Science, 82*(4), 248.

Kim, Morgan, Kakizaki, Kang, & Jee. (2013). Prevalence and risk factors for refractive errors: Korean National Health and Nutrition Examination Survey 2008-2011. *Plos One, 8*(11).

Kling, Bekesi, Dorronsoro, Pascual, & Marcos. (2014). Corneal viscoelastic properties from finite-element analysis of in vivo air-puff deformation. *Plos One, 9*(8), e104904.

Kling, & Hafezi. (2017). Corneal biomechanics - a review. *Ophthalmic & Physiological Optics, 37*(3), 240-252.

Kling, & Marcos. (2013). Contributing factors to corneal deformation in air puff measurements. *Investigative Ophthalmology & Visual Science, 54*(7), 5078-5085.

Kling, & Marcos. (2013). Effect of hydration state and storage media on corneal biomechanical response from in vitro inflation tests. *Journal of Refractive Surgery, 29*(7), 490-497.

Ko, Leung, Lam, & Leung. (2013). Characterization of corneal tangent modulus in vivo. *Acta Ophthalmologica, 91*(4), e263-269.

Ko, Liu, Chou, Chen, Hsu, & Liu. (2002). Comparisons of risk factors and visual field changes between juvenile-onset and late-onset primary open-angle glaucoma. *Ophthalmologica, 216*(1), 27-32.

Koh, Yang, Saw, Chan, Lin, Tan, . . . Ikram. (2014). Differences in prevalence of refractive rrrors in young Asian males in Singapore between 1996-1997 and 2009-2010. *Ophthalmic Epidemiology, 21*(4), 247-255.

Konomi, Hayashi, Nakayasu, & Arima. (1984). Localization of Type-V Collagen and Type-Iv Collagen in Human Cornea, Lung, and Skin - Immunohistochemical Evidence by Anti-Collagen Antibodies Characterized by Immunoelectroblotting. *American Journal of Pathology, 116*(3), 417-426.

Lagali, Germundsson, & Fagerholm. (2009). The Role of Bowman's Layer in Corneal Regeneration after Phototherapeutic Keratectomy: A Prospective Study Using In Vivo Confocal Microscopy. *Investigative Ophthalmology & Visual Science, 50*(9), 4192-4198.

Lam, Li, Lo, Guggenheim, & To. (2006). A chick retinal proteome database and differential retinal protein expressions during early ocular development. *Journal of Proteome Research, 5*(4), 771-784.

Lambert, Ivosev, Couzens, Larsen, Taipale, Lin, . . . Gingras. (2013). Mapping differential interactomes by affinity purification coupled with data-independent mass spectrometry acquisition. *Nature Methods, 10*(12), 1239-1245.

Larsen, Cordwell, & Roepstorff. (2002). Graphite powder as an alternative or supplement to reversed-phase material for desalting and concentration of peptide mixtures prior to matrix-assisted laser desorption/ionization-mass spectrometry. *Proteomics, 2*(9), 1277-1287.

Last, Liliensiek, Nealey, & Murphy. (2009). Determining the mechanical properties of human corneal basement membranes with atomic force microscopy. *Journal of Structural Biology, 167*(1), 19-24.

Lauber, & Oishi. (1987). Lid suture myopia in chicks. *Investigative Ophthalmology & Visual Science, 28*(11), 1851-1858.

Laurens, Koolwijk, & de Maat. (2006). Fibrin structure and wound healing. *Journal of Thrombosis and Haemostasis, 4*(5), 932-939.

Lee, Chang, Wong, Lai, Lee, & Singh. (2016). Assessment of corneal biomechanical parameters in myopes and emmetropes using the Corvis ST. *Clinical and Experimental Optometry, 99*(2), 157-162.

Leung, Lam, & Kee. (2013). Corneal shapes of Chinese emmetropes and myopic astigmats aged 10 to 45 years. *Optometry & Vision Science, 90*(11), 1259-1266.

Li, Iribarren, Kang, Li, Li, Liu, . . . Wang. (2016). Corneal power, anterior segment length and lens power in 14-year-old Chinese children: the Anyang Childhood Eye Study. *Scientific Reports, 6*, 20243.

Li, Troilo, Glasser, & Howland. (1995). Constant light produces severe corneal flattening and hyperopia in chickens. *Vision Research, 35*(9), 1203-1209.

Liebler, & Zimmerman. (2013). Targeted Quantitation of Proteins by Mass Spectrometry. *Biochemistry, 52*(22), 3797-3806.

Lim, Gazzard, Chan, Fong, Kotecha, Sim, . . . Saw. (2008). Corneal biomechanics, thickness and optic disc morphology in children with optic disc tilt. *British Journal of Ophthalmology, 92*(11), 1461-1466.

Lin, Shih, Hsiao, & Chen. (2004). Prevalence of myopia in Taiwanese schoolchildren: 1983 to 2000. *Annals Academy of Medicine Singapore, 33*(1), 27-33.

Liu, Kenning, Jobling, McBrien, & Gentle. (2017). Reduced Scleral TIMP-2 Expression Is Associated With Myopia Development: TIMP-2 Supplementation Stabilizes Scleral Biomarkers of Myopia and Limits Myopia Development. *Investigative Ophthalmology & Visual Science, 58*(4), 1971-1981.

Liu, & Roberts. (2005). Influence of corneal biomechanical properties on intraocular pressure measurement: quantitative analysis. *Journal of Cataract & Refractive Surgery, 31*(1), 146-155.

Long, Wang, Yang, Jin, Ai, & Li. (2015). Assessment of corneal biomechanical properties by CorVis ST in patients with dry eye and in healthy subjects. *Journal of Ophthalmology, 2015*, 380624.

Lu, Chong, Leung, & Lam. (2019). Characterization of corneal biomechanical properties and determination of natural intraocular pressure using CID-GAT. *Translational Vision Science & Technology, 8*(5).

Lu, Zhou, Zhao, Wang, Jia, Jiang, . . . Qu. (2006). Axial myopia induced by a monocularly-deprived facemask in guinea pigs: A non-invasive and effective

model. *Experimental eye research, 82*(4), 628-636.
Luce. (2005). Determining in vivo biomechanical properties of the cornea with an ocular response analyzer. *Journal of Cataract & Refractive Surgery, 31*(1), 156-162.
Ludwig, Gillet, Rosenberger, Amon, Collins, & Aebersold. (2018). Data-independent acquisition-based SWATH-MS for quantitative proteomics: a tutorial. *Molecular Systems Biology, 14*(8).
Lundberg, Fagerberg, Klevebring, Matic, Geiger, Cox, . . . Uhlen. (2010). Defining the transcriptome and proteome in three functionally different human cell lines. *Molecular Systems Biology, 6*.
Ly, & Wasinger. (2011). Protein and peptide fractionation, enrichment and depletion: tools for the complex proteome. *Proteomics, 11*(4), 513-534.
Ma, Pavlatos, Clayson, Pan, Kwok, Sandwisch, & Liu. (2019). Mechanical Deformation of Human Optic Nerve Head and Peripapillary Tissue in Response to Acute IOP Elevation. *Invest Ophthalmol Vis Sci, 60*(4), 913-920.
Maczynska, Rzeszewska-Zamiara, Jimenez Villar, Wojtkowski, Kaluzny, & Grulkowski. (2019). Air-puff-induced dynamics of ocular components measured with optical biometry. *Investigative Ophthalmology & Visual Science, 60*(6), 1979-1986.
Manadas, Mendes, English, & Dunn. (2010). Peptide fractionation in proteomics approaches. *Expert Review of Proteomics, 7*(5), 655-663.
Manzoni, Kia, Vandrovcova, Hardy, Wood, Lewis, & Ferrari. (2018). Genome, transcriptome and proteome: the rise of omics data and their integration in biomedical sciences. *Briefings in Bioinformatics, 19*(2), 286-302.
Marshall, Konstas, & Lee. (1991). Immunogold Fine-Structural Localization of Extracellular-Matrix Components in Aged Human Cornea .1. Types-I-Iv Collagen and Laminin. *Graefes Archive for Clinical and Experimental Ophthalmology, 229*(2), 157-163.
Marshall, Konstas, & Lee. (1991). Immunogold Fine-Structural Localization of Extracellular-Matrix Components in Aged Human Cornea .2. Collagen Type-V and Type-Vi. *Graefes Archive for Clinical and Experimental Ophthalmology, 229*(2), 164-171.
Marzani, & Wallman. (1997). Growth of the two layers of the chick sclera is modulated reciprocally by visual conditions. *Investigative Ophthalmology & Visual Science, 38*(9), 1726-1739.
McBrien, Cornell, & Gentle. (2001). Structural and ultrastructural changes to the sclera in a mammalian model of high myopia. *Investigative Ophthalmology & Visual Science, 42*(10), 2179-2187.
McBrien, & Gentle. (2003). Role of the sclera in the development and pathological complications of myopia. *Progress in Retinal and Eye Research, 22*(3), 307-338.

McBrien, Gentle, & Cottriall. (1999). Optical correction of induced axial myopia in the tree shrew: Implications for emmetropization. *Optometry and Vision Science, 76*(6), 419-427.

McBrien, Jobling, & Gentle. (2009). Biomechanics of the sclera in myopia: extracellular and cellular factors. *Optometry & Vision Science, 86*(1), E23-E30.

McBrien, Lawlor, & Gentle. (2000). Scleral remodeling during the development of and recovery from axial myopia in the tree shrew. *Investigative ophthalmology & visual science, 41*(12), 3713-3719.

Mcfadden, & Wallman. (1995). Guinea-pig eye growth compensates for spectacle lenses. *Investigative Ophthalmology & Visual Science, 36*(4), S758-S758.

McLellan, Marcos, & Burns. (2001). Age-related changes in monochromatic wave aberrations of the human eye. *Investigative Ophthalmology & Visual Science, 42*(6), 1390-1395.

McMonnies. (2012). Assessing Corneal Hysteresis Using the Ocular Response Analyzer. *Optometry and Vision Science, 89*(3), E343-E349.

Meade, Shiyanov, & Schlager. (2009). Enhanced detection method for corneal protein identification using shotgun proteomics. *Proteome Science, 7*.

Medeiros, & Weinreb. (2006). Evaluation of the influence of corneal biomechanical properties on intraocular pressure measurements using the ocular response analyzer. *Journal of Glaucoma, 15*(5), 364-370.

Meek. (2009). Corneal collagen-its role in maintaining corneal shape and transparency. *Biophysical Reviews, 1*(2), 83-93.

Meek, Blamires, Elliott, Gyi, & Nave. (1987). The Organization of Collagen Fibrils in the Human Corneal Stroma - a Synchrotron X-Ray-Diffraction Study. *Current eye research, 6*(7), 841-846.

Meek, & Boote. (2004). The organization of collagen in the corneal stroma. *Experimental eye research, 78*(3), 503-512.

Meek, & Fullwood. (2001). Corneal and scleral collagens - a microscopist's perspective. *Micron, 32*(3), 261-272.

Meek, & Knupp. (2015). Corneal structure and transparency. *Progress in Retinal and Eye Research, 49*, 1-16.

Meek, Tuft, Huang, Gill, Hayes, Newton, & Bron. (2005). Changes in collagen orientation and distribution in keratoconus corneas. *Investigative Ophthalmology & Visual Science, 46*(6), 1948-1956.

Metlapally, & Wildsoet. (2015). Scleral mechanisms underlying ocular growth and myopia. *Progress in Molecular Biology and Translational Science, 134*, 241-248.

Mi, Huang, Muruganujan, Tang, Mills, Kang, & Thomas. (2017). PANTHER version 11: expanded annotation data from Gene Ontology and Reactome pathways, and data analysis tool enhancements. *Nucleic Acids Research,*

45(D1), D183-D189.
Mitchell, Hourihan, Sandbach, & Wang. (1999). The relationship between glaucoma and myopia: the Blue Mountains Eye Study. *Ophthalmology, 106*(10), 2010-2015.
Mohan, Lee, & Panjwani. (1995). Molecular cloning of the E-cadherin cDNAs from rabbit corneal epithelium. *Current eye research, 14*(12), 1136-1145.
Molinari, Roche, Peoc'h, Tiers, Seveno, Hirtz, & Lehmann. (2018). Sample pooling and inflammation linked to the false selection of biomarkers for neurodegenerative diseases in top-down proteomics: A pilot study. *Frontiers in Molecular Neuroscience, 11*, 477.
Morgan, French, Ashby, Guo, Ding, He, & Rose. (2018). The epidemics of myopia: Aetiology and prevention. *Progress in Retinal and Eye Research, 62*, 134-149.
Moring, Baker, & Norton. (2007). Modulation of glycosaminoglycan levels in tree shrew sclera during lens-induced myopia development and recovery. *Investigative Ophthalmology & Visual Science, 48*(7), 2947-2956.
Murphy, Glasser, & Howland. (1995). The Anatomy of the Ciliary Region of the Chicken Eye. *Investigative Ophthalmology & Visual Science, 36*(5), 889-896.
Napper, Brennan, Barrington, Squires, Vessey, & Vingrys. (1995). The duration of normal visual exposure necessary to prevent form deprivation myopia in chicks. *Vision Research, 35*(9), 1337-1344.
Nawrocki-Raby, Gilles, Polette, Martinella-Catusse, Bonnet, Puchelle, . . . Birembaut. (2003). E-Cadherin mediates MMP down-regulation in highly invasive bronchial tumor cells. *The American Journal of Pathology, 163*(2), 653-661.
Newsome, Foidart, Hassell, Krachmer, Rodrigues, & Katz. (1981). Detection of Specific Collagen Types in Normal and Keratoconus Corneas. *Investigative Ophthalmology & Visual Science, 20*(6), 738-750.
Newton, & Meek. (1998). Circumcorneal annulus of collagen fibrils in the human limbus. *Investigative Ophthalmology & Visual Science, 39*(7), 1125-1134.
Newton, & Meek. (1998). The integration of the corneal and limbal fibrils in the human eye. *Biophysical Journal, 75*(5), 2508-2512.
Nickla, Wildsoet, & Wallman. (1998). The circadian rhythm in intraocular pressure and its relation to diurnal ocular growth changes in chicks. *Experimental eye research, 66*(2), 183-193.
Nickla, Wildsoet, & Wallman. (1998). Visual influences on diurnal rhythms in ocular length and choroidal thickness in chick eyes. *Experimental eye research, 66*(2), 163-181.
Nomura, Ando, Niino, Shimokata, & Miyake. (2004). The relationship between intraocular pressure and refractive error adjusting for age and central corneal thickness. *Ophthalmic and Physiological Optics, 24*(1), 41-45.
Norton. (1999). Animal models of myopia: learning how vision controls the size of

the eye. *Institute of Laboratory Animal Resources, 40*(2), 59-77.
Norton, & Rada. (1995). Reduced Extracellular-Matrix in Mammalian Sclera with Induced Myopia. *Vision Research, 35*(9), 1271-1281.
Norton, & Rada. (1995). Reduced extracellular matrix in mammalian sclera with induced myopia. *Vision Research, 35*(9), 1271-1281.
Nyquist. (1968). Rheology of the cornea: experimental techniques and results. *Experimental eye research, 7*(2), 183-188.
Pallikaris, Kymionis, & Astyrakakis. (2001). Corneal ectasia induced by laser in situ keratomileusis. *Journal of Cataract and Refractive Surgery, 27*(11), 1796-1802.
Pan, Ramamurthy, & Saw. (2012). Worldwide prevalence and risk factors for myopia. *Ophthalmic and Physiological Optics, 32*(1), 3-16.
Pardue, & Sivak. (1997). The functional anatomy of the ciliary muscle in four avian species. *Brain Behavior and Evolution, 49*(6), 295-311.
Park, Jeong, Lee, Lee, Ahn, Kim, & Seo. (2013). Acute changes in central corneal thickness according to experimental adjustment of intraocular pressure in normal canine eyes. *Journal of Veterinary Medical Science, 75*(11), 1479-1483.
Pavlatos, Ma, Clayson, Pan, & Liu. (2018). Regional Deformation of the Optic Nerve Head and Peripapillary Sclera During IOP Elevation. *Invest Ophthalmol Vis Sci, 59*(8), 3779-3788.
Pena-Garcia, Peris-Martinez, Abbouda, & Ruiz-Moreno. (2016). Detection of subclinical keratoconus through non-contact tonometry and the use of discriminant biomechanical functions. *Journal of Biomechanics, 49*(3), 353-363.
Phillips, Khalaj, & McBrien. (2000). Induced myopia associated with increased scleral creep in chick and tree shrew eyes. *Investigative Ophthalmology & Visual Science, 41*(8), 2028-2034.
Phillips, & McBrien. (1995). Form deprivation myopia: elastic properties of sclera. *Ophthalmic and Physiological Optics, 15*(5), 357-362.
Pinero, & Alcon. (2015). Corneal biomechanics: a review. *Clinical and Experimental Optometry, 98*(2), 107-116.
Plakitsi, O'Donnell, Miranda, Charman, & Radhakrishnan. (2011). Corneal biomechanical properties measured with the Ocular Response Analyser in a myopic population. *Ophthalmic and Physiological Optics, 31*(4), 404-412.
Qian, Jacobs, Liu, Camp, & Smith. (2006). Advances and challenges in liquid chromatography-mass spectrometry-based proteomics profiling for clinical applications. *Molecular & Cellular Proteomics, 5*(10), 1727-1744.
Qiao-Grider, Hung, Kee, Ramamirtham, & Smith. (2004). Recovery from form-deprivation myopia in rhesus monkeys. *Investigative Ophthalmology & Visual Science, 45*(10), 3361-3372.

Qiao-Grider, Hung, Kee, Ramamirtham, & Smith. (2010). Nature of the refractive errors in rhesus monkeys (Macaca mulatta) with experimentally induced ametropias. *Vision Research, 50*(18), 1867-1881.

Qiu, Lu, Zhang, Wang, & Zhang. (2016). Corneal biomechanics determination in healthy myopic subjects. *Journal of Ophthalmology, 2016*, 2793516.

Quantock, & Young. (2008). Development of the Corneal Stroma, and the Collagen-Proteoglycan Associations That Help Define Its Structure and Function. *Developmental Dynamics, 237*(10), 2607-2621.

Rad, Jabbarvand, & Saifi. (2004). Progressive keratectasia after laser in situ keratomileusis. *Journal of Refractive Surgery, 20*(5), S718-S722.

Rada, Achen, Penugonda, Schmidt, & Mount. (2000). Proteoglycan composition in the human sclera during growth and aging. *Investigative Ophthalmology & Visual Science, 41*(7), 1639-1648.

Rada, Achen, & Rada. (1998). Proteoglycan turnover in the sclera of normal and experimentally myopic chick eyes. *Investigative Ophthalmology & Visual Science, 39*(11), 1990-2002.

Rada, & Brenza. (1995). Increased latent gelatinase activity in the sclera of visually deprived chicks. *Investigative Ophthalmology & Visual Science, 36*(8), 1555-1565.

Rada, & Hollaway. (2011). Regulation of the biphasic decline in scleral proteoglycan synthesis during the recovery from induced myopia. *Experimental eye research, 92*(5), 394-400.

Rada, & Matthews. (1994). Visual deprivation upregulates extracellular matrix synthesis by chick scleral chondrocytes. *Investigative Ophthalmology & Visual Science, 35*(5), 2436-2447.

Rada, Nickla, & Troilo. (2000). Decreased proteoglycan synthesis associated with form deprivation myopia in mature primate eyes. *Investigative Ophthalmology & Visual Science, 41*(8), 2050-2058.

Rada, Perry, Slover, & Achen. (1999). Gelatinase A and TIMP-2 expression in the fibrous sclera of myopic and recovering chick eyes. *Investigative Ophthalmology & Visual Science, 40*(13), 3091-3099.

Rada, Shelton, & Norton. (2006). The sclera and myopia. *Experimental eye research, 82*(2), 185-200.

Radhakrishnan, Miranda, & O'Donnell. (2012). Corneal biomechanical properties and their correlates with refractive error. *Clinical and Experimental Optometry, 95*(1), 12-18.

Rehman, Ahsan, & Khan. (2013). Alpha-2-macroglobulin: A physiological guardian. *Journal of Cellular Physiology, 228*(8), 1665-1675.

Ritchey, Code, Zelinka, Scott, & Fischer. (2011). The chicken cornea as a model of wound healing and neuronal reinnervation. *Molecular Vision, 17*(264-65), 2440-2454.

Roark, & Young. (1989). *Roark's formulas for stress and strain* (6th ed.). New York: McGraw-Hill.

Roberts, & Liu. (2017). *Corneal Biomechanics: from theory to practice*: Kugler Publications.

Rodriguez-Calvo, Ferran, Alonso, Marti-Pamies, Aguilo, Calvayrac, . . . Martinez-Gonzalez. (2015). NR4A receptors up-regulate the antiproteinase alpha-2 macroglobulin (A2M) and modulate MMP-2 and MMP-9 in vascular smooth muscle cells. *Thrombosis and Haemostasis, 113*(6), 1323-1334.

Romero-Jimenez, Santodomingo-Rubido, & Wolffsohn. (2010). Keratoconus: A review. *Contact Lens & Anterior Eye, 33*(4), 157-166.

Rosales, & Marcos. (2009). Pentacam Scheimpflug quantitative imaging of the crystalline lens and intraocular lens. *Journal of Refractive Surgery, 25*(5), 421-428.

Ruberti, Sinha Roy, & Roberts. (2011). Corneal biomechanics and biomaterials. *Annual Review of Biomedical Engineering, 13*, 269-295.

Rucker, Britton, Spatcher, & Hanowsky. (2015). Blue light protects against temporal frequency sensitive refractive changes. *Investigative Ophthalmology & Visual Science, 56*(10), 6121-6131.

Sarker, Hardy, Haimour, Maksymowych, Botto, & Fernandez-Patron. (2019). Identification of fibrinogen as a natural inhibitor of MMP-2. *Scientific Reports, 9*.

Saw, Gazzard, Shih-Yen, & Chua. (2005). Myopia and associated pathological complications. *Ophthalmic and Physiological Optics, 25*(5), 381-391.

Saw, Katz, Schein, Chew, & Chan. (1996). Epidemiology of myopia. *Epidemiologic Reviews, 18*(2), 175-187.

Schaeffel, Burkhardt, Howland, & Williams. (2004). Measurement of refractive state and deprivation myopia in two strains of mice. *Optometry & Vision Science, 81*(2), 99-110.

Schaeffel, & Feldkaemper. (2015). Animal models in myopia research. *Clinical and Experimental Optometry, 98*(6), 507-517.

Schaeffel, & Howland. (1987). Corneal accommodation in chick and pigeon. *Journal of Comparative Physiology A, 160*(3), 375-384.

Schmid, & Wildsoet. (1997). Natural and imposed astigmatism and their relation to emmetropization in the chick. *Experimental eye research, 64*(5), 837-847.

Schubert, Gillet, Collins, Navarro, Rosenberger, Wolski, . . . Aebersold. (2015). Building high-quality assay libraries for targeted analysis of SWATH MS data. *Nature Protocols, 10*(3), 426-441.

Schweitzer, Roberts, Mahmoud, Colin, Maurice-Tison, & Kerautret. (2010). Screening of forme fruste keratoconus with the ocular response analyzer. *Investigative Ophthalmology & Visual Science, 51*(5), 2403-2410.

Scientific. (2016). Use of high pH reversed-phase peptide fractionation to analyze

proteins of medium to low abundance in complex mixtures [White Paper].
Sedaghat, Naderi, & Zarei-Ghanavati. (2010). Biomechanical parameters of the cornea after collagen crosslinking measured by waveform analysis. *Journal of Cataract and Refractive Surgery, 36*(10), 1728-1731.
Seko, Shimokawa, & Tokoro. (1995). Expression of Bfgf and Tgf-beta-2 in experimental myopia in chicks. *Investigative Ophthalmology & Visual Science, 36*(6), 1183-1187.
Shah, & Laiquzzaman. (2009). Comparison of corneal biomechanics in pre and post-refractive surgery and keratoconic eyes by Ocular Response Analyser. *Contact Lens & Anterior Eye, 32*(3), 129-132; quiz 151.
Shan, Tse, Zuo, To, Liu, McFadden, . . . Lam. (2018). Integrated SWATH-based and targeted-based proteomics provide insights into the retinal emmetropization process in guinea pig. *Journal of Proteomics, 181*, 1-15.
Shen, Fan, Xue, Wang, Zhou, & Lu. (2008). Biomechanical properties of the cornea in high myopia. *Vision Research, 48*(21), 2167-2171.
Sherman, Norton, & Casagrande. (1977). Myopia in the lid-sutured tree shrew (Tupaia glis). *Brain research, 124*(1), 154-157.
Shilov, Seymour, Patel, Loboda, Tang, Keating, . . . Schaeffer. (2007). The Paragon Algorithm, a next generation search engine that uses sequence temperature values and feature probabilities to identify peptides from tandem mass spectra. *Molecular & Cellular Proteomics, 6*(9), 1638-1655.
Shin, Vito, Johnson, & McCarey. (1997). The distribution of strain in the human cornea. *Journal of Biomechanics, 30*(5), 497-503.
Siegwart, & Norton. (1998). The susceptible period for deprivation-induced myopia in tree shrew. *Vision Research, 38*(22), 3505-3515.
Siegwart, & Norton. (1999). Regulation of the mechanical properties of tree shrew sclera by the visual environment. *Vision Research, 39*(2), 387-407.
Siegwart, & Norton. (2002). The time course of changes in mRNA levels in tree shrew sclera during induced myopia and recovery. *Investigative Ophthalmology & Visual Science, 43*(7), 2067-2075.
Skeie, Aldrich, Goldstein, Schmidt, Reed, & Greiner. (2018). Proteomic analysis of corneal endothelial cell-descemet membrane tissues reveals influence of insulin dependence and disease severity in type 2 diabetes mellitus. *Plos One, 13*(3).
Smolek. (1993). Interlamellar cohesive strength in the vertical meridian of human eye bank corneas. *Investigative Ophthalmology & Visual Science, 34*(10), 2962-2969.
Smoluch, Mielczarek, Drabik, & Silberring. (2016). 5 - Online and offline sample fractionation. In Ciborowski & Silberring (Eds.), *Proteomic Profiling and Analytical Chemistry (Second Edition)* (pp. 63-99). Boston: Elsevier.
Song, Congdon, Li, Zhou, Choi, Lam, . . . Sharma. (2008). Corneal hysteresis and axial

length among Chinese secondary school children: the Xichang Pediatric Refractive Error Study (X-PRES) report no. 4. *American Journal of Ophthalmology, 145*(5), 819-826. e811.

Spoerl, Huhle, & Seiler. (1998). Induction of cross-links in corneal tissue. *Experimental eye research, 66*(1), 97-103.

Suzuki, Amano, Honda, Usui, Yamagami, & Oshika. (2007). Longitudinal changes in corneal irregular astigmatism and visual acuity in eyes with keratoconus. *Japanese Journal of Ophthalmology, 51*(4), 265-269.

Szklarczyk, Gable, Lyon, Junge, Wyder, Huerta-Cepas, . . . Mering. (2019). STRING v11: protein-protein association networks with increased coverage, supporting functional discovery in genome-wide experimental datasets. *Nucleic Acids Research, 47*(D1), D607-D613.

Takahashi, Fujimoto, Honda, & Ogawa. (1992). Distributional change of fodrin in the wound healing process of the corneal epithelium. *Investigative Ophthalmology & Visual Science, 33*(2), 280-285.

Tan, Baker, Chen, Lewis, Shi, Swartz, & Wang. (2008). How keratoconus influences optical performance of the eye. *Journal of Vision, 8*(2).

Terai, Raiskup, Haustein, Pillunat, & Spoerl. (2012). Identification of biomechanical properties of the cornea: the ocular response analyzer. *Current eye research, 37*(7), 553-562.

Thibos, Wheeler, & Horner. (1997). Power vectors: an application of Fourier analysis to the description and statistical analysis of refractive error. *Optometry & Vision Science, 74*(6), 367-375.

Touboul, Roberts, Kérautret, Garra, Maurice-Tison, Saubusse, & Colin. (2008). Correlations between corneal hysteresis, intraocular pressure, and corneal central pachymetry. *Journal of Cataract & Refractive Surgery, 34*(4), 616-622.

Touzeau, Allouch, Borderie, Kopito, & Laroche. (2003). Correlation between refraction and ocular biometry. *J Fr Ophtalmol, 26*(4), 355-363.

Troilo, Li, Glasser, & Howland. (1995). Differences in eye growth and the response to visual deprivation in different strains of chicken. *Vision Research, 35*(9), 1211-1216.

Troilo, & Nickla. (2005). The response to visual form deprivation differs with age in marmosets. *Investigative Ophthalmology & Visual Science, 46*(6), 1873-1881.

Troilo, Smith, Nickla, Ashby, Tkatchenko, Ostrin, . . . Jones. (2019). IMI - Report on experimental models of emmetropization and myopia. *Investigative Ophthalmology & Visual Science, 60*(3), M31-M88.

Tur, MacGregor, Jayaswal, O'Brart, & Maycock. (2017). A review of keratoconus: Diagnosis, pathophysiology, and genetics. *Survey of Ophthalmology, 62*(6), 770-783.

UniProt. (2019). UniProt: a worldwide hub of protein knowledge. *Nucleic Acids Research, 47*(D1), D506-D515.

Van Aken, Papeleu, De Potter, De Laey, & Mareel. (2000). Cadherin expression in the eye. *Bulletin de la Societe Belge d'Ophtalmologie*(278), 55-59.

Verolino, Nastri, Sellitti, & Costagliola. (1999). Axial length increase in lid-sutured rabbits. *Survey of Ophthalmology, 44*, S103-S108.

Vinciguerra, Ambrosio, Elsheikh, Roberts, Lopes, Morenghi, . . . Vinciguerra. (2016). Detection of keratoconus with a new biomechanical index. *Journal of Refractive Surgery, 32*(12), 803-810.

Vogel, Silva, & Marcotte. (2011). Protein expression regulation under oxidative stress. *Molecular & Cellular Proteomics, 10*(12).

Wallman, & Adams. (1987). Developmental aspects of experimental myopia in chicks: susceptibility, recovery and relation to emmetropization. *Vision Research, 27*(7), 1139-1163.

Wallman, Turkel, & Trachtman. (1978). Extreme myopia produced by modest change in early visual experience. *Science, 201*(4362), 1249-1251.

Wang, Chen, Li, & Gao. (2008). *Biomechanical properties of experimental myopia in the guinea pig.* Paper presented at the International Work-Conference on Bioinformatics and Biomedical Engineering.

Wang, Huang, Tian, Kee, & Zheng. (2016). Measurement of corneal tangent modulus using ultrasound indentation. *Ultrasonics, 71*, 20-28.

Wang, Li, Jin, Yang, Zhao, & Long. (2015). Corneal biomechanical properties in myopic eyes measured by a dynamic Scheimpflug analyzer. *Journal of Ophthalmology, 2015*, 161869.

Whitford, Joda, Jones, Bao, Rama, & Elsheikh. (2016). Ex vivo testing of intact eye globes under inflation conditions to determine regional variation of mechanical stiffness. *Eye Vis (Lond), 3*, 21.

Wiesel, & Raviola. (1977). Myopia and eye enlargement after neonatal lid fusion in monkeys. *Nature, 266*(5597), 66-68.

Wilson, & Hong. (2000). Bowman's layer structure and function - Critical or dispensable to corneal function? A hypothesis. *Cornea, 19*(4), 417-420.

Wisely, Sayed, Tamez, Zelinka, Abdel-Rahman, Fischer, & Cebulla. (2017). The chick eye in vision research: An excellent model for the study of ocular disease. *Progress in Retinal and Eye Research, 61*, 72-97.

Wolffsohn, Safeen, Shah, & Laiquzzaman. (2012). Changes of corneal biomechanics with keratoconus. *Cornea, 31*(8), 849-854.

Wollensak, Spoerl, & Seiler. (2003). Riboflavin/ultraviolet-a-induced collagen crosslinking for the treatment of keratoconus. *American Journal of Ophthalmology, 135*(5), 620-627.

Wollensak, Spoerl, & Seiler. (2003). Stress-strain measurements of human and porcine corneas after riboflavin-ultraviolet-A-induced cross-linking. *Journal*

of Cataract and Refractive Surgery, 29(9), 1780-1785.
Wong, Klein, Klein, Knudtson, & Lee. (2003). Refractive errors, intraocular pressure, and glaucoma in a white population. *Ophthalmology, 110*(1), 211-217.
Wong, & Lam. (2015). The roles of cornea and axial length in corneal hysteresis among emmetropes and high myopes: A pilot study. *Current eye research, 40*(3), 282-289.
Woo, Kobayashi, Schlegel, & Lawrence. (1972). Nonlinear material properties of intact cornea and sclera. *Exp Eye Res, 14*(1), 29-39.
Xi, Yip, Shan, Rada, & Kee. (2017). Region-specific differential corneal and scleral mRNA expressions of MMP2, TIMP2, and TGFB2 in highly myopic-astigmatic chicks. *Scientific Reports, 7*(1), 11423.
Xiao, Prieto, Conrads, Veenstra, & Issaq. (2005). Proteomic patterns: their potential for disease diagnosis. *Molecular and Cellular Endocrinology, 230*(1-2), 95-106.
Xu, Wang, Li, Wang, Cui, Li, & Jonas. (2006). Causes of blindness and visual impairment in urban and rural areas in Beijing: the Beijing Eye Study. *Ophthalmology, 113*(7), 1134 e1131-1111.
Yokoi, Seko, Yokoi, Makino, Hatou, Yamada, . . . Azuma. (2012). Establishment of Functioning Human Corneal Endothelial Cell Line with High Growth Potential. *Plos One, 7*(1).
Younan, Mitchell, Cumming, Rochtchina, & Wang. (2002). Myopia and incident cataract and cataract surgery: the blue mountains eye study. *Investigative Ophthalmology & Visual Science, 43*(12), 3625-3632.
Young, Budynas, & Roark. (2002). *Roark's formulas for stress and strain* (7th ed.). New York London: McGraw-Hill.
Yu, Lam, Liu, Chun, Cheung, Li, & To. (2017). Isotope-coded protein label based quantitative proteomic analysis reveals significant upregulation of apolipoprotein A1 and ovotransferrin in the myopic chick vitreous. *Scientific Reports, 7*.
Yura. (1998). The relationship between the types of axial elongation and the prevalence of lattice degeneration of the retina. *Acta Ophthalmologica Scandinavica, 76*(1), 90-95.
Zhao, Pan, Sui, Munoz, Sperduto, & Ellwein. (2000). Refractive error study in children: results from Shunyi district, China. *American Journal of Ophthalmology, 129*(4), 427-435.
Zheng, Wang, Li, & Wang. (2014). *An OCT-based air suction-indentation probe for tissue elasticity measurement.* Paper presented at the SPIE BiOS.
Zhou, Cao, Wu, & Zhang. (2017). Role of corneal collagen fibrils in corneal disorders and related pathological conditions. *International Journal of Ophthalmology, 10*(5), 803-811.
Zhou, Chun, Wang, Zuo, Li, Lam, . . . To. (2018). Proteomic analysis of chick retina

during early recovery from lens-induced myopia. *Molecular Medicine Reports, 18*(1), 59-66.

Zhou, Lu, Xie, Jiang, Wen, Li, . . . Qu. (2007). Recovery from axial myopia induced by a monocularly deprived facemask in adolescent (7-week-old) guinea pigs. *Vision Research, 47*(8), 1103-1111.